AN ELECTRON BOMBARDMENT-MATRIX ISOLATION STUDY OF THE TROPOSPHERIC REACTIONS OF TOLUENE

by

Sasha Erin Campbell

A thesis submitted to the Department of Chemistry

In conformity with the requirements for

the degree of Master of Science

Queen's University

Kingston, Ontario, Canada

(November, 2013)

Abstract

The tropospheric reactions of toluene, acting as a model VOC, are investigated using an electron bombardment-matrix isolation system coupled with Fourier transform infrared spectroscopy. Initial experiments to produce the hydroxyl radicals used to initiate the toluene reactions via electron bombardment of water-argon mixtures are performed. The effects of electron current, water concentration, and gas flow rate are investigated.

A more efficient method of initiating the toluene reactions, by directly creating benzyl radicals through electron bombardment of toluene is then investigated, and the effects of toluene concentration and electron current on the production of the benzyl radicals is quantified. Benzyl radicals are successfully produced, and identified via FT-IR. The next step is the formation of benzylperoxy radicals, via electron bombardment of toluene-oxygen-argon gas mixtures. Experiments are performed using increasing concentrations of toluene and oxygen, in an attempt to observe the benzylperoxy radical. Two new absorptions are observed in the infrared spectra and are tentatively identified as due to the peroxy group on the benzylperoxy radical.

Computational work is also performed to confirm that benzylperoxy radicals can in fact be produced from benzyl radicals and oxygen. The vibrational frequencies of the benzylperoxy radical are also calculated, and used to confirm the possibility that the new absorptions seen in the infrared spectra could in fact be due to benzylperoxy radicals.

The overall results from this work demonstrate that it is likely to be possible to use electron bombardment-matrix isolation systems to investigate tropospheric reactions of volatile organics, and that further experiments could be enhanced by structural modifications to the system.

Acknowledgements

I would first like to thank my supervisor, J. Mark Parnis, without him this would not have happened. He is an incredible teacher, and I have been lucky to learn from him throughout this process, as well as in my undergrad years. His help and encouragement, and his belief that I could successfully complete this work, made this possible.

I would like to thank the staff and faculty of the chemistry departments at Trent and Queen's Universities, as well. I have been fortunate enough to be able to study from a number of excellent professors at both schools, and the help I have received has been invaluable. I would also like to thank everyone else in the Parnis Lab. Dr. Matthew Thompson – his help is one of the things that made this project possible, he was an incredible resource for discussing the project and offering solutions. Bryan Linford, Kaitlynn King, and Alena Celsie – their company in the lab, support, and friendship were a great help. Whether it was troubleshooting apparatus problems, or going on a doughnut run.

There are a few groups of friends that I need to thank. My knitting group was an excellent escape from the lab, and a great way to get rid of the products of my stress-baking. My roller derby teams were an awesome outlet, and helped keep me sane. The Pineau family – without you letting me live with you while I finished this, it would have taken even longer. I can't thank you enough.

And last, but in no way least, I need to thank my family: Marion Wilson, Michael Campbell, my sister Bridget, and everyone else. Without your support through this work, and without you pushing me, I never could have finished this.

Table of Contents

List of Figures

List of Tables

Chapter 1

Introduction

1.0 Overview and scope of present work

Atmospheric chemistry is an important and growing field, a major part of which involves investigating the fate of common contaminants, such as volatile organic compounds. Work has been performed to determine the reactions that these molecules undergo, how they are initiated, and how the molecules are ultimately removed from the atmosphere. Much of this work has made use of mass spectrometric techniques, which have been a traditional method for studying gas-phase chemistry. Mass spectrometry has been successful in determining reaction rates, mechanisms, and energetics, however there are some limitations to mass spectrometric analysis that mean that further investigations are still valuable.[1] Characterization of reactions, such as VOC reactions in the troposphere will necessarily be limited to either identification of final products along with suspected intermediates, or to identification of intermediates without isomer identification. This is because mass spectrometry uses mass-to-charge ratio to identify reaction products, it is therefore often unable to distinguish between structural isomers or isobaric pairs that have the same m/z ratio. In addition, it can only indirectly identify the structure of molecular ions produced.

One technique that can differentiate these pairs is infrared spectroscopy which, when used in tandem with a matrix isolation system, is an excellent method for investigating reaction products and intermediates (including neutral species), their structures, and their energy levels. The present work uses a matrix isolation system coupled with an infrared spectrometer to determine whether this system can be

successfully used to reproduce and observe atmospheric reactions of pollutants, to gain more insight into their mechanisms, products, structures, and branching ratios.

Previous studies in our lab using oxalyl chloride[2], acetone[3], and dimethyl ether[4] have shown that matrix isolation can be a useful method for investigating decomposition and isomerization chemistry, in addition to its more common applications characterizing unstable and reactive molecules. These studies, along with the present work use an electron-bombardment source coupled to the matrix isolation spectroscopy set-up (EBMIS) that is based on work by Szczepanski et al.[5] In addition to the benefits provided by the use of infrared spectroscopy, matrix isolation methods allow reaction intermediates to be directly observed and therefore characterized. This provides a mechanistic insight into previously-unclear areas of gas-phase chemistry. The EBMIS system also allows for the effects of a range of different variables to be investigated, so that their impacts on the chemistry occurring can be observed and analyzed.

The EBMIS system has been used previously in this lab to shed new light onto the gas-phase chemistry of a number of molecules, allowing for a more full understanding of decomposition and isomerization pathways and mechanisms. The present work is an attempt to determine whether the EBMIS system could also be a valuable new method for investigating the chemistry of common atmospheric pollutants, shedding new light on reaction mechanisms, intermediates, and branching ratios. Toluene is used as a model VOC, since it is a simple molecule, readily available for study, and common in the atmosphere.[6]

1.1 Matrix isolation

Matrix isolation, a technique that involves trapping molecules or atoms in solidified gas glasses, was first developed in the early 1930's, using organic compounds as the matrix gas. Ideally, the matrix gas is inert with respect to the sample gas being

studied, and is inactive in the spectroscopic region used for analysis. Based on these criteria, the use of organic matrix gases was clearly limited as they are not inert, and will produce strong absorbances throughout the infrared spectrum. Work by George Pimentel in the 1950's pioneered the use of noble gases, specifically xenon, as the matrix gas to isolate small organic compounds at 66K, and Pimentel is generally credited as the developer of the modern matrix isolation technique.[7] Despite this advance in the technique, the full potential of matrix isolation was not realized until it became possible to obtain lower temperatures. Before this, the matrices that were produced were not very rigid, and allowed both diffusion and bimolecular interactions to occur. Once lower temperatures became possible, so did the use of additional noble gases, such as argon, as matrix gases.

Argon is an ideal matrix gas for a number of reasons – many of its properties make it well-suited for use in matrix isolation. Argon is an atomic gas, having no molecular structure and therefore no vibrational modes, so it is transparent in the infrared range. In addition, it has a full outer shell of electrons making it non-reactive. Closed-cycle helium compressors are the main device currently used for matrix isolation, and the temperatures that these systems can obtain allow for argon matrices with rigid structures, since argon freezes at 83.8K. Argon is also relatively inexpensive, compared to other inert gases used for matrix isolation, due to its abundance in the atmosphere and its production as a byproduct of nitrogen purification.[8]

Matrix isolation has been used for a number of different types of studies, but it is especially suited to work studying transient species which would otherwise decompose or react under different conditions. It has also been used to study weakly-bound complexes, and some studies have attempted to use it as a synthetic tool. One area of study that is particularly useful is investigations into the mechanisms of chemical

reactions. An example is the use of matrix isolation to isolate and characterize short-lived intermediates that had previously only been suspected. The work presented here uses matrix isolation in order to capture the neutral products of neutral molecule-molecule reactions – these radical products do not have long lifetimes, and must be isolated and stabilized. The exothermicity of radical-radical reactions is what necessitates the stabilization of the reaction products, and the argon matrix created in the MI system is ideal for this. An electron bombardment setup is used in this work only as a convenient means to produce radicals, a function that will also be useful in similar future studies.

Generally, an electron bombardment matrix isolation experiment involves a gas sample containing the precursor species of interest (the “guest” molecules) heavily diluted in an inert gas (the “host” or “matrix” gas). The gas mixture is flowed towards a cold surface held well below the host gas freezing point, at a controlled rate. An electron beam is also present in the reaction chamber, and electrons collide with the gas mixture as it flows, ionizing the precursor and initiating typical gas-phase chemistry. As this is occurring, the mixture of products, reactants, and intermediates co-condenses on the cold surface diluted in the host gas. This isolates the various molecules from each other within the solid matrix, shown in Figure 1. Once condensation is complete, various spectroscopic techniques may be used to analyze the products and intermediates. As long as the matrix is kept frozen, this analysis can be completed at any time. In addition, the deposition of the gas sample onto the cold surface can take place over extended periods of time, from several hours up to days.

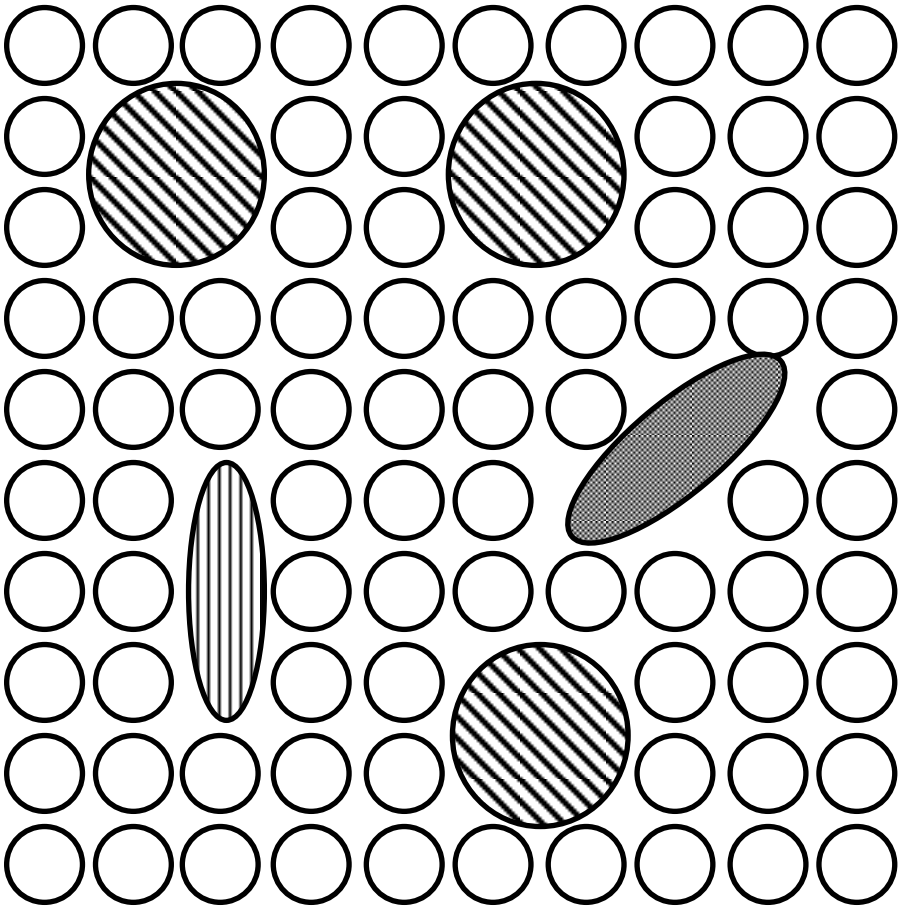

Figure 1. Graphical representation of guest molecules (shaded circles and ovals) matrix isolated in a host gas (clear circles).

Reactive and unstable species are stabilized during matrix isolation, allowing for analysis with whichever spectroscopic method is selected. The stabilization is thought to occur during condensation onto the cold surface – as the gas mixture condenses, the region containing the unstable species will have a higher pressure than usually encountered in gas-phase environments. This will increase the likelihood of collisions occurring between the products or intermediates and the inert host gas. The mean free path of any molecule produced during ionization will be significantly reduced in the solidifying matrix, so repeated collisions with the host gas will occur. These collisions allow for excess energy to transfer from the excited species to the host gas – if the gas

is inert rare gas atoms, the energy will be transferred as translational energy. If inert molecules are used in the host gas, they can accept additional excess energy, as they have vibrational and rotational modes which provide additional degrees of freedom. In either case, the combination of the transfer of excess energy and the lowering temperatures occurring during condensation results in the quenching of unstable or reactive species through a process called collisional deactivation. An important part of this process is keeping the matrix species isolated from one another. This is achieved by selecting a concentration of sample gas that is low enough that there will be a great excess of host gas – generally the ratio of sample to host gas is kept below 1:400. Since most molecules are significantly larger than the rare gas atoms forming the matrix, they will have to occupy multiple substitution sites in the face-centered cubic crystal structures of the rare gases[9]. This means that most molecules will be surrounded by at least twenty rare gas atoms, and they will be kept effectively isolated from one another. These molecules will not be able to diffuse once the matrix has formed, as long as temperatures are low enough to create a rigid matrix – the general rule is that the matrix temperature should be 30%[5] of the host gas freezing point. This means that as long as the temperature and concentration are low enough, bimolecular reactions will be prevented. An additional factor preventing these reactions is that the extremely low matrix temperatures make even small reaction barriers insurmountable, due to the lack of thermal energy available. This aspect of matrix isolation makes it particularly useful for this work, as the products of radical-radical reactions are short-lived as a result of their exothermic formations. The ability of matrix isolation to capture these initial products and isolate and stabilize them is key to our ability to characterize the compounds.

Matrix isolation does, however, have some disadvantages. One major disadvantage is the amount of equipment required to perform EBMIS experiments. Another is that there can be matrix interactions with the products generated, causing unexpected results. Depending on the type of study planned, the advantages to this technique often outweigh the disadvantages, particularly if the required equipment is already available. This is the case for the present work, in which an EBMI system is used coupled with Fourier-transform infrared spectrometry (FTIR).

1.2 FTIR and matrix isolation

Matrix isolation systems have been successfully coupled with many different types of spectroscopic techniques for analysis. The present work uses infrared absorption spectroscopy, which, along with UV/visible absorption spectroscopy and electron spin resonance spectroscopy, is one of the most common methods. One major aspect of infrared spectroscopy that makes it ideal for this work is its ability to distinguish between structural isomers, something that is not generally possible in gas-phase reaction kinetics studies. The coupling of matrix isolation with infrared spectroscopy allows for radical initial reaction products to be stabilized and characterized more thoroughly than other methods, where isomer identification is not possible.

For a molecule to absorb infrared radiation, its vibrational normal modes must become excited by infrared light of an energy that exactly matches the transition energy associated with a particular vibrational mode. The vibrational modes correspond to vibrations in the molecule occurring either through bond stretching, or non-stretching modes including bending, torsion, wagging, or deformation (this group will be referred to as “bending modes”). Using the number of atoms in a molecule, N, the number of vibrational modes can easily be calculated – 3N-6 for non-linear molecules or 3N-5 for

linear molecules. In addition, for a molecule to be infrared active, the vibrational mode that is excited must result in a change in the molecule's dipole moment.

The features of an infrared spectrum that correspond to stretching modes of a molecule can be easily modeled. This is because even in larger, more complex molecules, a stretching motion can be quite accurately simplified to involve only motion of the two atoms connected by the stretching bond. This means that the vibrational energy of a specific stretching mode can be accurately predicted by solving the harmonic oscillator problem,[10] where c is the speed of light in a vacuum, k is the force constant of the stretching bond, and μ is the reduced mass of the two nuclei involved.

$$\bar{\nu}_{stretch} = \frac{1}{2\pi c}\sqrt{\frac{k}{\mu}} \quad (1)$$

The feature of stretching modes that makes them easily predicted is the fact that their motion is quite simple. This is not true of bending modes, which cannot be predicted with accuracy due to their increased complexity. Since we can consider stretching modes to involve only motion of specific nuclei, we can identify absorption positions that are typical of the stretching modes of different functional groups. This means that stretching mode absorptions are ideal for use when identifying molecules, as they can be used to determine which functional groups are present. This method is the group frequency approach, and works because functional groups will always produce absorptions in the same known spectral ranges (generally occurring between 4000 and 1300 cm^{-1}). As an example, a hydrogen-bonded O-H group stretch appears as a broad feature around 3600 cm^{-1}, while a C=O stretch in an aldehyde will appear as a large sharp feature around 1700 cm^{-1}. As previously mentioned, bending motions are more complicated than stretching motions. The energy of these motions is also typically lower

than the energy of stretching motions, and therefore they appear at lover wavenumbers. This region is called the fingerprint region, and occurs between 1300 and 900 cm^{-1}. This region usually appears quite complex compared to the functional group region, but is useful for confirming specific structures when there are multiple similar structures possible according to the functional groups identified.

Interpretation of gas-phase infrared spectra at room temperature becomes more difficult as several complicating factors must be taken into account. Molecules have thermal energy that allows them to rotate, and occupy different rotational states that cause absorptions to broaden. Some of these complications are eliminated or diminished when infrared spectroscopy is used in conjunction with matrix isolation, or when gas phase work is performed at very low temperatures. When molecules are trapped in a rare-gas matrix, their ability to rotate is inhibited, lowering the bandwidth of absorbances. The matrix can, however, hold some percentage of the molecules in different orientations from the others, which will not broaden absorbances but will cause a small, shifted peak to appear in the spectrum[11]. These effects are shown in Figure 2, reproduced from Dunkin's book on matrix isolation techniques.

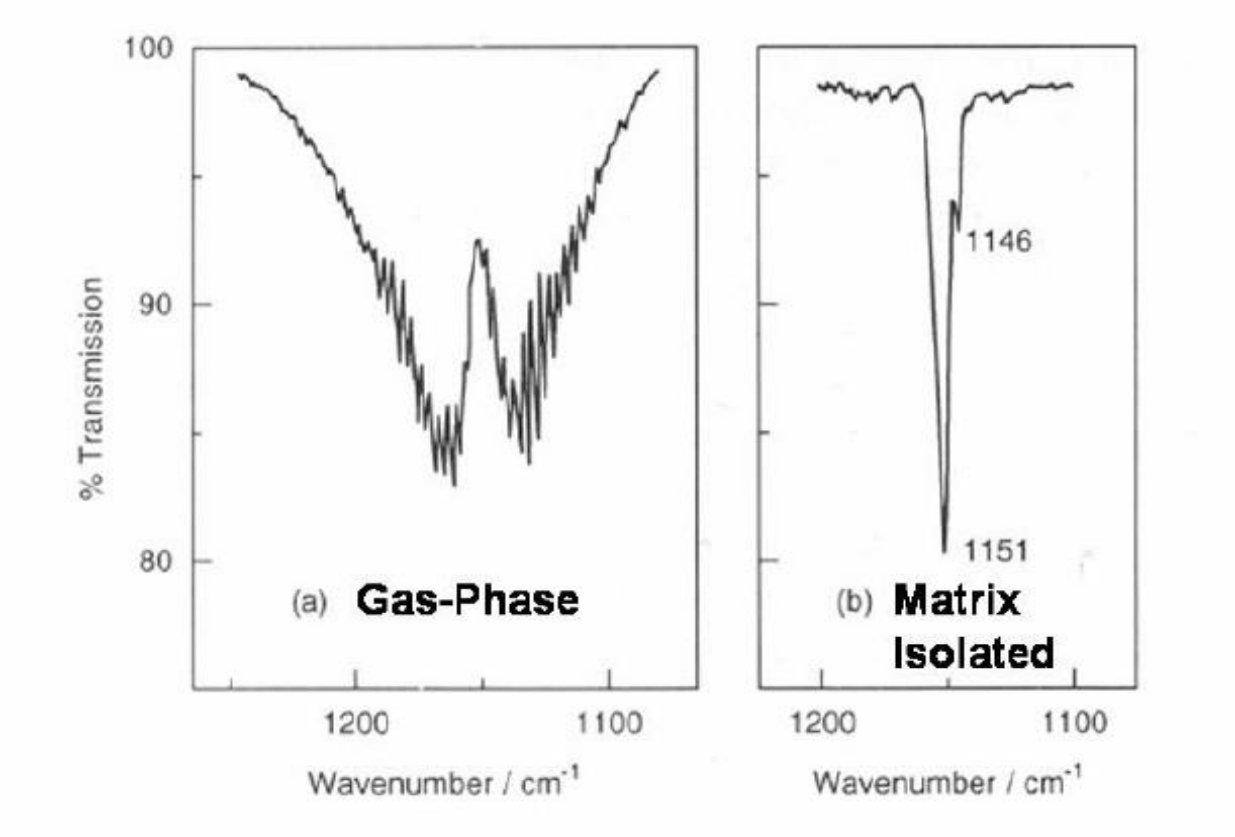

Figure 2. Comparison, from Dunkin[11], of the IR modes of SO_2 in the gas phase (a) and matrix isolated (b). Splitting caused by a sample of the gas held in a different environment from the rest is also visible.

Also, although molecules are generally isolated from one another, at higher concentrations aggregations can occur which may cause interactions and complex formation that will complicate the spectrum. This is occasionally desired, for example in experiments when the goal is to observe a reaction between compounds. When it is not a desired outcome, it can easily be avoided by working at lower concentrations. Lower concentrations will generally result in smaller absorbances, but deposition time can be increased so that larger quantities of the gas sample are condensed into the matrix, helping to mitigate this issue. Deposit time is however limited by matrix scattering and

opacity, at typical flow rates this creates an upper limit on deposition time of about six hours.

One additional complication that can occur with matrix isolation, briefly mentioned in the previous section, is matrix-site effects – these are vibrational shifts that are caused by matrix-guest interactions. These interactions alter the electronic structure of the guest molecules, which then changes their vibrational spectrum. Overall, this means that the observed wavenumber at which a particular mode absorbs for a matrix-isolated species will be different from the wavenumber observed for the same mode in the gas phase. The larger the difference, the greater the interaction between the host and guest molecules – generally the difference is small, the fundamental absorbances of most argon matrix-isolated species is only different from their gas phase absorbances by about 1%, and only very few absorptions will be more than 2% off from their gas-phase counterparts. This simply means that while the gas phase absorbances may be known for a molecule of interest, the molecule will likely not be observed at the exact same wavenumbers when matrix-isolated – the known gas-phase values serve as a guide for where to look, but will not provide exact locations.

In general, infrared spectroscopy is extremely useful in a variety of applications. It does have some disadvantages, including the tendency for rotational movement, overtones, or other features to complicate the spectrum. As explained above, the low temperatures and immobilization that occur in a rare gas matrix mean that some of these problems are often eliminated or significantly diminished when infrared spectroscopy is used in conjunction with a matrix isolation system. In the present work, IR spectroscopy is used to identify products and intermediates in the typical expected reactions of toluene trapped in an argon matrix using matrix isolation techniques. The next section of this

chapter will discuss the commonly observed gas-phase chemistry that occurs in the EBMIS apparatus.

1.3 Gas-phase chemistry relevant to EBMIS system

Gas-phase chemistry is a field that has been extensively studied, through both theoretical and experimental work. A major feature of gas-phase chemistry that is important to the present work is that one-electron oxidation creates a localized charge in a molecule, which can result in structural changes that include bond weakening. This means that working in the gas phase allows reactions to occur that would not occur in condensed phases, where energy transfer to the surrounding medium would result in the removal of the excess energy that could otherwise cause dissociation. These reactions lead into extremely diverse sets of results that make this field especially interesting. The chemistry occurring in the EBMIS apparatus, while not identical to ideal gas-phase chemistry, can be interpreted and understood using much of the same principles and theory as unimolecular decomposition of isolated ions in the gas phase. The fit of these principles and theory is not exact, as the molecules studied are not single isolated molecules and bimolecular reactions are possible, but knowledge of both the basic concepts and methods for the study of gas-phase chemistry is useful.

Gas-phase chemistry can be described by theoretical models, the currently accepted model being Rice-Ramsperger-Marcus-Kassel (RRKM) theory. A complete description of this theory is not within the scope of this work; however, a simplified theory, quasi-equilibrium theory (QET) is also applicable, and assumes that energized molecules can only redistribute energy internally[1]. An understanding of the assumptions of this theory presented by Gross[1] is useful for discussion of decomposition of molecules.

The initial assumption made is that ionization occurs vertically, rather than adiabatically – the molecular geometry of the ion that is formed does not change and relax to a lower energy configuration. Using the Born-Oppenheimer Approximation, it is possible to ignore the nuclear motion involved in the molecule's vibrational modes, as the electronic motion is assumed to occur essentially instantaneously. Therefore, the positions of the atoms within the molecule can be assumed to remain constant when ionization takes place, as the molecule transfers to a cationic potential energy surface. The Franck-Condon principle states that excitation occurs through vertical transitions, and that the probability for an electronic transition is highest where the wavefunctions associated with the vibronic ground and ionized states overlap most strongly. In addition, an ion may have multiple low-lying electronic states. These overlap and cause energy transitions to occur from excess electronic energy into vibrational energy. The molecule can remain intact long enough for this transition to occur, randomly distributing the excess electronic energy as vibrational energy, as long as the low-lying excited state lifetimes are significantly longer than the vibrational energy time period. The rate of dissociation of the ion is determined by the probability that this randomly distributed vibrational energy will concentrate in specific regions that will cause a dissociation or rearrangement[1]. Lastly, if the initially formed ion has enough internal energy, fragment ions produced by its dissociation may still have enough energy to undergo secondary decomposition[1].

QET is especially useful when working with unimolecular reactions and their rates. In relation to the present work, however, the difference in rates between simple cleavages and rearrangement reactions is the most important point. When a molecule is fragmenting, it can do this via simple heterolytic bond cleavage or through a rearrangement process. Bond cleavage involves what is termed a loose transition state

(TS), meaning that the molecule does not need to be in a specific orientation for the cleavage to proceed, it requires only enough energy to overcome the involved bond's dissociation energy. Rearrangement processes involve a tight TS, where the molecule must obtain a specific orientation to proceed. In the case where rearrangements lead to products that are thermodynamically lower in energy than those of bond cleavage processes, they will generally dominate at higher internal energies. However, since cleavages require only a loose TS, and can occur from any orientation, if there is an excess of energy available and both reactions are possible, the cleavage reaction dominates kinetically. The internal energy possessed by an ionized molecule will directly impact the chemistry that follows. Product distributions can differ significantly depending on whether an ion is left with a small or large amount of excess internal energy. This remaining internal energy left with the molecule after ionization depends on the ionization process that occurred.

Discussion of gas-phase ion chemistry cannot occur without knowledge of the ionization processes that can or will occur. Atoms and molecules can be characterized by their ionization potentials, the minimum amount of energy that they must absorb in their ground state to eject an electron and form a ground state ion. Frequently, the amount of energy that a molecule absorbs during ionization is larger than its IP, and after ionization it will be left with an excess of internal energy to disperse through its vibrational modes. This dispersed energy can often exceed the molecule's bond dissociation energies, and cause extensive fragmentation. Appearance energy is one factor used to characterize unimolecular fragmentation reactions – this is the minimum amount of energy that the neutral precursor needs to absorb in order for a specific fragmentation process to occur, producing a specific product for detection.

There are three possible ionization processes that can occur in the EBMIS apparatus used in the present work. These are electron ionization, charge transfer ionization, and Penning ionization. Electron ionization involves an interaction between energetic electrons and the molecule which causes a transient electronic disturbance. This can cause excitation of the molecule, or it can cause an electron to be ejected from the valence shell, resulting in ionization of the molecule if the disturbance involves energy greater than the ionization potential. This is shown for argon in the gas phase in equation (2), below:

$$Ar + e^{-} \rightarrow Ar^{+\bullet} + 2e^{-} \qquad (2)$$

The second process, charge transfer ionization, requires a charged molecule to interact with the neutral molecule of interest. The neutral molecule must have a lower ionization energy than the electron affinity of the charged molecule, so that the charged molecule can pull off an electron while ionizing the other species. In the present work, charge transfer ionization would be most likely to occur between charged argon, ionized via electron ionization, and the guest molecules, M. This is shown below, in equation (3):

$$Ar^{+\bullet} + M \rightarrow M^{+\bullet} + Ar \qquad (3)$$

The thermodynamics of this reaction would be dictated by the ionization potential of the neutral species as well as the electron affinity (EA) of the charged radical cation. EA is defined as the energy released when the species in question gains an electron, and while some of this energy will be transferred as translational motion, most is carried away by the product as excess internal energy. The maximum amount of energy that a molecule, M, will possess after charge transfer ionization can be determined using equation (4).

$$E_{\text{internal}}(M^{+\bullet}) \leq EA(Ar^{+\bullet}) - IP(M) \qquad (4)$$

As an example, argon has an electron affinity of 15.8 eV, while a typical organic species has an ionization potential of around 10 eV. This means that if the organic species were ionized via charge transfer from an argon radical cation, it would be left with up to 6 eV of excess internal energy, approximately 580 kJ/mol. This is enough energy to cause extensive fragmentation of the organic species, since C-C and C-H bond dissociation energies are generally well below this level.

The final method of ionization is Penning ionization, shown in equations (5) and (6). This occurs when an internally excited, but not ionized, argon atom interacts with a molecule, M, and transfers its energy. If the ionization energy of M is lower than the energy of the excited argon atom, ionization may occur.

$$Ar + e^{-} \rightarrow Ar^{*} + e^{-} \qquad (5)$$

$$Ar^{*} + M \rightarrow M^{+\bullet} + e^{-} \qquad (6)$$

These ionization processes will be discussed further in the next chapter, using studies performed with the EBMI apparatus that determined which methods were most likely to be occurring. An in-depth discussion of the chemistry that occurs upon oxidation of toluene in the atmosphere is also present in the next chapter. This chemistry provides an outline of what can be expected to occur in the EBMI system, if it successfully models the atmospheric conditions under which toluene oxidation occurs.

1.4 Calculations

This section will provide a brief explanation and discussion of the calculations performed in the present work. The reaction between the benzyl radical and molecular oxygen is expected to be significantly exothermic, since both species contain unpaired

electrons. In order to confirm that it would in fact proceed, a series of calculations were performed to determine the reaction energy. In addition, the reaction energies of a series of other key processes were determined.

This work was performed by building the structures of the key neutral, radical, and ionized molecules and atoms examined in this work - such as toluene, oxygen, and the benzyl radical, for example – into Gaussian software[12], in order to use computational techniques to determine the energies of each species. The initial method used was Austin Model 1 (AM1), a semi-empirical method for calculating molecular electronic structures. The results of these calculations were used as the starting point for Density Functional Theory (DFT) calculations using the 3-21G basis set. The calculations were repeated, starting from the results of the previous calculation, using increasingly complex basis sets to obtain increasingly accurate results. The final basis set used was the 6-31G** basis set, and the results of these calculations were used in determining the reaction energies of the key processes in this work. The method used, increasing the complexity of the calculations performed, starting from the previous results, allowed for accurate results to be obtained without excessively long wait times for the results.

Once the enthalpies of formation (H_f) had been obtained, they were used to determine the reaction energy, the enthalpy change of reaction (ΔH_R) using equation (7). The reaction energy is the sum of the enthalpies of formation of the products, minus the sum of the enthalpies of formation of the reactants.

$$\Delta H_R = \sum H_f(\text{products}) - \sum H_f(\text{reactants}) \quad (7)$$

A positive enthalpy change of reaction indicates that the reaction is endothermic, and requires an energy input to occur. If the enthalpy change is negative, the reaction is exothermic, and will proceed spontaneously, giving off energy in the process. The

reaction between the benzyl radical and molecular oxygen is expected to be exothermic. In comparison, the loss of a hydrogen atom from toluene to form the benzyl radical is expected to be endothermic – the toluene requires an addition of energy to eject the hydrogen atom and form the radical. In the current work, this additional energy could be provided by an electron impact, or transferred from an argon radical cation.

Chapter 2

Literature Review

2.0 Brief introduction to environmental relevance of aromatic hydrocarbons

Aromatic compounds are common atmospheric pollutants due to their widespread use, production as by-products of combustion, and high volatility. For this reason, their activity in, and their removal from, the atmosphere are of significant interest to environmental scientists.

The most likely reactions of aromatic hydrocarbons in the troposphere are with hydroxyl radicals ($OH^{\bullet}$).[13] These reactions are generally either an addition of the radical to the hydrocarbon forming a new radical species, or abstraction of a hydrogen by the hydroxyl radical, forming a water molecule and a new radical species. These radical species then go on to react in the atmosphere, via reaction pathways that lead to the formation of components of photochemical oxidizing smog.[13]

In order to study these reaction pathways, toluene was selected as a model aromatic hydrocarbon compound. Toluene was selected for a number of reasons, discussed in more detail later in this section. As one example of toluene's prevalence, and therefore its relevance as a model species for study, Canada's total atmospheric release of toluene alone has been estimated at over 100 kilotonnes per year – these releases are largely due to toluene-containing solvents, and vehicle emissions.[14] For comparison, Canada's 2010 emissions of HFC's, PFC's and SF_6 were reported to be 9000 kilotonnes[15] – the mass of toluene released is more than 1% that of these major greenhouse gases.

Experiments were performed in an electron bombardment-matrix isolation apparatus that attempted to reproduce the reactions that toluene would undergo in the atmosphere. This review of the available literature will discuss the history of the EBMI apparatus, and its use and development in the Parnis lab; the importance of the hydroxyl radical in the atmosphere, the reactions that it is involved in, its isolation and observation in EBMI experiments; the selection of toluene as a model VOC, the reactions that toluene undergoes in the atmosphere, and previous work regarding the observation using infrared spectrometry of toluene and its reaction products in EBMI and EBMI-type systems.

2.1 The electron bombardment-matrix isolation (EBMI) apparatus

The technique of matrix isolation and how it works was previously discussed in Chapter 1, along with the gas-phase ionization of molecules and why gas phase chemical theories can be applied to the chemistry occurring in a matrix isolation system. Electron bombardment is one method of ionizing molecules that are to be studied, and in this section the coupling of electron bombardment techniques with matrix isolation systems will be discussed. The initial development of the electron bombardment-matrix isolation (EBMI) systems will be covered as well as its use – and the new understandings of the technique that have resulted from its use in the Parnis lab.

2.1.1 Development of the EBMI system

The early development of the use of electron bombardment in conjunction with a matrix-isolation system came about through the desire to capture charged species in the frozen matrix for analysis. This had previously been possible with the use of a number of methods, including reactive atomic sources, photolysis, radiolysis, and lasers, while electron bombardment had only been used in the gas phase.[16,17] Some of the first work

coupling electron bombardment with matrix isolation was performed by Milligan and Jacox,[18] and Breeze et al.[19]

Milligan and Jacox[18] used a series of methods to isolate NO_2^- in an argon matrix, including electron bombardment during deposition of a NO_2/Ar onto the matrix substrate. The work by Breeze et al.[19] used electron bombardment, among other methods, to isolate charged carbonyl species in argon matrices by bombarding the neutral compounds as they were deposited. The paper in which this work was published also discusses the potential mechanisms by which the ions are being formed after electron bombardment – electron capture by a neutral molecule, or dissociative electron capture by the neutral parent molecule. The method of ion formation in our EBMIS system will be discussed in more detail later in this section. Suzer and Andrews[16,20] were also among the first research groups coupling electron bombardment to matrix isolation for use with vibrational spectroscopy. In two studies, they used a tungsten filament as a low-energy electron source for electron bombardment of H_2O/Ar and NH_3/Ar mixtures. Both experiments produced new infrared absorptions that were assigned to the hydroxyl anion and neutral radical,[16] and the amide anion and neutral radical.[20]

The capture and study of positively charged species in a rare-gas matrix was first reported by Knight et al.[21] Their work studied $^{14}N_2^+$ and $^{15}N_2^+$ trapped in neon matrices, and developed a new technique – using electron bombardment matrix isolation to trap species for analysis with electron spin resonance. They based the new technique on the previous coupling of electron bombardment matrix isolation with vibrational spectroscopy, and continued to use it to study additional molecular cation radicals.[22]

The previously-discussed early electron bombardment matrix isolation studies all used an apparatus setup where the electron beam was aimed directly at the matrix deposition surface. The matrix was bombarded with electrons as it condensed, and the gas sample molecules did not encounter the electrons before condensing. This apparatus was modified by Szczepanski et al.[5] to a setup where the electron beam is aimed at an anode positioned beside the deposition surface, so that it intersects the gas sample before the sample reaches the surface. With this setup, the ionization occurs in the gas phase before condensation, rather than being an irradiation of a solid surface, as in the previously-discussed work. The apparatus used in this work is based on the Szczepanski design, with some modifications. The electron beam in this apparatus is not perpendicular to the gas flow, but parallel. The electrons and gas sample both originate at the same end of the reaction cell, and travel together towards the deposition surface. The anode towards which the electrons are flowing is ring-shaped, and sits slightly above the deposition surface. This allows the ionization to occur in the gas phase, since the gas sample is able to interact with the electron beam while flowing towards the deposition window.

The work done by Szczepanski and coworkers[5] explored a number of aspects of the electron bombardment-matrix isolation system. Their main goal was to acquire the infrared spectrum of the matrix-isolated naphthalene radical cation, for comparison with unidentified interstellar IR emission features. To do this, they prepared gas samples containing naphthalene (Np) and carbon tetrachloride (CCl_4) diluted in argon, which were subject to electron bombardment before condensing on a window held at 12K. The purpose of the CCl_4 was to act as a matrix ion stabilizer by providing an electron trap that would balance the charge of the cations under observation. When subject to

electron bombardment, the CCl_4 produces multiple fragmentation products: CCl_3^+, CCl_3, CCl_3•Cl, Cl^-, and Cl. Since chlorine has a high electron affinity, the use of carbon tetrachloride as an electron trap is common – the chlorine will capture low-energy electrons produced from electron impact with argon atoms, and chlorine anions will be produced. If the condensed matrix contained only the neutral argon atoms and the cations of interest, the potential created in front of it would be enormous – approximately 1 megavolt, according to Szczepanski. This demonstrates the need for balancing negative charges to be present, to allow for successful formation of the matrix and the ability to study the positively-charged species of interest. The opposite is obviously true when creating negatively charged species for study – positively-charged species are required for charge balance.

In addition to acting as a matrix stabilizer, Szczepanski's results[5] indicated that the carbon tetrachloride was also acting as an ionization enhancer. The intensity of the visible bands they observed for the naphthalene cation was significantly increased by the addition of CCl_4 to the sample gas mixture. They also observed that the presence of argon increased the ionization of the naphthalene, and proposed two different methods by which the CCl_4 and Ar could be causing ionization of naphthalene. The first was charge transfer from CCl_4:

$$CCl_4 + e^- \rightarrow CCl_3^+ + Cl + 2e^- \qquad (1)$$

$$CCl_3^+ + Np \rightarrow CCl_3 + Np^{+\bullet} \qquad (2)$$

The second possible method was through Penning ionization. Because the energy required to ionize the naphthalene (IP) is lower than the energy of the excited metastable state of argon, Penning ionization can occur:

$$Ar + e^- \rightarrow Ar^* + e^- \quad (3)$$

$$Ar^* + Np \rightarrow Np^{+\bullet} + Ar + e^- \quad (4)$$

2.1.2 EBMIS work in the Parnis lab

The electron bombardment-matrix isolation system used in the Parnis research lab is based off of the design developed by Szczepanski, et al.[5] with some modifications. Although the original Parnis modification involved the same perpendicular electron flow configuration, for the present work, the electron flow is parallel to the gas sample flow, while still allowing for gas-phase sample ionization.

The ongoing EBMI work in this research lab has contributed to the furthered understanding of the functioning of the EBMI apparatus, as newer work has built on previously explained concepts and revealed new aspects to investigate and consider. This work has built the foundation of the knowledge of the EBMI apparatus and its functioning in this lab. Research using the EBMI apparatus has focused on a number of different areas, including looking at ionization mechanisms.

Despite the current work being the first study of the feasibility of the use of EBMI techniques for study of atmospheric reactions, much of the knowledge developed over the Parnis lab's history of EMBI work is relevant. In particular, the understanding of the ionization mechanism occurring in the apparatus that has been gained through research in this lab will be highly useful.

2.1.2.1 Ionization mechanisms in the EBMI system

The discussion earlier in this chapter of research performed by Breeze et al.[19] and Szczepanski et al.[5] touched briefly on the mechanism of ionization that was occurring with electron bombardment of the sample gas mixtures. The potential

mechanisms that were mentioned were electron capture (possibly followed by dissociation) by the neutral parent molecule, charge transfer ionization by the inert matrix gas, or Penning ionization by the inert matrix gas. Research in the Parnis lab has led to the conclusion that the ionization of the molecules of interest occurs via charge transfer from the neutral matrix gas. This conclusion is supported by the results of multiple experiments, including work by Fridgen and Parnis[2], and by Fridgen et al[23].

The work by Fridgen and Parnis[2] was focused on the study of the gas-phase ion chemistry of oxalyl chloride ($C_2O_2Cl_2$, OxCl) using the EBMI technique, and compares the likelihoods of two mechanisms of ionization – charge transfer, and Penning ionization. They use the thermodynamics of one of the major ion processes observed to argue that Penning ionization is not occurring. An important product that is observed in the infrared spectra is the carbonyl chloride radical, $ClCO^{\bullet}$. They state that the most likely route to this product is the C-C bond cleavage of the oxalyl chloride radical cation ($OxCl^{+\bullet}$), to produce $ClCO^{\bullet}$ and $ClCO^{+}$. Due to the excess energy that would remain with the products, and the low barrier for decomposition of the radical product, it is likely that the $ClCO^{\bullet}$ observed in the matrix is the result of the cation being neutralized near or in the matrix.

Penning ionization requires the matrix gas to be excited to a metastable state, and then transfer this excess energy to the target molecules. The metastable states of argon that could be causing Penning ionization exist between 11.5 and 11.8 eV above the ground state, and are not high enough in energy to cause the C-C bond dissociation that is observed to occur. The metastable states of krypton are even lower in energy, yet the carbonyl chloride radical product is still observed, indicating that C-C bond dissociation is still happening. This demonstrates that Penning ionization is unlikely to

be the ionization mechanism taking place. Charge transfer is another possible ionization mechanism. Since the matrix gas atoms are the most abundant species in the reaction chamber, they are the most likely to be directly ionized via electron impact. The cation that results will then continue to exist until it can re-capture an electron, or collide with a species that has a lower ionization potential than itself. In the matrix isolation system currently being discussed, this would be the oxalyl chloride molecules present, and an electron would be transferred from the OxCl to the argon via charge transfer:

$$Ar + e^- \rightarrow Ar^{+\bullet} + 2e^- \qquad (5)$$

$$Ar^{+\bullet} + OxCl \rightarrow Ar + OxCl^{+\bullet *} \qquad (6)$$

When the ionized argon (or other rare gas) atom is returned to its ground state after charge transfer, there is an excess of energy (*) that is equal to the difference between the electron affinity of the rare gas and the ionization potential of the other molecule. This excess energy can then lead to rearrangements and unimolecular dissociation of the other molecule. In this case, there is enough excess energy left with the oxalyl chloride radical cation to cause the C-C bond cleavage that results in formation of the carbonyl chloride radical product. Charge transfer therefore offers the best explanation for the observed results of the experiment.

Further work by Fridgen and coworkers[23] was research using the EBMI apparatus and infrared spectroscopy to study the isomerization and fragmentation products of dihalomethanes in rare-gas matrices, particularly dichloromethane (CH_2Cl_2). As part of their evidence for charge transfer ionization, they state that the rare gas cations that are formed by electron impact, and necessary for charge transfer, have infinite lifetimes when in the absence of species with lower ionization potentials than

their own. They would therefore still have significant lifetimes when they vastly outnumber a species with a lower IP, as they do in matrix isolation conditions. In contrast to this, the lifetimes of excited metastable states of rare gases, which are required for Penning ionization to occur, are relatively short.

In addition to this, they compare the results of EBMI experiments performed using gas samples of CH_2Cl_2 diluted in three different rare gases (Ar/CH_2Cl_2, Kr/CH_2Cl_2, and Xe/CH_2Cl_2) to further demonstrate that Penning ionization is unlikely, and the more probable ionization mechanism is charge transfer. The ionization potential of dichloromethane is 11.32 eV, which falls in between the excitation energies of neutral argon's first excited states (11.72 and 11.55 eV) and above the first excited states of neutral krypton (10.56 and 9.92 eV). The first excited states of neutral xenon are even lower than those of kryption, at 9.54 and 8.32 eV. Based on this information, only collisions with metastable argon atoms would ionize dichloromethane, while collisions with metastable krypton or xenon would not. If Penning ionization were the mechanism occurring in the EBMI system, ionization products would only be expected to occur in the Ar/CH_2Cl_2 experiments, and only the parent compound would be seen in the spectra taken from the Kr and Xe experiments. This was not the case, and similar products were observed in all three experiments. Based on this evidence, the ionization method occurring is consistent only with charge transfer, occurring between the rare gas radical cation and the dichloromethane molecule.

These studies, and others performed in this lab, have led to a wider understanding of the ionization occurring in the EBMI system, and general acceptance that charge transfer is responsible. This information is key to the current work being performed on the system, in that it will allow for some prediction of expected products.

This is possible by looking at the photoelectron-photoion coincidence spectra (PEPICO spectra) and breakdown curves of the molecules being studied, and looking at the products created at 15.8 eV, the ionization energy of argon.

2.2 Hydroxyl radicals

Hydroxyl radicals are vitally important in the troposphere because they are responsible for initiating the oxidation of most trace tropospheric gases. Despite being only a minor component of the atmosphere, they begin the processes that lead to the removal of most trace gases through precipitation or other means. The reactions that hydroxyl radicals undergo to remove these trace gases are generally catalytic, so relatively large steady concentrations of hydroxyl radicals are maintained in the troposphere.[24]

2.2.1 OH radical formation and maintenance in the troposphere

Hydroxyl radicals in the troposphere are produced by the reaction between water vapour and excited $O(^1D)$ atoms.[25] The oxygen atoms are the result of reactions between ozone and solar UV radiation. The UV radiation reaching the troposphere is too low-energy to photolyze the compounds that make up the majority of the atmosphere, but it is able to react with ozone. This reaction is a very important piece of the overall tropospheric chemistry, particularly when it involves UV radiation with wavelengths lower than 320nm, which produce electronically excited oxygen atoms. This reaction process will actually proceed with UV radiation shorter than 340nm, but at a lower yield than with wavelengths <320nm. The steps are shown below[24,26,27]

$$O_3 + h\nu \rightarrow O^1D + O_2, \lambda \leq 340nm \quad (7)$$

$$O^1D + M \rightarrow O^3P + M \quad (M = O_2, N_2) \qquad (8)$$

$$O^1D + H_2O \rightarrow OH + OH \qquad (9)$$

Reaction (7) above shows the actual photolysis of the ozone molecule, producing O^1D, the excited oxygen atom. The following reaction (8) is the pathway that occurs the majority of the time – the excited atom collides with nitrogen or oxygen molecules and is quenched to O^3P. In a minority of cases, reaction (9) will occur, and the excited oxygen will collide with water vapour, producing hydroxyl radicals. Since water vapour is present in large quantities in the troposphere and the rate constant of reaction (9) is significantly higher than that of reaction (8), the quenching pathways, a reasonable percentage (10% in some geographic locations) of O^1D atoms eventually generate OH radicals.[24]

The reactions that the hydroxyl radicals undergo in the atmosphere (see Section 2.2.2 for more detail) are generally chain reactions in which either hydroxyl radicals, hydroperoxy radicals ($HOO^{\bullet}$), or both (HO_X) are produced,[24] A number of common reaction chains produce hydroperoxy radicals as a final product – this radical can then undergo additional reactions, sometimes producing hydroxyl radicals.[27,28] In regions with low NO concentrations, the hydroperoxy radicals will generally undergo self-reaction, and be consumed to produce hydrogen peroxide (generally removed from the atmosphere in rain).[24,27] When in the presence of NO, hydroxyl radicals and nitrogen dioxide will be produced when hydroperoxy radicals oxidize the NO. The nitrogen dioxide is then quickly photolyzed to produce nitric oxide and atomic oxygen. This highlights two major atmospheric functions of NO_X – NO reacts with hydroperoxy

radicals to produce more-reactive hydroxyl radicals, and NO_2 is photolyzed to produce O^3P atoms which will quickly react with O_2 to form ozone.[24,27] These steps, the conversion of a hydroperoxy radical into a hydroxyl radical and, eventually, an ozone molecule, are shown below.

$$HO_2 + NO \rightarrow NO_2 + OH \qquad (10)$$

$$NO_2 + h\nu \rightarrow NO + O^3P \qquad (11)$$

$$O^3P + O_2 + M \rightarrow O_3 + M \qquad M = O_2, N_2 \qquad (12)$$

These reaction cycles are responsible for secondary production of hydroxyl radicals, through recycling, and serve to maintain a relatively constant OH radical concentration ([OH]) in the troposphere. The concentration cannot be entirely spatially or temporally constant for a few reasons. Since the production of OH radicals from ozone relies on solar UV radiation, there are obviously diurnal and seasonal cyclic variations in concentration.[24] In addition, the production of OH radicals from ozone and production of the OH radicals by recycling requires the presence of additional compounds, such as water vapour or nitrogen oxides. Concentrations of these compounds will vary geographically, causing the concentration of hydroxyl radicals to also have some geographic variation. These temporal and spatial variations in concentration mean that while local [OH] can be directly measured, results of those measurements do not accurately reflect global [OH], or how it responds to the different processes that affect OH radical production and loss.[29] Global [OH] values are generally arrived at by observing selected trace gases whose major tropospheric sink is the reaction with hydroxyl radicals, and whose global emission rate is known.[29, 30] This is

obviously not an extremely precise or accurate method of calculating global hydroxyl radical concentrations.

2.2.2 Hydroxyl radical reactions with molecules in atmosphere

As previously stated, hydroxyl radicals are responsible for initiating the oxidation of most atmospheric contaminant gases, often as the rate determining step.[24] The majority of hydroxyl radicals that are formed will go on to react with carbon monoxide or methane – approximately 70% will react with CO, and 30% with CH_4.[27] The simplest reaction the radical undergoes is with carbon monoxide to form carbon dioxide and a very reactive hydrogen atom:

$$CO + OH^{\bullet} \rightarrow CO_2 + H^{\bullet} \qquad (13)$$

The hydrogen atom can then go on to react with oxygen, forming a reactive hydroperoxy radical:

$$H^{\bullet} + O_2 \rightarrow HO_2^{\bullet} \qquad (14)$$

These hydroperoxy radicals will sometimes go on to produce hydroxyl radicals, as discussed in Section 2.2.1.

Generally, the reactions between hydroxyl radicals and other atmospheric chemicals result in products that are more water-soluble than the original contaminants, making the products easier to be removed from the atmosphere via precipitation. Some examples include the conversion of nitrogen and sulfur dioxides into nitric and sulfuric acid, as well as the partial oxidation of hydrocarbons into ketones, alcohols, aldehydes, and other compounds.[30]

Alkane loss in the atmosphere proceeds almost entirely by reactions with hydroxyl radicals – a hydrogen atom is abstracted from a carbon-hydrogen bond to produce an alkyl radical.[27] These alkyl radicals will then react with oxygen to produce alkylperoxy radicals. Alkenes present in the atmosphere, particularly ethene and propene, mainly react with hydroxyl radicals by addition reactions where OH-alkene adducts are formed.[27] These adducts behave similarly to alkyl radicals during later reactions. This is known to occur in dienes as well, studies investigating mechanisms and products formed from the reaction between hydroxyl radical and 1,3-butadiene showed the reaction to proceed via addition of the OH followed by addition of an oxygen molecule to form alkyl peroxy products.[31] These products undergo further reactions, often forming aldehyde products such as 4-hydroxy-2-butenal, which was confirmed for the first time by Berndt and Böge,[31] and the carbonyl-containing products of its reaction with hydroxyl radical were observed.

Hydroxyl radicals are important molecules in the oxidation of isoprene and other terpenes in the troposphere. Isoprene is the most abundant non-methane hydrocarbon in the atmosphere,[31] it is produced mainly by biogenic sources, and is oxidized by hydroxyl radicals, generally via OH-addition to one of multiple possible sites on the isoprene.[32] A number of studies on the tropospheric activity of isoprene have been performed, investigating its reactions with hydroxyl radicals, the products formed, the reaction rate constants, and the further reactions that the initial products undergo.[32,33,34] Monoterpenes are a class of molecules that are another highly abundant biogenic tropospheric component. They are known to react with hydroxyl radicals, and this reaction is important in the formation of ozone and organic aerosols, but understanding of the reaction mechanisms is still limited. A study by Librando and Tringali[35] is one of

many that investigate the kinetics and product formation of terpene-OH radical reactions. They specifically look at the gas- and aerosol-phase reaction products of a number of important monoterpenes, and propose mechanisms to explain how the degradation products of these terpenes could influence the formation and growth of organic aerosols in the troposphere.

Hydroxyl radicals are responsible for the removal of many other atmospheric pollutants beyond carbon monoxide, simple hydrocarbons, and the terpenes. Polychlorinated biphenyls (PCBs) are a group of pollutant molecules that have become ubiquitous in the environment. Experiments performed by a number of groups between 1986 and 1995 are discussed by Anderson and Hites,[36] and have demonstrated that a major loss process for PCBs with up to two chlorine atoms present is the reaction with hydroxyl radicals - OH radicals will react with these PCBs at environmentally significant rates. They will also react with PCBs containing more than two chlorine atoms, but these reaction rates have only been calculated, and have not been experimentally determined – the calculated reaction rates show that the major loss method for these PCBs is also reaction with hydroxyl radicals.[36]

Simple aromatic hydrocarbons and their activity in the atmosphere have been studied extensively, as discussed by Arey et al.[37] and Obermeyer et al,[38] and have been found to also participate in oxidation reactions with hydroxyl radicals. They react via OH radical addition far more frequently than via H-atom abstraction, and the products of their reactions include multiple different carbonyl and aldehyde compounds.[37,38] Polycyclic aromatic hydrocarbons (PAHs) are another major atmospheric pollutant – their main Canadian source is forest fires, though they are also produced in large amounts by transportation sources.[39] PAHs containing two to four aromatic rings are present mainly

in the gas phase, and the main process for their loss from the atmosphere is reaction with hydroxyl radicals.[40] As discussed by Atkinson and Arey,[40] little is known about the oxidation chemistry of PAHs, since there is such variety and complexity of the potential products – their study identified many products and mechanisms for the oxidation of naphthalene, one of the simplest of the PAHs.

Oxidized volatile organic compounds (OVOCs) are another class of compounds found in the troposphere. Their sources include the oxidation of volatile organic compounds (such as isoprene and other previously-discussed species) in the troposphere by hydroxyl radicals, biogenic emissions, and anthropogenic emissions. These compounds influence tropospheric photochemistry, just as VOC and other pollutants do. Methanol is one of the most abundant OVOCs observed in the upper troposphere. Ethanol is also observed, but at lower concentrations; the main loss process for both species is reaction with hydroxyl radicals, eventually producing formaldehyde and acetaldehyde, respectively, among other products.[41] The experimental kinetics study of hydroxyl radical reactions with both methanol and ethanol performed by Dillon et al.[41] determined that due to the rate constant of the OH radical-ethanol reaction, ethanol is an important source of acetaldehyde, an important species involved in NO_x transport, despite its low tropospheric concentration.

Reactions with hydroxyl radicals are also a key step in the removal of other, less common, atmospheric pollutants. Organosilicons are one of these species – reaction with OH radicals is known to be the main cause of oxidation, and work by Markgraf and Wells[42] has begun to fill in gaps in the knowledge of the environmental impact of these compounds by identifying the mechanisms and products of the reactions with OH radicals. Among other atmospheric trace compounds, hydroxyl radicals are also an

important molecule in the oxidation of sulfur-containing species, specifically dimethyl sulfide and dimethyl sulfoxide – the reactions that these species undergo with hydroxyl radicals, their mechanisms, and products are discussed in detail in a review by Barnes, et al.[43] Dimethyl sulfide is particularly important, as it makes up approximately 50% of biogenic emissions of sulfur-containing compounds; while biogenic sources are greatly outweighed by anthropogenic sources in industrialized areas, they are important to the sulfur budget on a global scale (making up 50-60% of sulfur emissions in the Southern Hemisphere).[43] Longer-chain sulfur-containing compounds are also of interest to atmospheric scientists, and are also oxidized by hydroxyl radicals. Study of these compounds includes work performed in 2010 to determine kinetic data for, and identify products of, the reactions between hydroxyl radicals and ethyl methyl sulfide[44]

Anthropogenic and biogenic sources are responsible for the release of massive quantities of organic compounds into the atmosphere every year. These compounds can then go on to react in the troposphere, by one of many methods including photolysis by UV radiation, reactions with ozone, reactions with radical species (including hydroxyl radicals and nitrate radicals), and others. These reactions generally create radical products, and years of research have resulted in the reaction rates and mechanisms for many of these initial reactions being well-known. The reaction rates, mechanisms, and products of subsequent reaction steps, however, are less well-known, though still important. As discussed by atmospheric scientist Roger Atkinson,[45] there are two major routes to studying and learning about the products of these atmospheric reactions – one can study the products and mechanisms of the individual reactions involved in the degradation of the compounds (such as self-reactions of the alkyl peroxy radicals produced or reactions between the alkyl peroxy radicals and hydroperoxy radicals), or

one can study the products of the OH radical, NO_3 radical, and ozone reactions with the specific compound of interest. There is value in these studies of the products of oxidation of specific molecules, where the first-generation products have already been identified and reaction mechanisms are known.[45] This work is an effort to determine the feasibility of performing studies of the products and mechanisms of the tropospheric reactions of volatile organic compounds in the electron-bombardment matrix-isolation system. These studies would be of the second type discussed by Atkinson,[45] investigating oxidation products past the first product generation of specific organic compounds.

2.2.3 Hydroxyl radicals in the EBMI apparatus

Hydroxyl radicals have been isolated in rare-gas matrices and observed using infrared spectroscopy in a number of studies. An early study by Acquista et al.[46] used vacuum-ultraviolet photolysis to irradiate a frozen water ($H_2{}^{16}O$)-argon solid at 20.4 and 4.2K, producing infrared absorptions that they assigned to hydroxyl radicals. The pair of absorptions that were observed occurred at 3452.3 and 3428.2 cm^{-1}; they were compared to the sets of absorptions observed when hydrogen peroxide or hydroperoxy radicals are isolated in argon to rule out either of these compounds. Further experiments were performed using a mixture of $H_2{}^{16}O$ and $H_2{}^{18}O$, using $D_2{}^{16}O$ alone, and using a $D_2{}^{16}O$- $D_2{}^{18}O$ mixture to confirm the peak identification.

A later study by Suzer and Andrews,[16] whose work is frequently referenced in the Parnis lab due to their similar experimental procedures, supported these results. In their experiment, they prepared a mixture of argon with less than 0.1% H_2O, and condensed it at 12K while it was continuously bombarded by electrons created by a low energy source. In addition to the known hydroperoxy radical and water IR absorptions, five new

absorptions were observed – 3554.0, 3548.9, 3452.7, 3428.1, and 903.7 cm^{-1}. The 3452.7 and 3428.1 cm^{-1} absorptions were assigned to the hydroxyl radical on the basis of their agreement with the results aquired by Acquista et al,[46] and confirmed by repeating the experiment using water containing different isotope mixtures (ie $H_2{}^{18}O$, HDO, D_2O, etc.). The 3546.9 cm^{-1} absorption was assigned to one matrix site of OH^-, as it is fairly close to the OH^- absorption observed in the gas phase.

An additional study, performed by Cheng et al.,[47] shortly after the Suzer and Andrews work[16] was published, contradicts the previous assignments of the hydroxyl radical IR absorption. Atomic hydrogen and deuterium were produced using microwave discharge and thermal dissociation with a tungsten filament, and then reacted with NO_2, O_3, and atomic O. The reaction mixture was then condensed in an argon matrix at 12K. D and $^{18}O_2$ were used as isotopic labels and experiments using isotopically-labelled reactants, along with additional control experiments were used to confirm peak identifications. An absorption was produced at 3548.20 cm^{-1} when H atoms were reacted with NO_2, O_3, or ^{16}O. This absorption shifted to 3537.10 cm^{-1} when ^{18}O was used in place of ^{16}O, and lines appeared at both wavenumbers when a mixture of the two oxygen isotopes was used. When D was used in place of H, the absorption shifted from 3548.20 to 2616.10 cm^{-1}. When D and ^{18}O were reacted, the absorption appeared at 2600.30 cm^{-1}, and when ^{18}O was reacted with a mixture of H and D, the lines appeared at 3537.10 and 2600.30 cm^{-1}. Because only two lines appear when H and D mixtures are reacted with a single oxygen isotope, and when ^{18}O and ^{16}O mixtures are reacted with a single hydrogen isotope, it is clear that the compound responsible for the absorption contains a single hydrogen atom and a single oxygen atom. The compound is also shown to contain only hydrogen and oxygen, and no other elements, since it

appears when reactants that contain only hydrogen and oxygen are used, as well as when NO_2 is used.

Further control experiments included a set of experiments where the temperature was temporarily increased to 25K. In these experiments, the absorptions at 3548.20 and 2616.10 cm^{-1} decreased much more significantly than other observed absorptions known to be caused by stable species. These absorptions decreased only slightly when the samples were illuminated by an Hg lamp to photolyze them after deposition. The behavior of the absorptions when the matrix was warmed shows that the species is reactive. It is shown to be not easily photolyzed, and stable to UV light, by the experiments using the Hg lamp. In addition, the shift in wavenumbers when H or D are used, or when ^{16}O or ^{18}O are used, are consistent with the shift in wavenumber that occurs in gas-phase OH molecules, but not OH^+ or OH^- molecules. Also supporting the theory that the absorption is due to a neutral species is the fact that no hydrogen cations or anions are produced by the microwave discharge of H_2 at the temperatures used by Cheng et al.[47] Their study concludes that the hydroxyl radical produces an absorption at 3548.20 cm^{-1}, and the absorptions previously assigned to OH by Acquista et al.,[46] and Suzer and Andrews[16] are potentially caused by the hydroxyl radical in a complex with water or argon atoms.[47] The assignment of the absorption at 3548.2 cm^{-1} to the hydroxyl radical is supported by computational work performed by Cabral.[48]

This work will attempt to produce hydroxyl radicals via electron bombardment of water in the EBMI apparatus. It is likely that this will be successful, and production of OH will be confirmed by the observation of an infrared absorption at 3548.20 cm^{-1}.

2.3 Toluene

Volatile organic compounds are a major source of atmospheric pollution, as previously discussed. A significant number of these VOCs are aromatic hydrocarbons, largely coming from vehicle emissions and industrial sources. Toluene is a common aromatic hydrocarbon, widely used in industry and emitted in vehicle exhaust, and it has the highest typical ambient concentration in urban areas of the aromatic compounds.[6] Like other VOCs, its removal from the atmosphere largely proceeds via reactions with hydroxyl radicals. These reactions result 90% of the time in addition of the OH to the aromatic ring, and 10% of the time in H-atom abstraction from the methyl group.[49] Toluene is one of the simpler aromatic hydrocarbons, is easily available for EBMI work, and is very common in the atmosphere. For these reasons, it was selected as the model VOC that would be used in determining whether the EBMI apparatus would be useful for the investigation of atmospheric VOC reactions and their intermediate products.

2.3.1 Toluene reactions in the atmosphere

As discussed by Molina et al.[49] and others,[6] in 10% of cases oxidation of toluene by hydroxyl radicals will proceed via abstraction of a methyl hydrogen. H-atom abstraction from toluene produces benzyl radicals, which can then go on to react with oxygen to form benzylperoxy radicals. These radicals are then able to react with NO_2, and form benzaldehyde and benzyl nitrate.[6] These radical chain reactions will continue, as the benzaldehyde is a carbonyl compound that can react with hydroxyl radicals and then oxygen to form another peroxy radical, which will continue to react and can form carboxylic acids.[37,49] The benzyl radical reaction with oxygen to produce benzylperoxy radicals is well-known, but the later oxidation reactions of the benzylperoxy radicals have not been fully characterized and further study would be valuable.[50]

In the other 90% of cases, the hydroxyl radical will add to the aromatic ring, forming a toluene-OH adduct, the methyl hydroxycyclohexadienyl radical.[49] This radical will then react with oxygen, forming peroxy radicals, which can continue to react with oxygen and NO_2. The toluene-OH adduct ultimately produces phenols, 1,2-dicarbonyls, and unsaturated 1,4-dicarbonyls.[37,38,49] The carbonyl products of the OH-toluene adduct reactions have been extensively studied by the research groups of Arey[37] and Obermeyer,[38] among others – they have identified many of the products, and proposed potential product formation pathways.

The major products of the oxidation of toluene by hydroxyl radicals, independent of initial reaction pathway, are benzaldehyde and its later carboxylic acid products, along with phenols, and 1,2- and 1,4-dicarbonyls. These compounds are all found in the troposphere, and the oxidation of hydrocarbons (including toluene) by hydroxyl radicals is largely responsible for their concentrations. In particular, although 1,2-dicarbonyls are released directly to the atmosphere from motor exhaust and other sources, this is believed to be a minor source of the carbonyls when compared to their production from the oxidation of both non-aromatic VOCs and aromatic hydrocarbons.[38] The majority of experimental research that investigates the oxidation of toluene and other VOCs has been performed using mass spectrometry. This has allowed for the identification of products by molecular formula, and the proposal of potential reaction pathways, but only allows for indirect determination of the molecular structures of the products that they observe. In addition, there is uncertainty over many of the mechanisms of the OH-initiated toluene oxidation reactions, and there have been few direct experimental studies of the radical intermediates formed during these reactions.[49]

The use of the electron bombardment-matrix isolation apparatus will make it possible to react toluene with hydroxyl radicals in the presence of oxygen, to produce peroxy radicals. Modifications of the apparatus could then allow for additional gas inlets, so that the newly created peroxy radicals are exposed to NO_2 and can then react further. The nature of the matrix isolation system means that reactants, products, and any intermediates can be trapped in the frozen argon matrix, unable to react further. This will allow for the observation of the radical intermediates created during the oxidation process. Since the EBMI apparatus is coupled with a Fourier-transform IR spectrometer, the spectra that will be obtained of the reaction products and intermediates will be useful to determine their molecular structures.

2.3.2 Observation of toluene and its oxidation products in EBMI-type systems

Many of the oxidation products of toluene have been previously studied, and their matrix-isolated infrared spectra exist in the literature. This will allow us to confirm their presence or absence in the spectra obtained in our experiments. For those compounds that do not have matrix-isolated IR spectra available, gas- or liquid-phase IR spectra have generally been recorded, and are available. While the vibrational frequencies observed in these spectra will not exactly match those expected in matrix isolation conditions, they do provide a good starting point for determining whether a particular compound is present.

Toluene itself is a compound for which matrix-isolated infrared vibrational frequency assignments are unavailable in the literature. However, there have been many studies performed that have determined the IR absorptions and their assignments for toluene in the vapour-,[51,52,53] liquid-,[51,54] and solid-phase.[55] Infrared spectra of matrix-isolated toluene do exist, but the observed absorbances are not listed or assigned to

specific vibrational modes. Hoops and Ault[56] have performed IR analysis of matrix-isolated mixtures of $CrCl_2O_2$ and toluene as part of an investigation into the photochemical reactions of methyl-substituted benzenes with $CrCl_2O_2$, and published the resulting spectra in a 2006 paper. The pre-irradiation reference spectrum shows the absorbances of the toluene and $CrCl_2O_2$ mixture before any reactions can take place and create product compounds. Although the individual absorbances are not assigned, the spectral figure could be useful as a comparison with our own toluene/argon spectra.

Using this spectral information, and comparing spectra that we obtain of matrix-isolated toluene with "blank" argon-only reference samples, we will be able to determine which spectral features we observe are due to toluene. In addition, matrix-isolated infrared spectra of benzene are available in the literature, with observed vibrations assigned.[57,58,59] These spectra may also be useful in confirming the assignments of potential toluene absorptions, as the spectra of the two molecules can be expected to share some similarities, due to the similar structures of benzene and toluene.

The benzyl radical, the radical product of H-atom abstraction by hydroxyl radicals, has been characterized using matrix isolation and infrared spectroscopy, and its infrared-region vibrational frequencies have been assigned, by Baskir et al.[60] Their research used the pyrolysis of benzyl bromide and dibenzyl in the gas phase to produce benzyl radicals, which were then trapped in an argon matrix at 12K for infrared spectroscopic analysis. They provide the resulting spectrum, and have assigned each IR absorption to a vibrational mode of the benzyl radical – the observed IR bands are discussed further in Chapter 4. The absorbances identified by Baskir and coworkers[60] will be used to determine whether benzyl radical has been produced in our experiments.

There is a lot of additional research on the benzyl radical available in the literature, including a number of studies of the production of the radicals from toluene. Two of these studies focused specifically on the production of benzyl radicals via photolysis of toluene.[61,62] Others also produced benzyl radicals by photolysis of toluene, and then performed different types of spectroscopic analysis to study them.[63,64] These studies indicate that excited toluene will decompose to produce the benzyl radical, raising the possibility that the benzyl radical could be produced directly from toluene in the EBMIS system. Studies have also been performed investigating the decomposition of excited benzyl radicals, determining that it fragments to produce C_7H_6.[65,66] It would therefore be useful to know the matrix-isolated IR spectrum of C_7H_6 and its potential rearrangement and reaction products, if they are available, in case the fragmentation of benzyl radicals to C_7H_6 occurs in the EBMIS system.

Benzaldehyde is another toluene decomposition product that has been studied by matrix isolation IR spectroscopy previously. Work by Kuş and coworkers[59] presents the infrared spectrum of benzaldehyde matrix-isolated in both an argon matrix and a xenon matrix, and discusses the effects of changing the matrix gas. Parker and Davis[67] have performed research looking at the matrix isolated products of the reactions between toluene and oxygen after UV irradiation. This work may be useful for determining whether reactions are occurring in our system between oxygen and toluene, as it discusses the matrix isolated spectra of methylphenol, benzyl alcohol, and a ketene product.

A major product for which matrix isolated infrared spectra are unavailable is the benzylperoxy radical, the product of the reaction that occurs between oxygen and the benzyl radical. Many studies have been performed on the formation of the benzylperoxy

radical, and the kinetics and thermodynamics of its formation are well-known. Little work exists, however, presenting any form of spectroscopic analysis of the radical. The best resource found for use in determining whether the benzylperoxy radical has been produced in the EBMIS system is a paper by Murakami et al.[68] that presents unscaled, calculated infrared vibrational frequencies of the benzylperoxy radical, as part of a study to determine rate constants for different reaction pathways at high temperatures. They have also calculated vibrational frequencies for a number of other possible products and transition states of the benzyl radical/oxygen reaction, which may be useful.

While only calculated infrared absorptions have been found for benzylperoxy radicals, matrix isolation studies have been performed on a number of other alkylperoxy radicals, presented in a series of papers by Snelson and coworkers.[69,70,71,72] The infrared absorptions of methyl-,[69] ethyl-,[70] isopropyl-,[71] and tert-butylperoxy[72] radicals matrix-isolated in argon at 12K are given. In addition, the matrix-isolated IR spectrum of the phenylperoxy radical is also available in the literature.[73] Using the known frequencies of these other alkylperoxy compounds, and readily available information on the inductive effects of benzene groups, we can predict at least a portion of the infrared spectral range in which we might observe absorptions due to benzylperoxy radicals, helped by the calculated values also available.

Chapter 3

Experimental Methods

3.0 Overview

This section will describe the technical details of the equipment required for this research, as well as the experimental protocols used. The main pieces of equipment typically used in this research are a gas handling line used for sample preparation, and the electron bombardment matrix isolation infrared spectroscopy (EBMIS) apparatus in which experiments are run.

3.1 Gas handling line

The gas handling line is a stainless steel, high-vacuum apparatus separate from the EBMIS system, where samples are prepared (Figure 3).

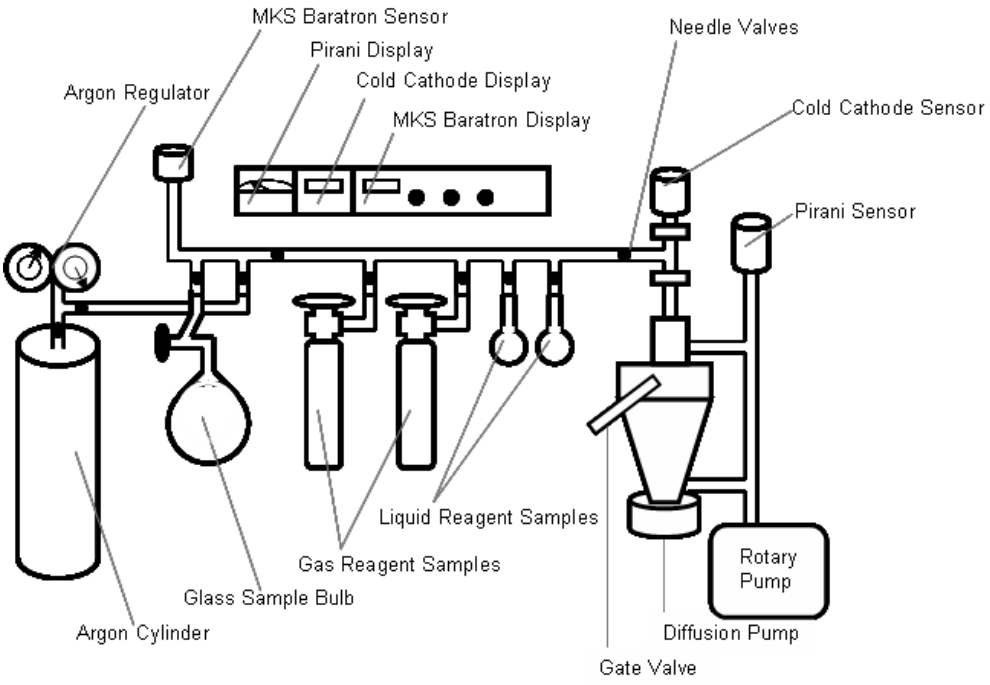

Figure 3. Gas handling line for preparation of samples

High-vacuum conditions are required in the gas handling line to ensure that the prepared samples are free of contaminants. A two-stage pumping system is used to achieve and maintain high-vacuum conditions in the line. The first stage is a rotary pump, which evacuates the system and achieves pressures between 10^{-2} and 10^{-3} Torr. The pressure is measured during evacuation with the rotary pump by a Pirani gauge, which will measure down to 10^{-3} Torr. Once the pressure has dropped below 5×10^{-2} Torr, the second stage is activated. The second stage is an oil diffusion pump which is used to achieve pressures of $10^{-6} – 10^{-7}$ Torr. Upon activation of the diffusion pump, pressure in the system is measured using a cold cathode ion gauge. When evacuating the system from high pressures, a bypass valve is used initially to isolate the diffusion pump until a low enough pressure is reached for its activation.

A digital MKS Baratron sensor is used to measure the absolute pressure in the line, to 10^{-1} Torr accuracy. The argon gas cylinder, other gas and liquid reagents, and the gas sample bulb are all attached to the line using Ultratorr compression fittings. Needle valves are used to control the flow in and out of the line of the various attached components, they are manipulated to allow small amounts of gases into the system from the gas cylinders. All gas samples are prepared in 1 or 2 liter, single- or multi-component glass bulbs.

3.2 Sample preparation

The first step in the preparation of a new gas sample is the evacuation of the sample bulb. The glass bulbs are attached to the sample line and are evacuated to high vacuum using the two-stage pumping system. They are left open and attached to the line for at least several hours, and often overnight.

Once the sample bulb has been totally evacuated, the line is closed off from the pumps and the MKS sensor is zeroed so that the sample can be prepared. The first component of the sample added is the reagent gas – this gas is present in smaller amounts in the sample than argon, and will therefore have a lower partial pressure. Adding the reagent gas first means that when argon gas is added, which will have a higher partial pressure, the reagent gas is less able to escape the sample bulb and the final concentration of the reagent gas in the sample will be more accurate.

To add the reagent gas, the valve on the sample bulb is first opened, and will be left open until the sample is completely prepared. With both the needle valve controlling the flow between the reagent gas cylinder and the gas line and the valve on the

connector between the cylinder and the gas line closed, the valve on top of the gas cylinder is opened and quickly closed. This allows an amount of gas out of the cylinder, and means that reagent gas entry into the system can be controlled more easily, without the high pressure created by leaving the cylinder open. The valve on the controller is then opened, and the needle valve controlling flow into the gas line is manipulated to allow the correct amount of reagent gas into the system. Once the MKS sensor reads the correct pressure, the needle valves that connect the gas cylinder and sample bulb to the gas line are closed, and the gas line is opened to vacuum to evacuate the reagent gas remaining in the line.

Once the desired amount of reagent gas has been added to the sample bulb and the gas line has been evacuated to high-vacuum, the final step is the addition of argon. The gas line is again isolated from the vacuum system, and the needle valve connecting the sample bulb is left closed. The argon gas cylinder is opened, and argon is allowed to flow into the system using the needle valve connecting it to the gas line. Once the MKS sensor reads a pressure of at least 400 Torr, the needle valve to the sample bulb is opened and the flow of argon is increased slightly. This is done to create a pressure gradient that will prevent any reagent gas from escaping the sample bulb during argon addition. Argon is further added to the system until the desired final pressure (generally 800 Torr) is attained, at which point the needle valves connecting the argon and the sample bulb to the system are closed. The valve on the sample bulb is then closed, and it is removed from the gas handling system, allowed to equilibrate for at least eight hours to ensure full mixing, and can then be used for experiments.

The amount of each gas to be used to attain a specific reagent to rare gas mole ratio is calculated by treating all gases as ideal, and using Dalton's law of partial

pressures. As an example, to prepare a sample where toluene and argon are present in a 1:200 mole ratio, we would add 4.0 Torr of toluene and 800.0 Torr of argon, for a total sample pressure of 804.0 Torr. The mole ratio can be calculated using the ideal gas law (since the volume and temperature of the system do not change between gas additions V, T, and R cancel):

$$\frac{n_{toluene}}{n_{Ar}} = \frac{P_{tol}V/RT}{P_{Ar}V/RT} = \frac{P_{toluene}}{P_{Ar}} = \frac{4.0Torr}{800.0Torr} = \frac{1}{200}$$

To prepare any samples with a reagent to rare gas mole ratio lower than 1:800, a sample is prepared with a mole ratio twice the desired ratio and then diluted to the required ratio. As an example, for a sample with a final mole ratio of 1:1600, a 1:800 sample is prepared. This sample bulb is left open to the gas line, and the whole system is evacuated to 400 Torr. Argon is then added back into the sample until the MKS sensor reads 800 Torr, diluting the sample by half to give a 1:1600 sample. This is done following the same procedures described earlier for sample preparation.

3.3 EBMIS apparatus

The EBMIS apparatus used in this research (Figure 4) is based on the original design of Szczepanski et al.[5] The four main components of the apparatus are: the gas handling inside the apparatus; the cooling system; the electron source; and the reaction chamber.

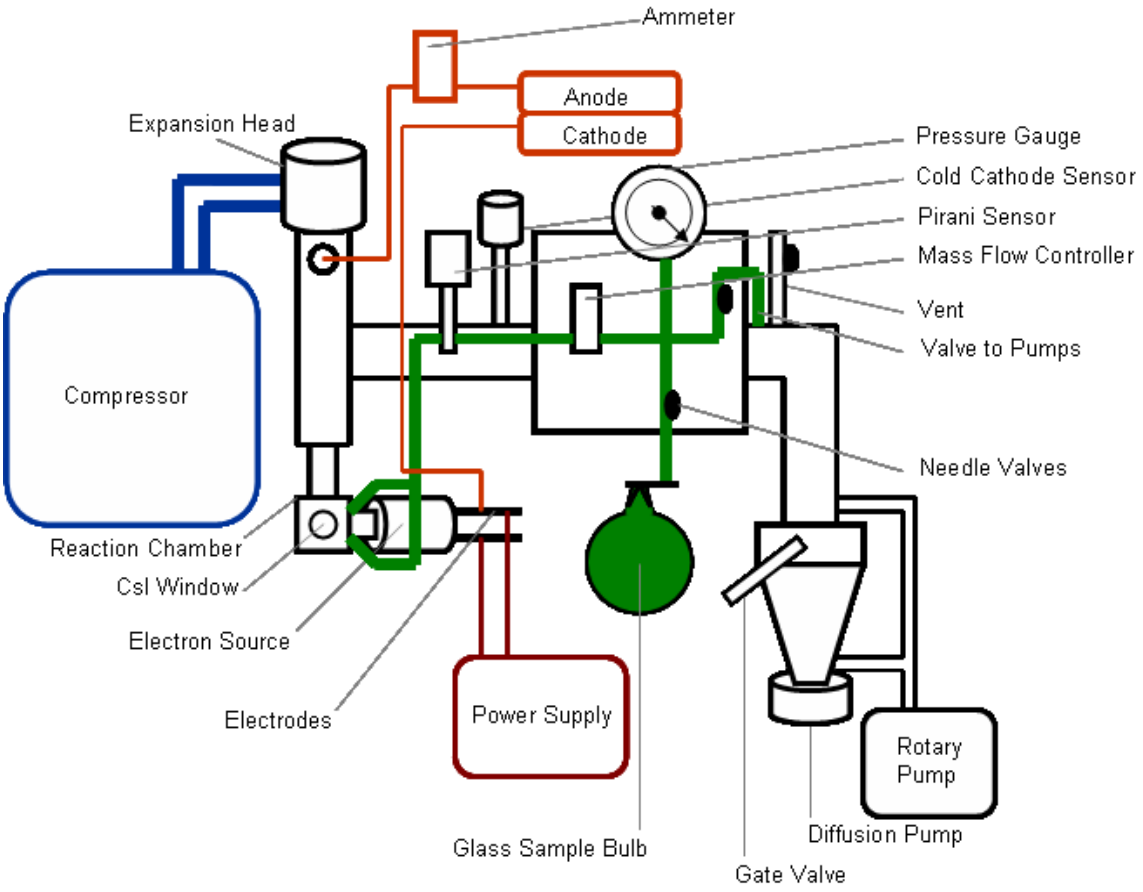

Figure 4. Electron bombardment-matrix isolation apparatus

3.3.1 Gas handling in EBMIS apparatus

The EBMIS system is held at a high vacuum by a two-stage pump system identical to that used in the gas handling line. The system pressure is measured by a Pirani gauge (low vacuum) and a cold cathode ion gauge (high vacuum). A needle valve on the apparatus gas line isolates the EBMIS system from the vacuum, and is kept closed when experiments are performed. Upon completion of an experiment, the bypass valve is closed to isolate the diffusion pump, and the needle valve is opened to allow the rotary pump to evacuate gas present in the system down to at least 5×10^{-2} Torr. When this pressure is reached, the bypass valve is shifted to the “backing”

position, and the gate valve is opened to allow the diffusion pump to evacuate the system to high-vacuum levels. The sample bulb is attached to the EBMIS system using an Ultratorr compression fitting, and a needle valve is used to isolate the fitting and bulb from the rest of the system when removing and replacing sample bulbs. The valve on the sample bulb is used to allow or stop gas flow from the bulb into the system.

When the sample bulb is opened to the rest of the system, the amount of sample gas can be determined using the helicoid pressure gauge connected to the gas-handling line. The bulbs are initially filled to 800 Torr, which is enough gas for several experiments at the conditions generally used in this research. Below approximately 200 Torr, the mass flow controller becomes unstable and thus less reliable, so experiments were not generally run with this little gas remaining. Once the sample bulb has been opened, the flow of gas through the apparatus into the reaction zone and towards the cold window is controlled by an MKS mass flow controller. The mass flow controller allows the user to set the desired flow rate (in cm^3/min) and maintains this rate through the entire experiment. Once the mass flow controller is switched on to allow the gas sample through, the gas flows through the apparatus and enters the reaction zone, where it flows towards the cold CsI window and freezes into a solid matrix. The CsI window is connected to the expander head, and is rotated to be perpendicular to the gas flow during gas deposition. The head is then rotated to be perpendicular to the IR spectrometer beam (parallel to gas flow) for analysis.

3.3.2 EBMIS cooling system

The cooling system used in this research is an APD Cryogenics Displex closed-cycle helium refrigeration system, which is turned on once the system has been

evacuated to high vacuum levels. This system pumps helium into the expander head, where the gas expands and cools. The helium is then pumped out, and this cycle repeats itself, further cooling the apparatus. Continued cycling for approximately an hour is generally sufficient to cool the cold tip, to which the CsI spectroscopic window is attached, down to 13 K. The compressor is left on, and can maintain the required low temperature for the entire length of the experiment.

The temperature is monitored using a Lakeshore temperature controller, which also allows for annealing. The annealing temperature can be set on the controller, and it will raise the temperature at the cold window to this target temperature. The cold window will be held at the target temperature for as long as desired, and will quickly lower back to 13 K when annealing is stopped.

3.3.3 EBMIS electron source

The electron source in the EBMIS apparatus is a thoriated tungsten filament, which acts as the cathode. When a current is applied to the filament, it generates an electron beam that is accelerated to the anode, an insulated wire ring that sits just in front of the CsI window. The anode and cathode are biased to -200 V and +80 V, respectively, creating a 300 V potential difference between them.

The kinetic energy of the generated electrons can be calculated using the following equation:

$$E_k = qV$$

Where E_k is the kinetic energy, q is the charge, and V is the potential difference. When we define q as e, the charge on an electron (1.6021×10^{-19} coulombs), and the

potential difference is in volts, we get a kinetic energy in electron volts, the kinetic energy on an electron when it has accelerated through a potential difference of 1 V. Using this information, the kinetic energy is determined to be 300eV.

The electron current is measured using an ammeter, and can be controlled by varying the current to the filament using the power supply. For this research, currents from 10 μA to 50 μA were used.

3.3.4 EBMIS reaction chamber

The reaction chamber (Figure 5) contains the CsI window, held at 13 K by the cooling system, the filament that acts as electron source and cathode, the anode, and the sample gas inlets.

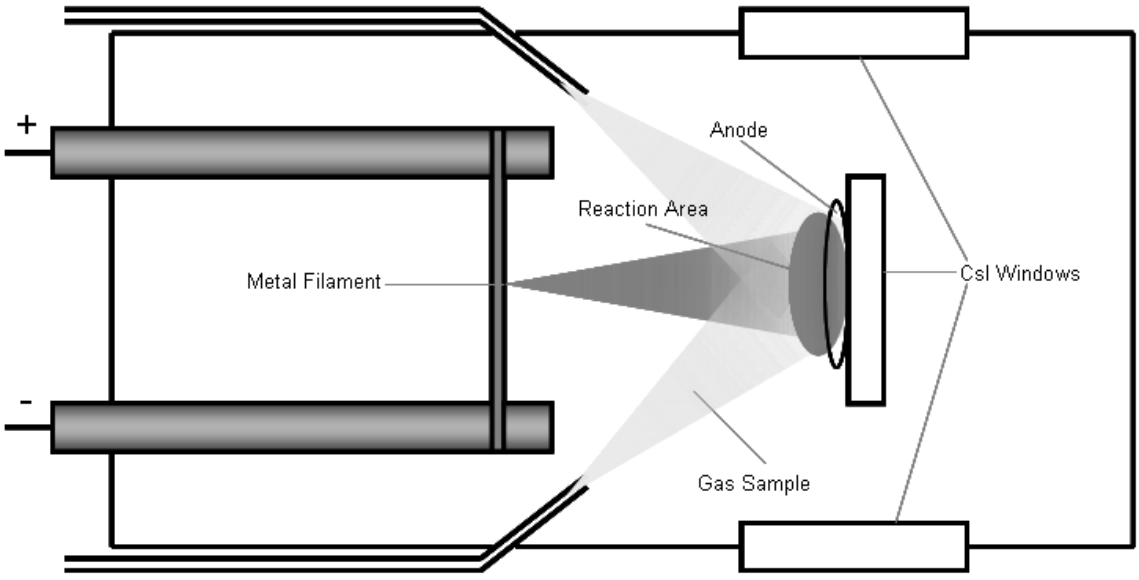

Figure 5. Reaction chamber of the EBMIS apparatus

The sample gas enters the reaction chamber through two inlets, at the top and bottom of the tube holding the filament assembly. The gas flows at the rate determined

using the flow meter during experiment setup. Located on the same face of the reaction chamber is the thoriated tungsten filament. Upon application of a current from the power source, this filament produced electrons which are accelerated towards the anode. This means that the sample gas and the electron current are flowing in the same direction, and their paths intersect as they approach the cold window and anode.

The anode towards which the electrons are accelerated is ring-shaped, and located directly in front of the CsI window (between the window and the electron source. This focuses the electrons on the area directly above where the gas sample will be condensing, creating a reaction area where gas molecules are most likely to collide with electrons.

The CsI cold window can be rotated through 90°, to allow for sample deposition or for an infrared spectrum to be obtained. When the window is oriented as shown in Figure 3, it is perpendicular to the direction of electron current and gas flow, and the gas sample will condense on the window to form a matrix. After sample deposition, the window can be rotated until it is in line with the two windows on the walls of the reaction chamber. In this orientation, it is perpendicular to the beam of the IR spectrometer, and spectra can be obtained.

3.4 EBMIS system experimental protocol

The sample bulb is connected to the apparatus, and with the valve on the bulb kept closed, the rest of the system is evacuated to high-vacuum conditions. Once the system has been pumped out, the compressor is switched on and the system is cooled to 13 K. When the system is adequately cooled, the expander head is rotated so that the CsI window is perpendicular to the IR beam, and a background spectrum is

recorded. All spectra consist of 100 co-added scans, at a resolution of 1 cm^{-1}. Once the background spectrum is complete, the expander head is rotated so that the CsI window is perpendicular to the gas flow direction, and an experiment can begin.

For each gas sample, a reference experiment is performed before any electron bombardment experiments. This produces a spectrum showing only the reagents present in the sample, for comparison with the electron bombardment spectra which will show both reagents and products. To run a reference sample, the system is closed off from the vacuum, and the sample bulb is opened. The mass flow controller is set with the desired flow rate, and then zeroed. The mass flow controller is switched on, to allow gas to flow into the rest of the apparatus, and simultaneously a timer is started for the desired experiment length. Experimental conditions for this research were a flow rate of 1.00 cm^3/min and a deposition time of 4 hours, unless otherwise indicated. Upon completion of the experiment, the mass flow controller is switched off, to stop the flow of gas, and the sample bulb is closed. The CsI window is then rotated into the IR beam, and a reference spectrum is collected. When the spectrum collection is complete, the compressor is turned off, and the system is opened to the pumps to warm up so that the condensed matrix sublimes and is removed. Following this, the system is pumped until it re-attains high vacuum.

To perform an electron bombardment experiment, the apparatus is cooled as before, and a background spectrum of the clean and cold CsI window is recorded. Once the gas bulb is opened and the mass flow controller is set and zeroed, the anode and cathode are biased to a 300V potential difference. The mass flow controller is switched on, and the timer started. Immediately following this, the power supply for the filament

current is turned on, and the current is adjusted to the desired value, displayed on the ammeter (generally from 10 to 50 μA in this research). Just prior to the end of the experiment (in the last ~30 seconds), the current is turned down and the power supply switched off. When the experiment ends, the mass flow controller is switched off and the sample bulb is closed. The CsI window is again rotated into the IR beam, and the electron bombardment spectrum is collected. The apparatus is then warmed and evacuated as before, and is ready for future experiments.

Chapter 4

Results

4.0 Overview

This chapter presents the experimental results of the investigation into the reactivity of toluene under conditions relevant to atmospheric chemistry, using an electron bombardment matrix isolation system. The first experiments performed were done to determine how best to produce benzyl radicals in the system. The initial plan was to produce hydroxyl radicals from water, and then use the reaction between the hydroxyl radicals and toluene to produce benzyl radicals. It will be demonstrated here that this was unsuccessful, such that the focus was shifted to the production of benzyl radicals by electron bombardment of toluene. Experiments were then performed to investigate the reaction between oxygen and benzyl radicals, in an attempt to produce and observe the highly-reactive benzylperoxy radical. All reaction product identifications in this section were made using information from previous work in this lab, or from the literature.

All gas mixtures were prepared using the gas handling system described above. All experiments were performed using the EBMIS apparatus described above, with a flow rate of 1 standard cubic centimeter per minute (SCCM), and at a temperature of 13 K, unless otherwise stated.

4.1 Hydroxyl radical experiments

This series of experiments was performed to determine the best conditions in the EBMIS system for the production of hydroxyl radicals. Gaseous mixtures of water in argon were prepared, and reference and electron bombardment spectra were obtained. The

concentration of water in the samples and the electron current used in the experiments were varied in an attempt to optimize hydroxyl radical production

4.1.1 1:800 H_2O:Ar

A 1:800 gas mixture of water in argon was prepared and used for the initial set of experiments. A reference deposition was run for four hours, without electron bombardment. A spectrum was taken at two hours, and after four hours at the end of the deposition. This procedure was repeated for an electron bombardment (EB) experiment, using an ionizing electron current of 50 μA. The reference spectra contained only peaks corresponding to water[74,75], as well as small peaks corresponding to common matrix impurities, such as CO[76] and CO_2[77]**.** The observed infrared absorptions of water, CO, and CO_2 are given in Table 1, below.

After electron bombardment, a significant decrease was seen in the water absorptions, along with an increase in several contaminant peaks, including CO and CO_2. A new peak was observed at 903 cm^{-1}, which is known to be caused by Ar_2H^+, a product observed in all electron bombardment experiments using this apparatus[78]. Additionally, another new absorption was seen at 3548 cm^{-1}, which is assigned to the hydroxyl radical, based on work by Cheng, et al.[47]. In the reference spectra, all absorptions increased in size from the 2-hour to the 4-hour spectrum. This was expected, as more of the gas sample will be deposited onto the cold window with increased deposition time. The same trend was observed in the EB spectra – all product absorptions increased with increased deposition time and all reactant absorptions, though decreased with respect to the reference, increased proportionally as well.

Table 1. Observed absorptions of CO_2, CO, and H_2O, and their assignments

Observed Absorption (cm^{-1})	Assignment
	CO_2[77]
662.0	v_2^h
663.5	v_2^1
2339.3	v_3^1
2345.2	v_3^h
	CO[76]
2138.4	v_a
2149.0	v_m
	H_2O[74,75]
1573.0	
1589.7	non-rotating monomer
1592.9	non-rot. monomer, or dimer
1608.1	dimer, or v_2 bend
1623.9	polymer, or v_2 bend
1636.7	
1661.3	
3574.4	dimer
3706.4	v_1 symmetrical stretch
3711.2	dimer
3756.3	v_3 anti-sym. stretch
3776.9	v_3 anti-sym. stretch

A portion of the reference and EB spectra is shown below, in Figure 6, demonstrating the destruction of water that occurs with electron bombardment. Figure 7 shows the

peak at 3548 cm^{-1}, corresponding to the hydroxyl radical – its absence in the reference spectra and appearance with electron bombardment is evident.

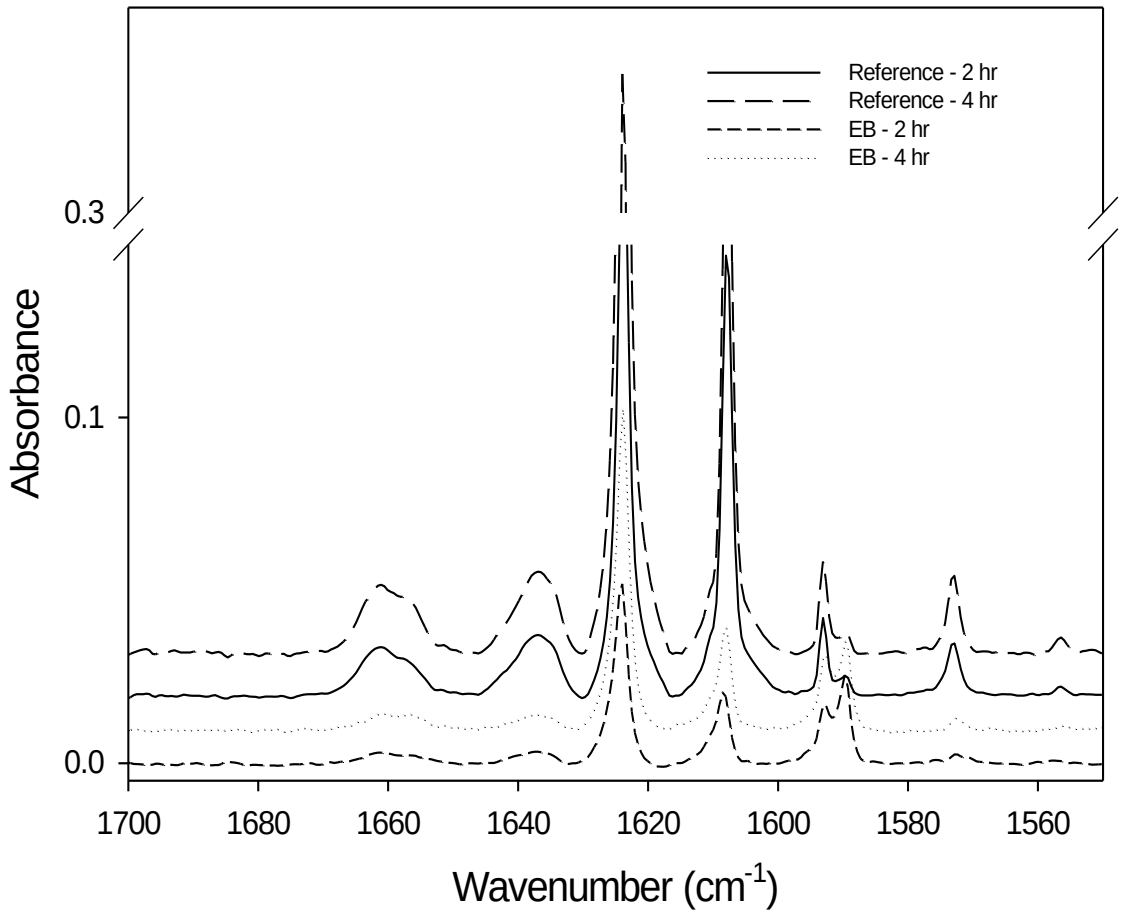

Figure 6. 1700 - 1550 cm^{-1} water region of reference and 50 µA electron bombardment spectra of 1:800 H_2O:Ar gas sample, demonstrating destruction of water by electron bombardment, shown by decrease in peaks around 1608 and 1624 cm^{-1}

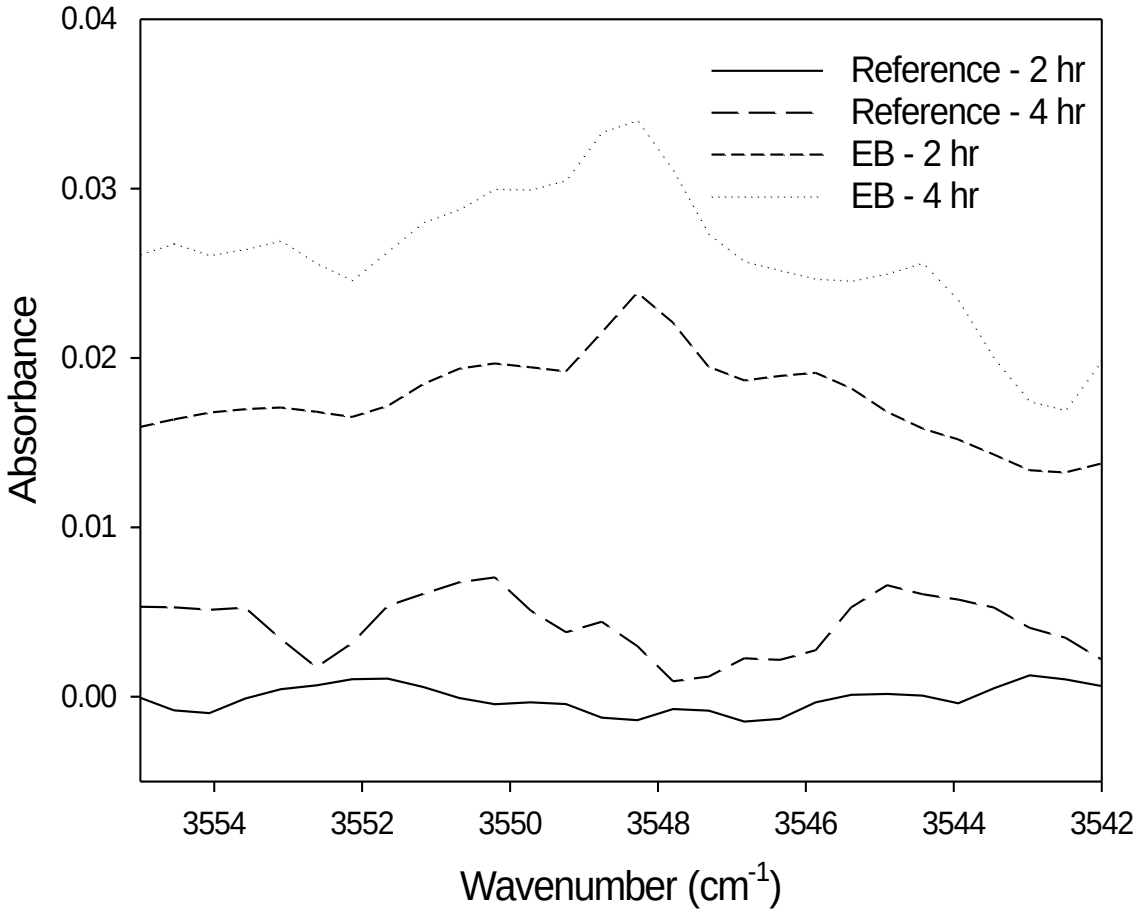

Figure 7. 3540 - 3555 cm^{-1} region of 1:800 H_2O:Ar reference and EB spectra, showing hydroxyl radical peak at 3548 cm^{-1} appearing after electron bombardment of water-argon mixture

4.1.2 1:1600 H_2O:Ar

1:800 H_2O:Ar is a highly concentrated sample, compared to the concentrations generally used in this lab. The next set of experiments involved lowering the concentration of water in the sample to observe the effect on the hydroxyl radical production. A gas sample containing 1:1600 H_2O in argon was prepared for this set of

experiments. All experiments had a deposition time of 4 hours, and the electron current was varied from 0 (reference experiment) to 50 μA. The peaks corresponding to water and hydroxyl radicals were measured in all spectra to track the changes in water destruction and hydroxyl radical production with increasing electron current. Figure 8 shows a section of the spectra, demonstrating the decrease in water absorption with increasing electron current. Figure 9 demonstrates the reverse trend, for the hydroxyl radical absorption.

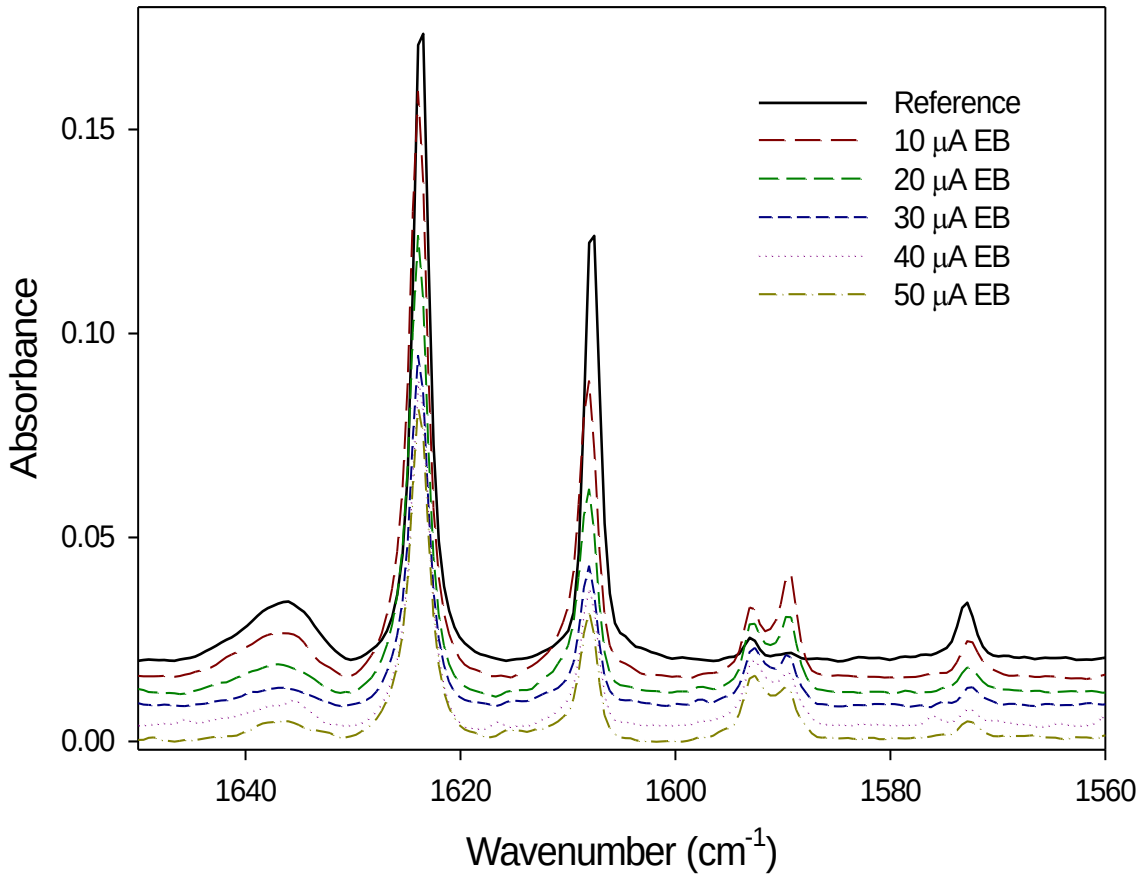

Figure 8. 1650 - 1560 cm^{-1} region of 1:1600 H_2O:Ar reference and electron bombardment spectra, showing that destruction of water increases with electron current

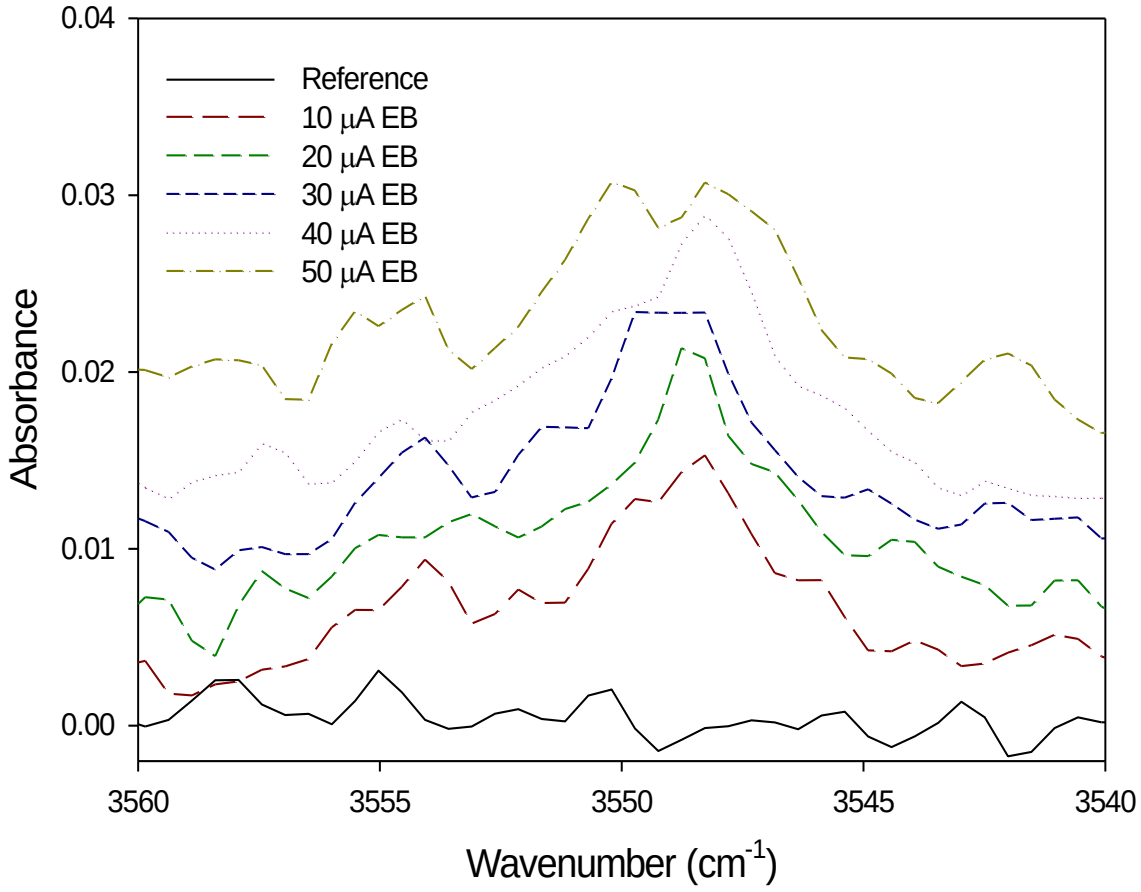

Figure 9. 3560 - 3540 cm^{-1} region of 1:1600 H_2O:Ar reference and EB spectra, hydroxyl radical peak is present at 3548 cm^{-1} in EB spectra, demonstrating creation of hydroxyl radicals after electron bombardment

The peak areas of the water absorptions in all spectra were integrated, and the relative percent destruction was calculated. This value corresponds to the percentage of the water initially present in the sample that is destroyed by the electron current, and is calculated as follows:

$$relative\%destruction = \frac{(area_{REF} - area_{EB})}{area_{REF}} \times 100\%$$

Where $area_{REF}$ is the integrated area under the water absorption in the reference spectrum, and $area_{EB}$ is the integrated area under the water absorption in the electron bombardment spectrum. This value was calculated for all electron bombardment experiments performed, and was plotted against the electron current, as shown in Figure 10.

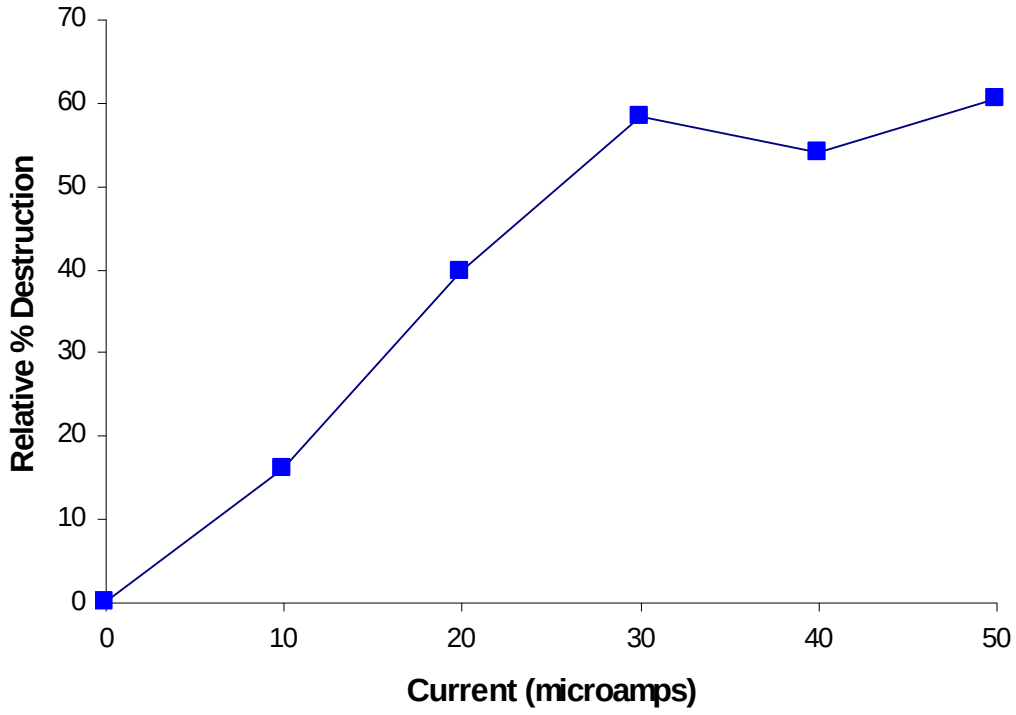

Figure 10. Relative percent destruction of water with respect to electron current, for 1:1600 H_2O:Ar gas sample

The areas under the hydroxyl radical absorptions were also integrated, and normalized relative to the largest area. These values were then plotted against the electron current as shown in Figure 11.

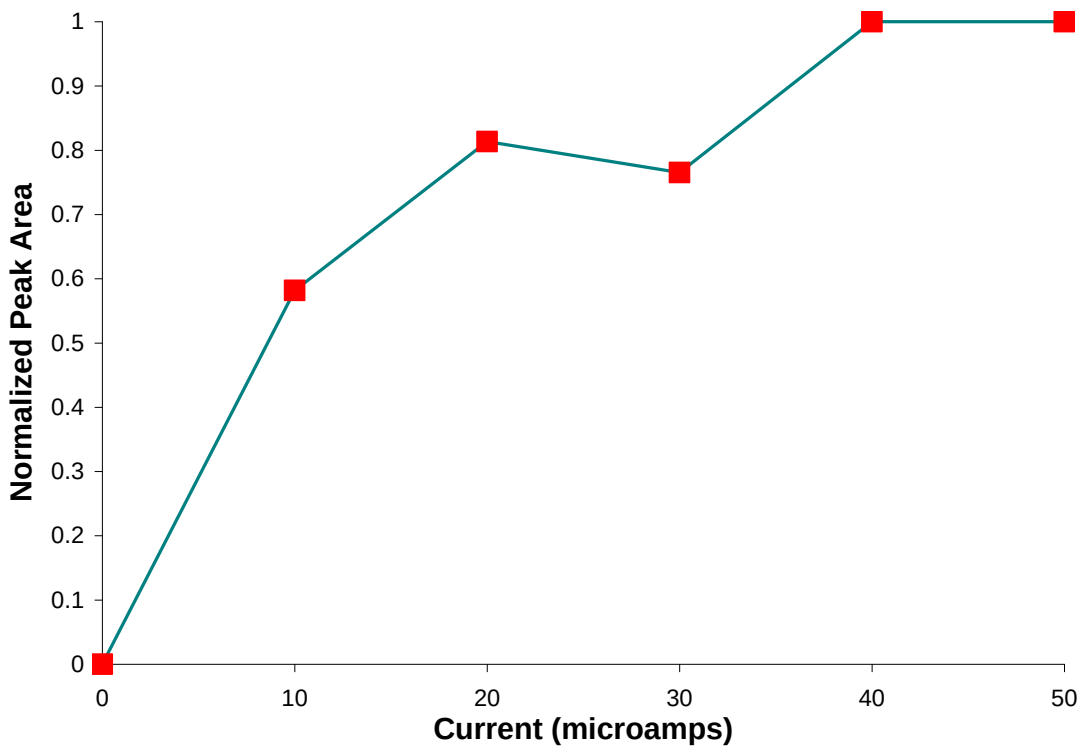

Figure 11. Normalized peak area of hydroxyl radical with respect to electron current, for 1:1600 H_2O:Ar gas sample

From Figure 10 and Figure 11, it was determined that both hydroxyl radical production and water destruction increase with electron current up to around 30 μA, at which point they plateau. This information was useful in the selection of conditions for future experiments.

No significant change in hydroxyl radical production was observed when halving the water concentration from 1:800 to 1:1600 in argon. The spectra shown in Figure 12 are from experiments that used two different electron currents – 50 μA for the 1:800 sample, and 20 μA for the 1:1600 sample. Based on the plot shown in Figure 11, the hydroxyl peak produced by EB of a 1:1600 water sample is slightly larger with a current of 50 μA,

but not significantly larger. Figure 12 shows that even at a lower water concentration and lower electron current, the magnitude of the hydroxyl radical absorption remains quite consistent, and a significant change in hydroxyl radical production is not occurring. The next set of experiments halved the water concentration again, to 1:3200 H_2O:Ar, to determine the threshold for observable hydroxyl radical production.

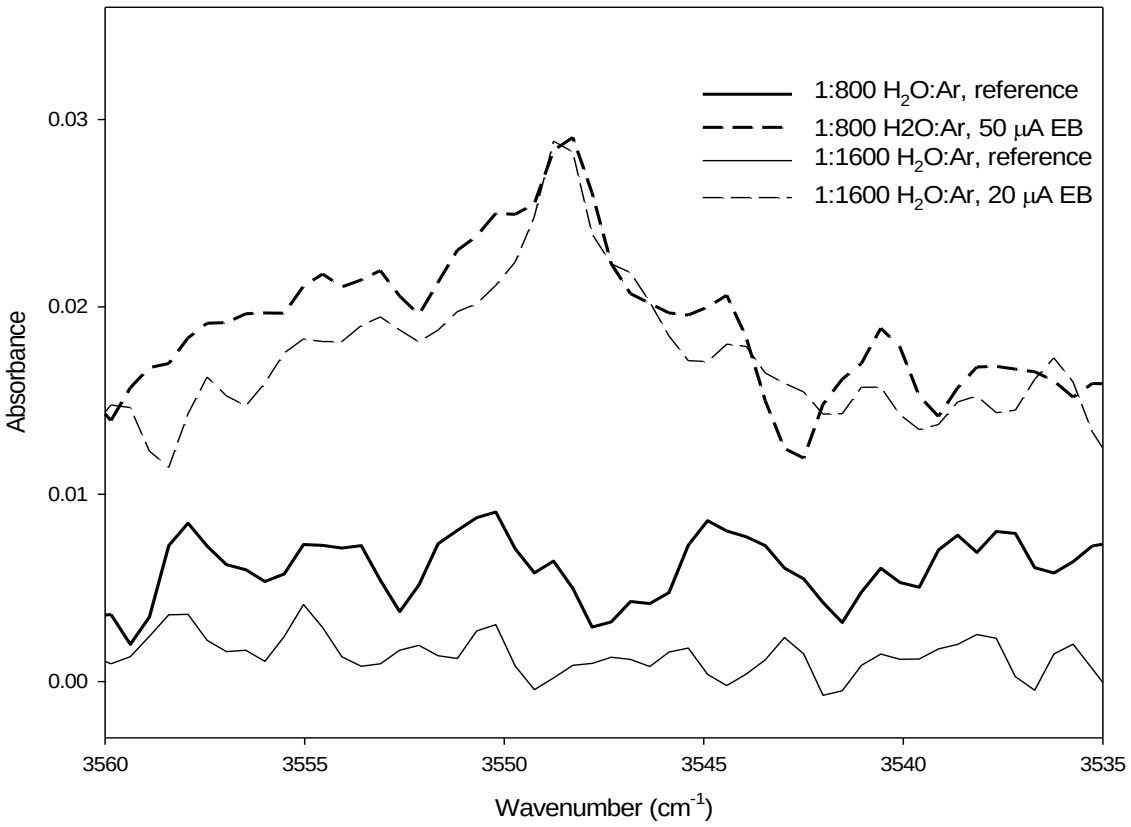

Figure 12. 3548 cm^{-1} hydroxyl radical peak in the 1:800 and 1:1600 H_2O:Ar reference and EB spectra, showing that hydroxyl radical is created with electron bombardment in similar amounts despite changing water concentration

4.1.3 1:3200 H_2O:Ar

A gas sample of 1:3200 H_2O in argon was prepared, to compare to the previous two samples. A reference experiment was performed, along with EB experiments with electron currents of 10, 20, 30, and 50 μA. When the water absorptions in these spectra were compared to those seen in the 1:1600 spectra, they were seen to be the same size. This is shown in Figure 13, the peaks are nearly identical which was unexpected, as the water concentration had been halved.

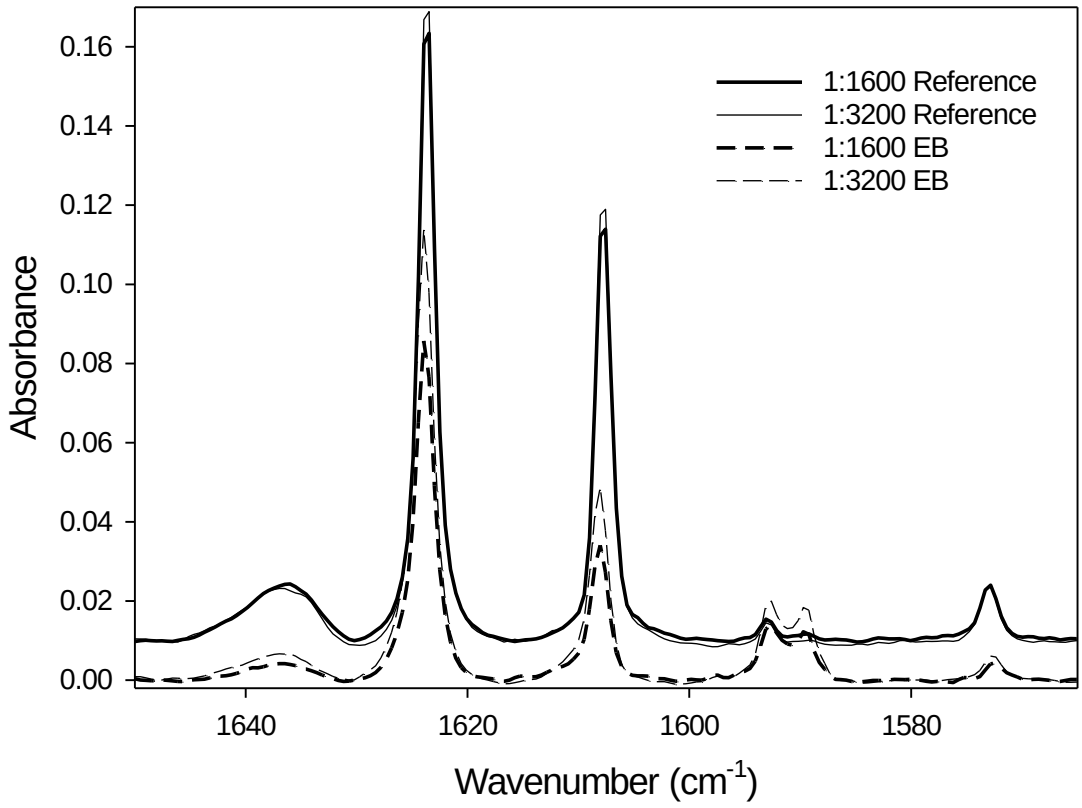

Figure 13. Reference and 30 μA EB spectra of 1:1600 & 1:3200 H_2O:Ar gas mixtures, showing slight increase in water absorptions with doubled water concentration

The hydroxyl radical absorption was still observed at this concentration. The peak size is not smaller than the peak seen in the 1:1600 experiments, as would be expected. These observations led to the possibility of a leak of atmospheric air into the apparatus. The next set of experiments used a sample of pure argon gas, to test this hypothesis.

4.1.4 Pure argon

The sample bulb used in this set of experiments was filled with pure argon gas, and no additional water. A reference experiment and two EB experiments, at 25 and 50 μA electron current, were performed.

The presence of a leak was confirmed by the presence of water absorptions. When these are compared to the water absorptions present in the 1:1600 and 1:3200 H_2O:Ar experiments, as in Figure 14, they are the same size. This indicates that the amount of water being introduced into the apparatus by this leak is greater than the amount in a 1:1600 H_2O:Ar sample.

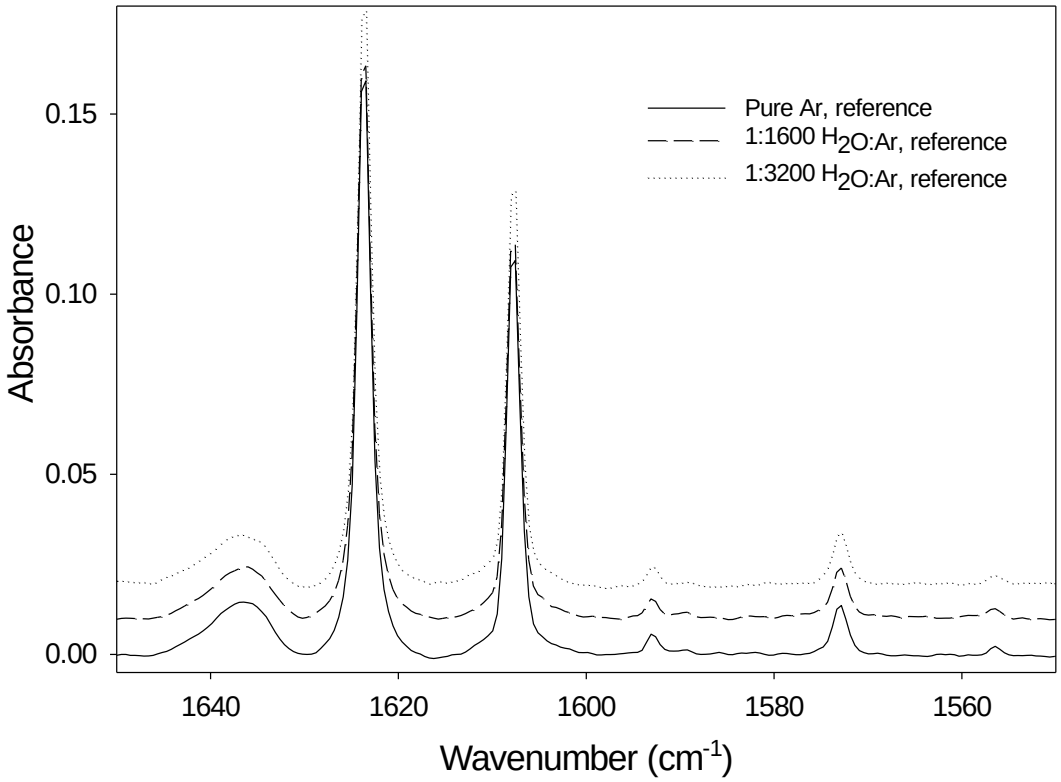

Figure 14. Comparison of water absorptions in reference spectra of pure argon, 1:1600 H_2O:Ar, and 1:3200 H_2O:Ar, demonstrating the existence of a water leak as peaks in the pure argon spectrum are the same size as those in the spectra of the water-argon mixtures

4.1.5 Hydroxyl radical production

The leak in the apparatus means that water does not need to be included in prepared gas samples for it to be present in the reaction chamber of the EBMIS system, and take place in the reactions occurring there. The amount of hydroxyl radical produced by the water present in the system was not very large, however. It remained relatively constant even when the water concentration was increased from 1:1600 to 1:800 in argon. This increase in concentration resulted in larger water absorptions, indicating that more water

was in fact present, but did not result in an increase in the hydroxyl radical absorptions, as shown in Figure 15.

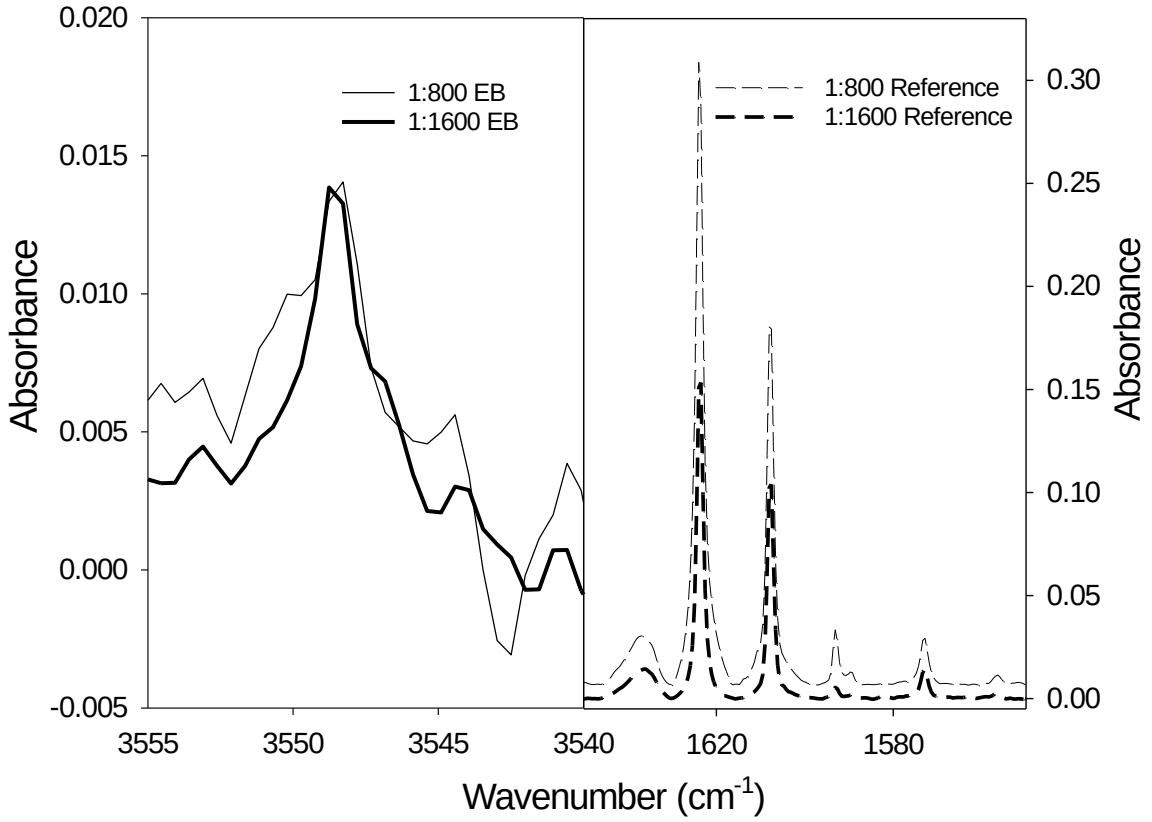

Figure 15. Comparison of water (1550 - 1650 cm^{-1}) and hydroxyl radical (3548 cm^{-1}) peaks between 1:800 and 1:1600 H_2O:Ar, showing that increasing water concentration increased the water peaks, but not the hydroxyl radical peak

The fact that the hydroxyl radical production appears to plateau at such a low amount makes it less useful as a reactant in the production of benzyl radicals. The next sets of experiments investigated the production of benzyl radicals directly from electron bombardment of toluene gas, as it was decided that the quantity of hydroxyl radicals produced was not enough to produce adequate amounts of benzyl radical.

4.2 Oxygen experiments

A brief series of experiments were performed using a mixture of 1:1600 oxygen in argon. The purpose of this was to record an electron bombardment spectrum of oxygen, and identify any major products. This knowledge would then be useful in identifying products from later experiments using a mixture of oxygen and toluene. We found that primarily ozone and hydroperoxy radicals were produced.

4.2.1 1:1600 O_2:Ar

A gas sample made up of 1:1600 oxygen in toluene was prepared, and four hour reference and electron bombardment experiments were run. The electron bombardment experiment used an electron current of 50 μA. A spectrum was obtained at the end of each experiment.

The electron bombardment spectrum was compared to the reference spectrum, and also to the EB spectrum of the pure argon sample acquired previously. Peaks that appeared with oxygen that were not present previously, and existing peaks that increased in size with the presence of oxygen were assumed to be the products of electron bombardment of oxygen. Due to the leak present in the system that allows room air in to the reaction chamber, small amounts of oxygen EB products are expected, even in spectra from gas samples that do not contain oxygen. This is why we do not rule out peaks that are present without oxygen and increase with it as possible oxygen EB products.

An existing pair of peaks around 1040 cm^{-1} was seen to increase in size. These were identified as being ozone absorptions[79], along with peaks at 1104 cm^{-1} and 704 cm^{-1}. The 1040 cm^{-1} pair of ozone peaks observed in this experiment are shown in Figure 16, below.

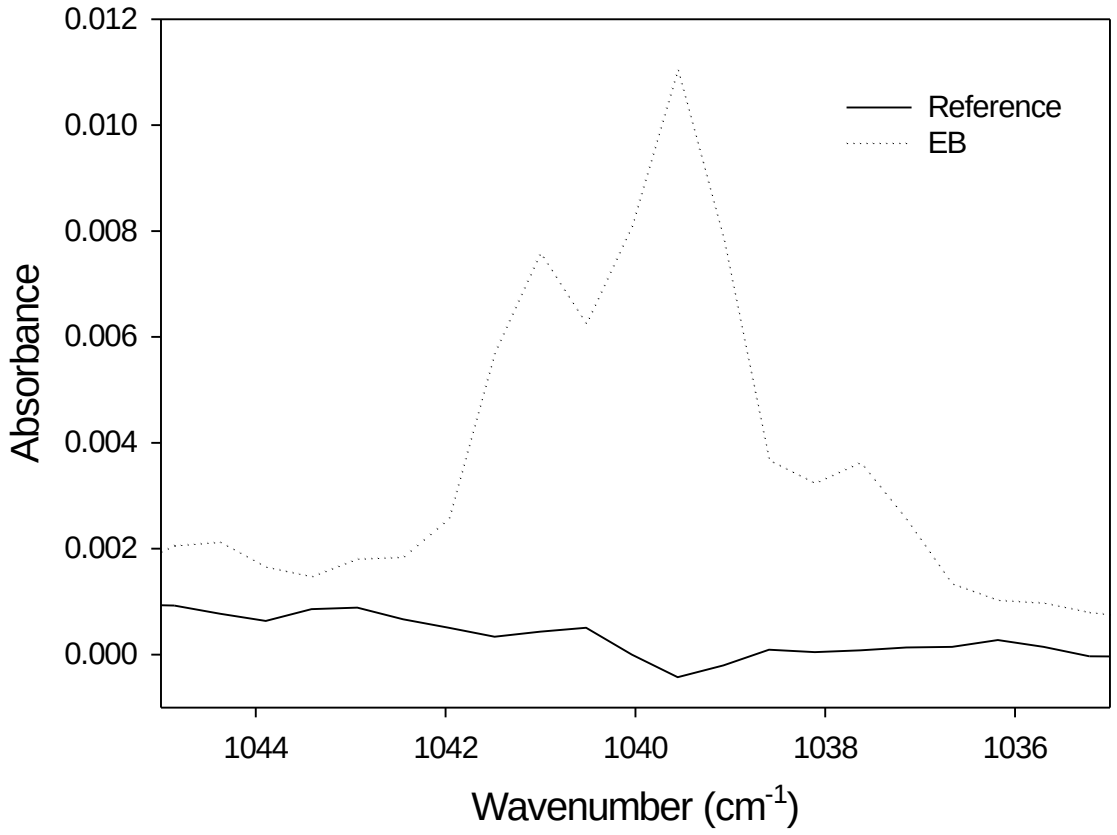

Figure 16. Ozone peaks visible in 1:1600 O_2:Ar electron bombardment spectrum, indicating creation of ozone after electron bombardment of oxygen-argon mixtures

Figure 17 shows peaks that were observed at 1101 and 1388 cm^{-1} in the electron bombardment spectrum. These were identified as being absorptions of the hydroperoxy radical ($HO_2^{\bullet}$) using work published by Milligan and Jacox[80,81].

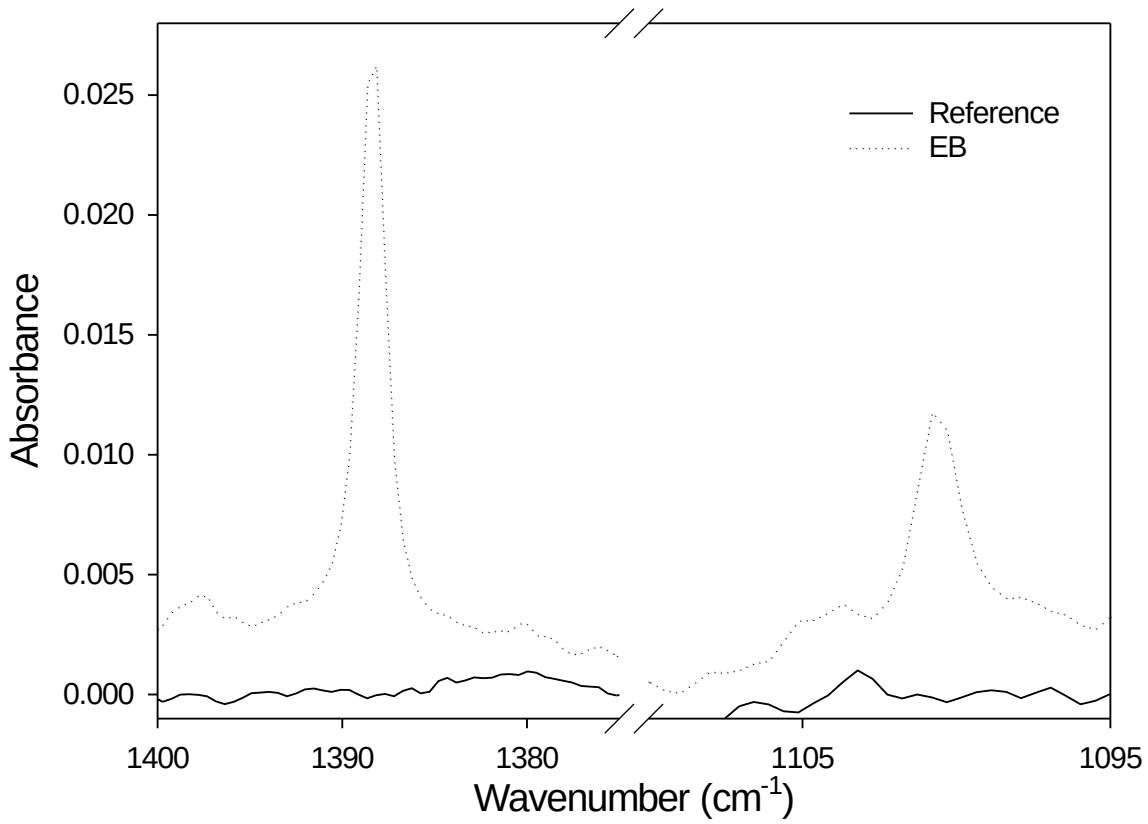

Figure 17. Hydroperoxy radical peaks present at 1101 & 1388 cm^{-1} in 1:1600 O_2:Ar electron bombardment spectrum, indicating production of hydroperoxy radical after electron bombardment of oxygen-argon mixtures

Hydroperoxy radicals produce a third absorption, at 3412 cm^{-1}. This peak is the weakest of the three absorptions, and is in a region of the spectrum where there is a significant amount of noise. In later experiments with increased oxygen concentration, this peak increases in magnitude relative to the surrounding noise, confirming its identification.

Ozone and hydroperoxy radicals were the two main products of electron bombardment of oxygen that could be observed in spectra obtained with the EBMIS system. These products are expected to appear in EB spectra of oxygen and toluene

mixtures, and having identified them now allows them to be ruled out as possible products of oxygen/toluene reactions.

4.3 Initial toluene experiments

A series of experiments was performed using gas mixtures of toluene in argon, the purpose being to confirm that the benzyl radical could be produced by electron bombardment of toluene, and to optimize its production yield. Electron current and gas flow rate were both varied during separate sets of experiments, to determine the optimal conditions for benzyl radical production.

4.3.1 Initial tests – 1:1600 Toluene:Ar

This initial set of experiments was performed simply to determine whether the benzyl radical could be observed at all in the EBMIS system. A 1:1600 gas mixture of toluene in argon was prepared, and reference and electron bombardment experiments were run. Each experiment had a deposition time of four hours, and the electron bombardment experiment used an electron current of 50 μA. 1:1600 is a medium concentration of toluene in argon, this concentration is frequently used in gas samples in the EBMIS system in this lab.

The spectrum obtained from the reference experiment allowed us to identify peaks corresponding to toluene absorptions. This was done by comparing the spectrum to the reference spectrum of pure argon. Any peaks not present in the pure argon spectrum were identified as toluene peaks, those that were also present in the pure argon spectrum included peaks corresponding to water, carbon dioxide, and other contaminants. Peaks corresponding to toluene absorptions that did not have any overlap with peaks from other compounds, and that were located in regions of the

spectrum without excessive amounts of background noise were selected for analysis. These peaks were used for all analysis of toluene behaviour in all experiment sets. Figure 18, below, shows some of the major absorptions used for analysis – the absence of the peaks in the argon spectrum (also shown) confirms that they are caused by toluene.

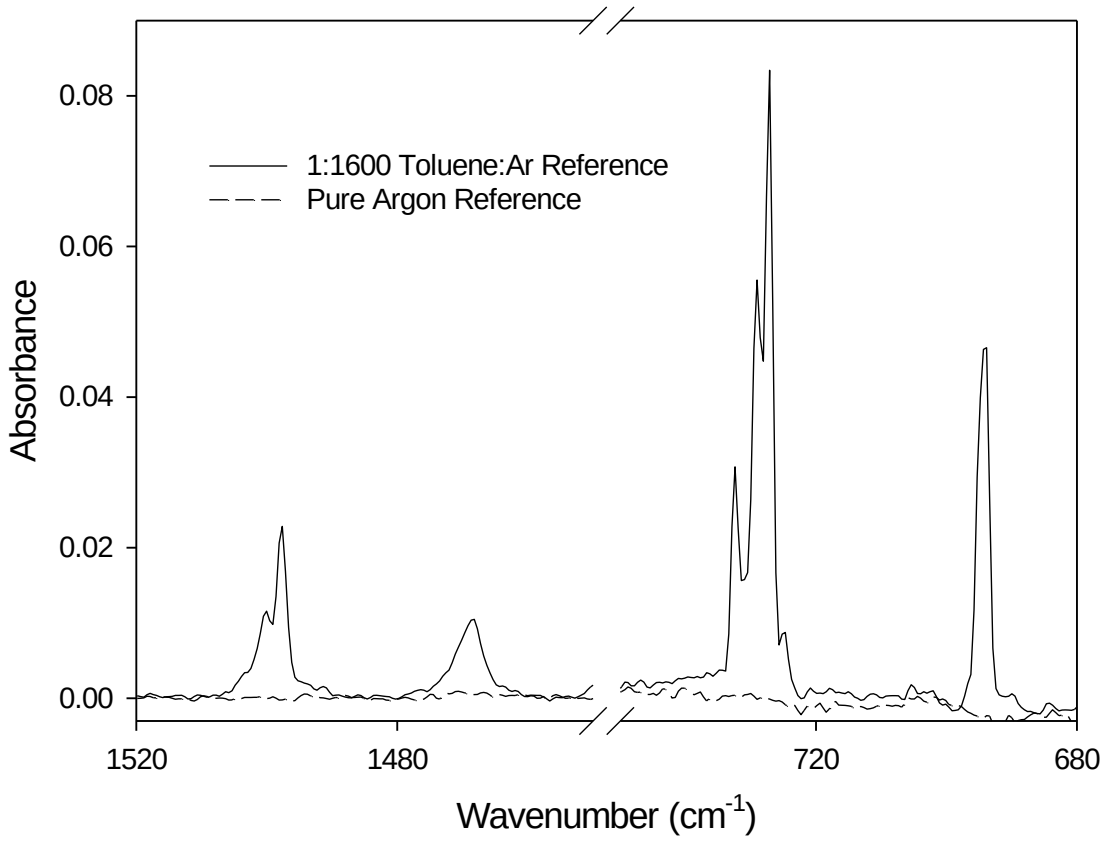

Figure 18. 1:1600 Toluene:Ar reference spectrum, showing toluene absorptions that will be used for analysis, identification of the peaks is confirmed by their absence in the pure argon reference spectrum

The 50 μA electron bombardment experiment was performed, and a spectrum was obtained. Peaks in this spectrum were identified using the analysis of the EB spectra

obtained from the previous work with pure argon, water in argon, and oxygen in argon. This allowed us to determine which peaks were present only in the toluene EB spectrum, and were therefore products of electron bombardment of toluene.

The infrared spectrum of the benzyl radical in an argon matrix is known, from work performed by Baskir, et al.[60] The EB spectrum was compared to the least of expected benzyl radical absorptions, and many were identified. The Baskir paper does not specify the concentration of benzyl radical or its precursors, only that they were frozen onto a CsI window with "excess" argon. Many of the absorptions of the benzyl radical present as only weak or medium peaks, with only two strong peaks present in the region visible in our spectra. The two strong benzyl radical peaks are visible at 667 and 762 cm^{-1}, and are shown in Figure 19, below – they clearly appear with electron bombardment of the toluene sample.

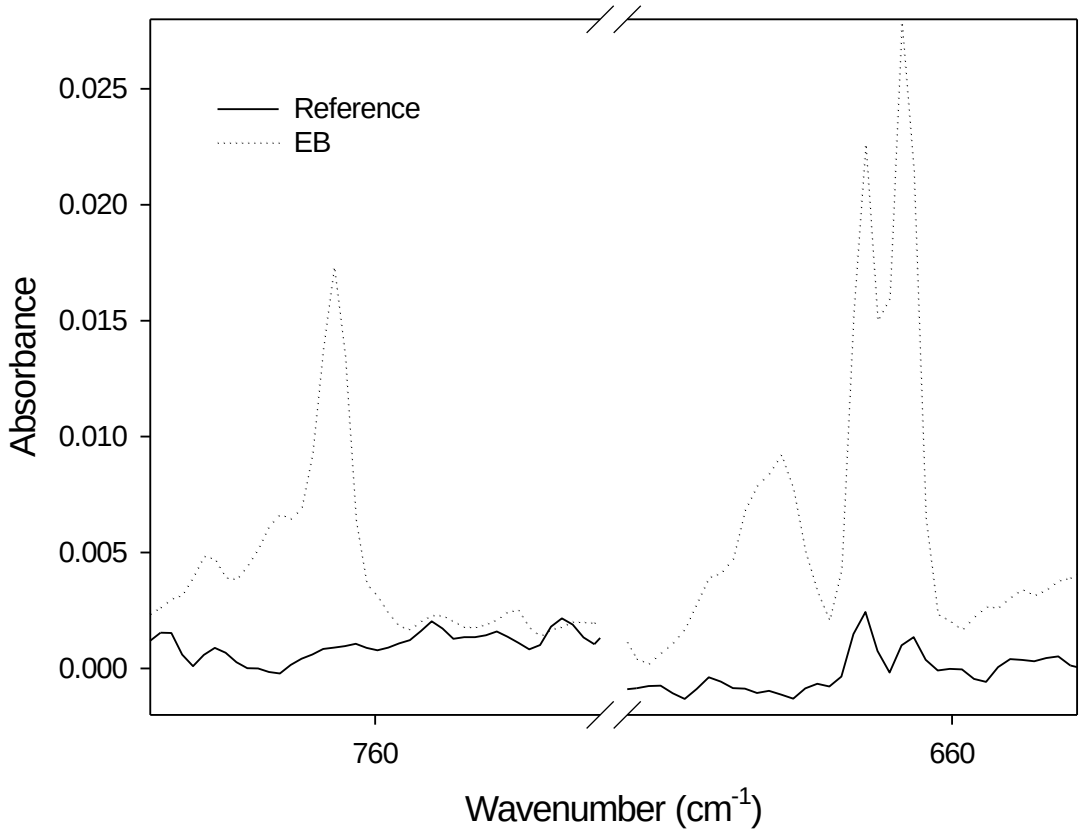

Figure 19. Appearance of peaks at 667 and 762 cm^{-1} in electron bombardment spectrum of 1:1600 toluene:Ar mixture, indicating creation of benzyl radicals after electron bombardment

These are the peaks that are used for any analysis of benzyl radical behaviour. The other benzyl radical peaks can be identified in the EB spectrum but all are too weak, or have too significant an overlap with other peaks in the spectrum, to be used for analysis. Another major observable feature of the electron bombardment spectrum is the destruction of toluene. The peaks corresponding to toluene have decreased in magnitude when compared to those present in the reference spectrum. This is expected, as destroying toluene via electron bombardment to produce benzyl radicals is

the main goal of these experiments. The decrease in toluene peak size from reference to electron bombardment is shown below, in Figure 20.

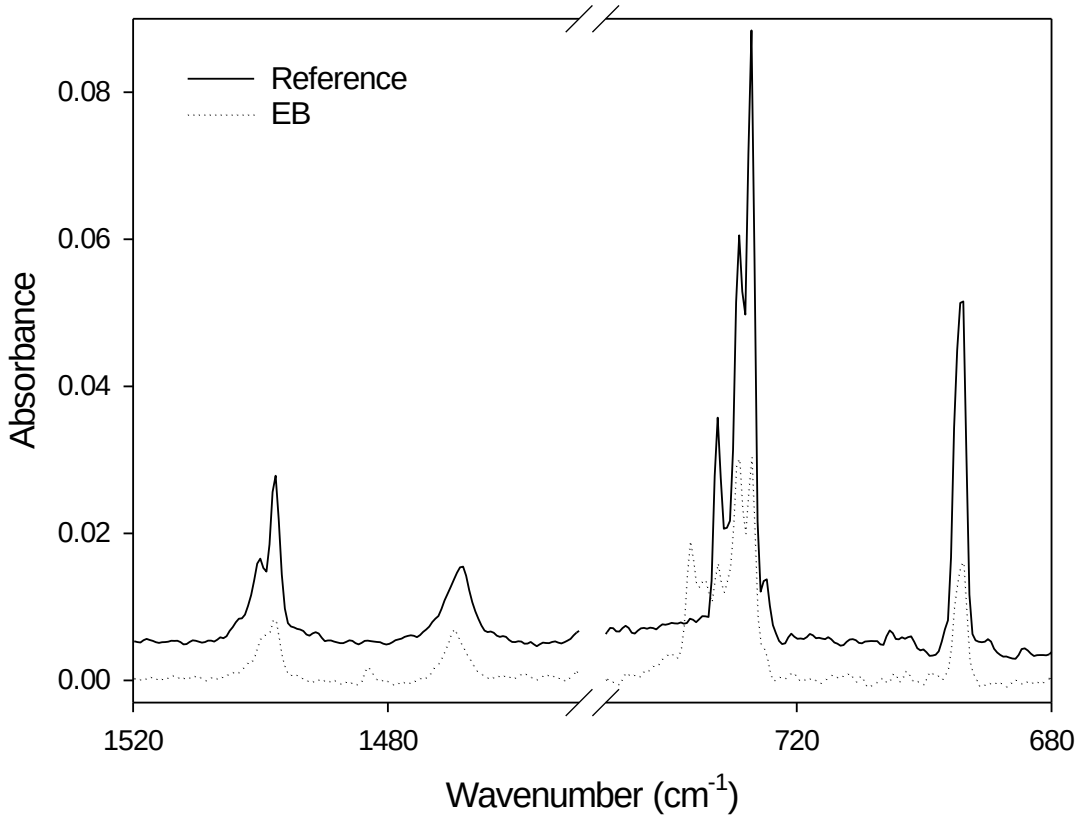

Figure 20. Decreased peak size in 1:1600 toluene:Ar electron bombardment spectrum compared to reference spectrum indicates destruction of toluene with electron bombardment

These experiments confirmed that it is possible to produce benzyl radicals from electron bombardment of toluene in the EBMIS system, and that we can observe them in infrared spectra. The next set of experiments used a new, larger gas sample, still with a concentration of 1:1600 toluene:Ar, to observe the results of varying the electron bombardment current on toluene destruction and benzyl radical production.

4.3.2 Varied electron current – 1:1600 Toluene:Ar

Once it was confirmed that benzyl radicals could be produced and observed in the EBMIS system, the next experiments performed were done to determine the best conditions for optimal benzyl radical production. This set of experiments used a 1:1600 toluene:Ar gas sample and varied the electron current between EB experiments to observe the effect that this had on the destruction of toluene and production of benzyl radical. A reference experiment was performed, along with a series of five electron bombardment experiments – at electron currents of 10, 20, 30, 40, and 50 μA. Each experiment had a deposition time of four hours.

When comparing the toluene and benzyl radical peak sizes between the different EB spectra, it is clear that both absorptions vary with electron current. Figure 21 shows some of the clearer toluene peaks, and the decrease in peak size with increasing electron current is clearly visible.

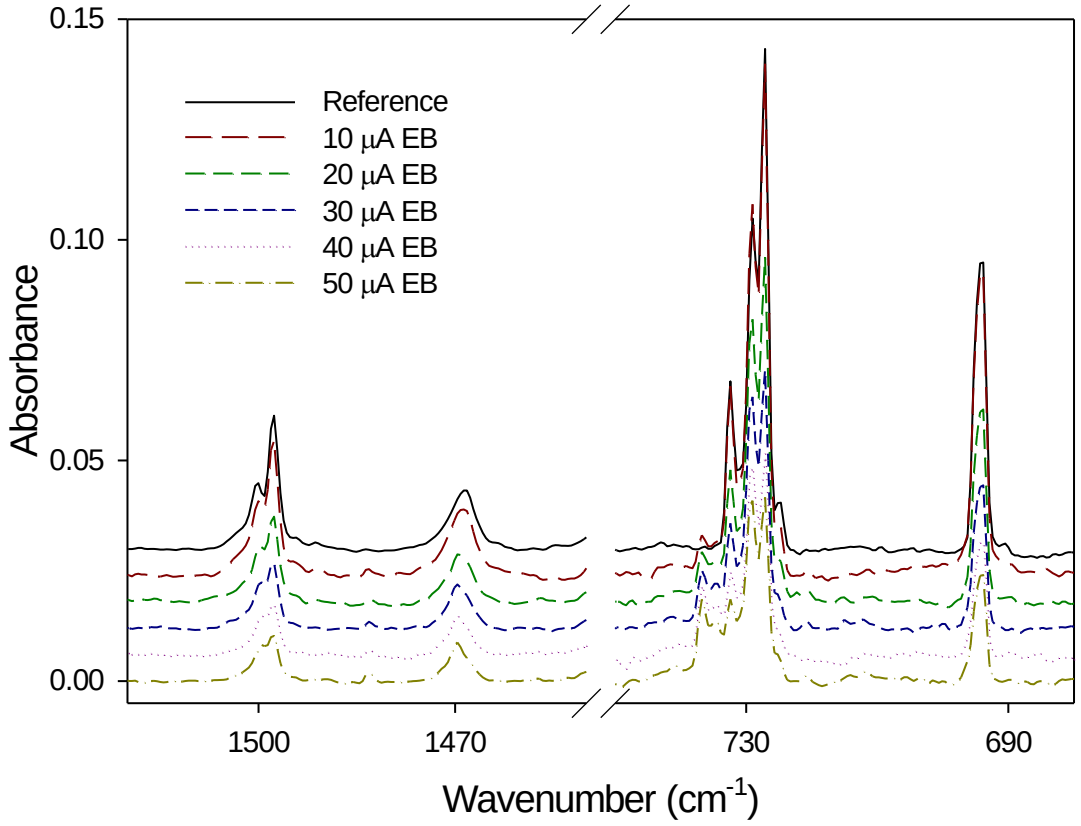

Figure 21. Decreasing toluene peak size with increased electron current indicates that toluene destruction increases with electron current

In order to better see the change in the toluene absorptions that occurred with varying electron current and verify the trend occurring, the four toluene peaks at 694, 727, 1081, and 1497 cm^{-1} were integrated, and the relative percent destruction was calculated as described previously. This calculation was performed on each selected toluene peak from each electron bombardment spectrum. These values show the percentage of the toluene that was initially present in the reference experiment that has been destroyed in each electron bombardment experiment. These numbers were plotted against the electron current, to illustrate the increase in destruction; this is shown in Figure 22.

From this plot, it is clear that toluene destruction increases with electron current in a fairly linear manner, and that it may show evidence of plateauing.

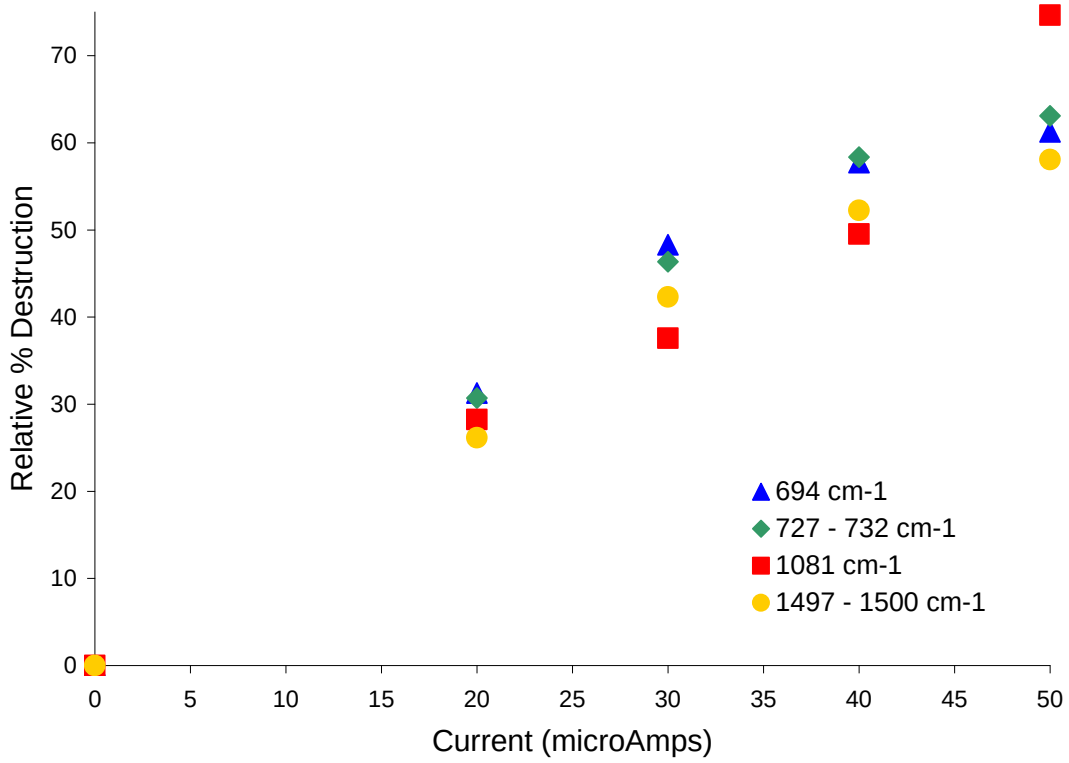

Figure 22. Relative percent destruction of toluene with respect to electron current

The benzyl radical absorptions used for analysis are shown in Figure 23, below. Similar to the toluene absorptions, it is clear that the peak magnitudes are changing with changing electron bombardment current, however in this case the peaks increase in size with increasing electron current.

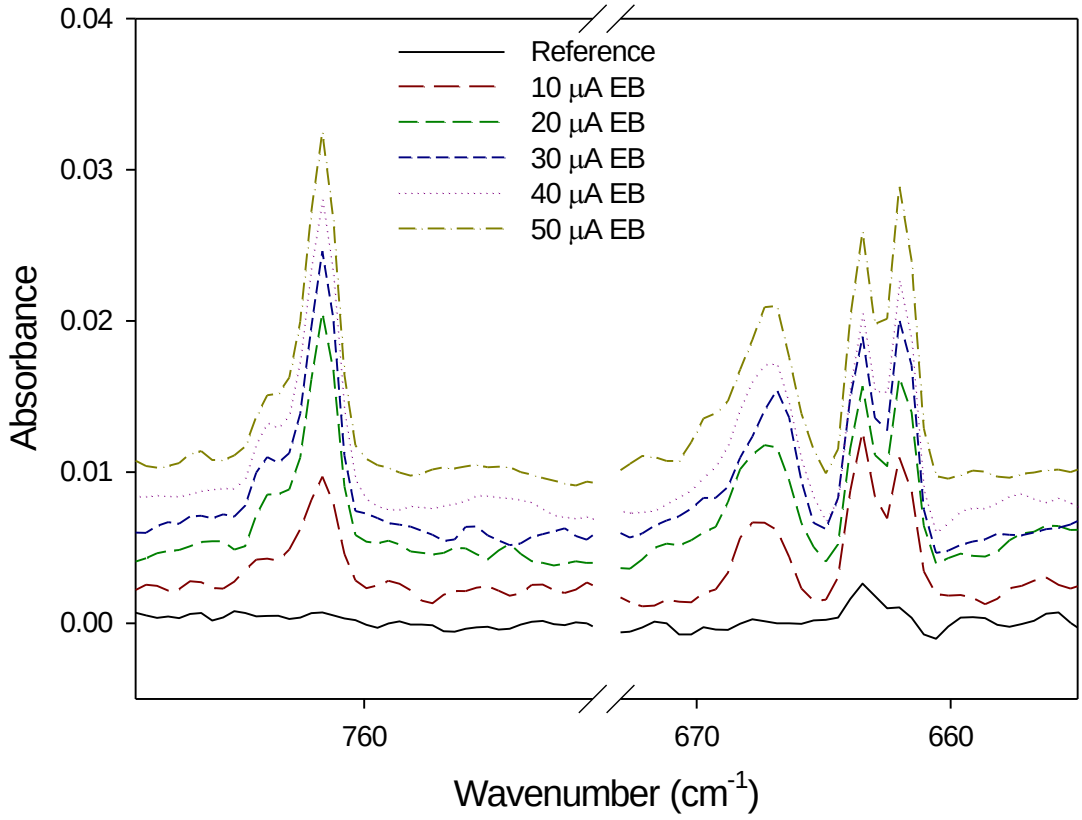

Figure 23. Benzyl radical absorption (762 & 667 cm^{-1}) in electron bombardment and reference spectra of 1:1600 toluene:Ar gas mixture demonstrating increased production of benzyl radical with increased electron current

Again, analysis was performed to better visualize and verify this trend. The two clearest benzyl radical peaks were integrated in each electron bombardment spectrum. The values of each peak were normalized against the values of the same peak from each different electron current – each peak integration was divided by the largest integration value for that peak. This allows for the relative size of the peak to be compared across EB current values more easily. These values were then plotted against the electron current so that the relationship between electron current and benzyl radical production could be observed. This plot is shown in Figure 24, and it demonstrates that the benzyl

radical production increases with the electron current and, like the toluene destruction, may show evidence of plateauing above 40 µA

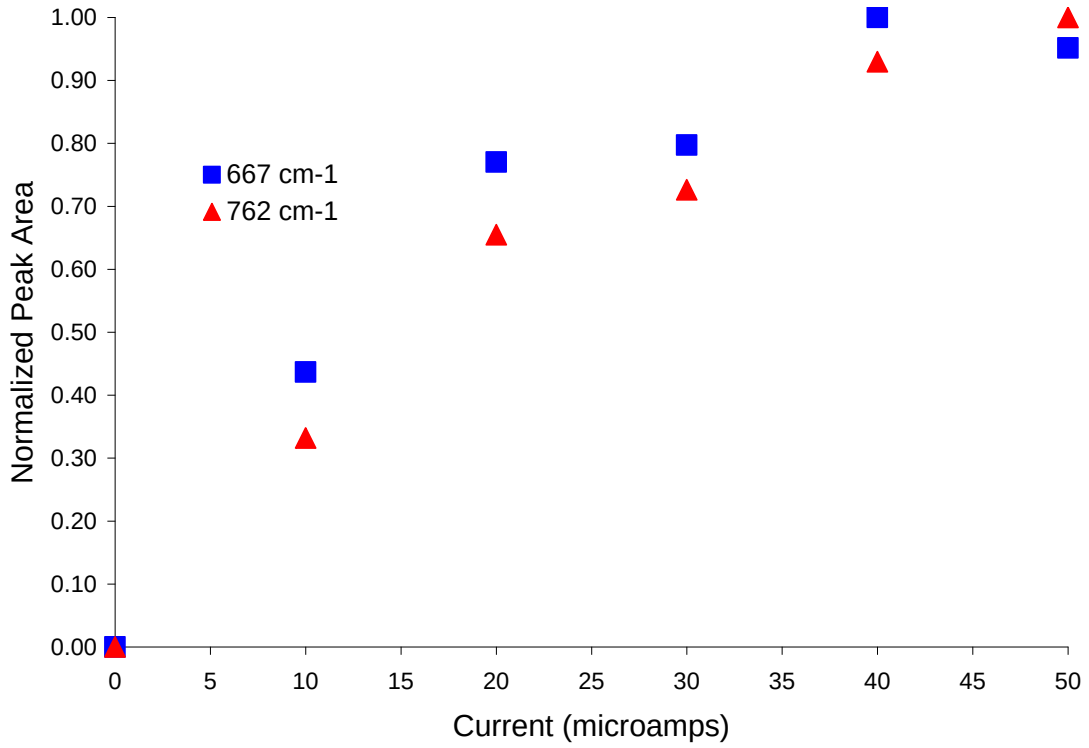

Figure 24. Normalized peak areas of benzyl radical absorptions with respect to electron current

This set of experiments clearly demonstrated that toluene destruction increases with increasing electron current, and that benzyl radical production increases with increased electron current and toluene destruction. From the data analysis performed, it was determined that this increase slows above 30 µA electron current, so increasing the electron current past 50 µA is unlikely to significantly improve either toluene destruction or benzyl radical production. The next set of experiments was performed using another

1:1600 toluene:argon sample, and the sample flow rate was varied, again to determine the effect on toluene destruction and benzyl radical production.

4.3.3 Varied flow rate – 1:1600 Toluene:Ar

These sets of experiments each used a gas sample with a 1:1600 mixture of toluene in argon, the same concentration as all previous toluene work. The rate of gas flow was varied between experiments, so to keep the total amount of gas deposited constant, the deposition time was also varied. A reference and an electron bombardment experiment were run at each different gas flow rate/deposition time combination, the EB experiments were all run at an electron current of 50 μA.

4.3.3.1 Varied flow rate – initial test

This set of experiments involved a reference and an EB experiment at three different flow rate/deposition time combinations. These combinations were: 1 SCCM for 4 hours; 2 SCCM for 2 hours; and ~4 SCCM for 1 hour. The 4 SCCM/1 hour electron bombardment experiment was the final experiment from the sample bulb. Due to low gas pressure the flow rate was extremely variable, ranging from 4.5 to 2.8 SCCM.

The change in toluene destruction with changing flow is shown in Figure 25, below.

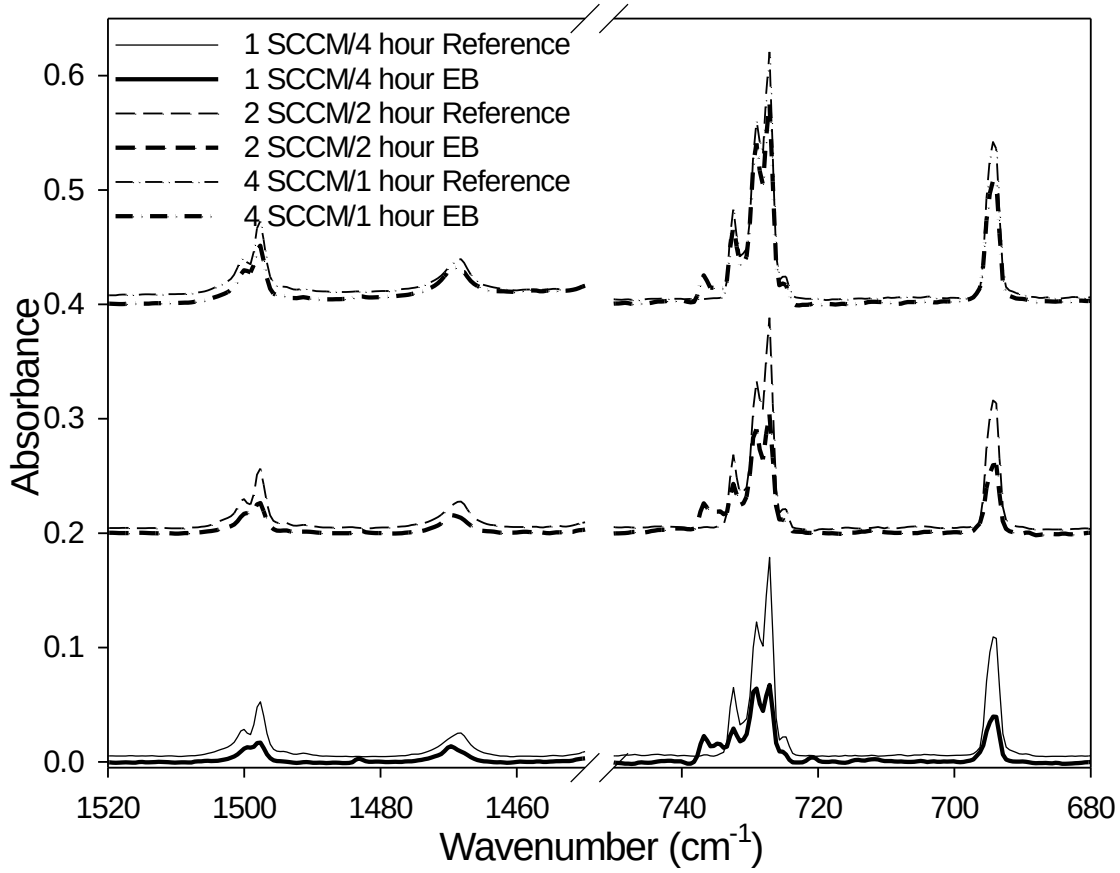

Figure 25. Reference and electron bombardment spectra from each flow rate/deposition time combination, showing that a flow rate of 1 SCCM and deposition time of 4 hours results in the greatest destruction of toluene

The relative percent destruction of each toluene peak was calculated for each EB spectrum, and these values were plotted against flow rate to more quantitatively demonstrate the change in destruction. This plot is shown in Figure 26. From these two figures, it is clear that while more toluene is deposited onto the cold window overall in experiments with a higher flow rate and shorter deposition time, the amount of toluene destroyed decreases as flow rate increases.

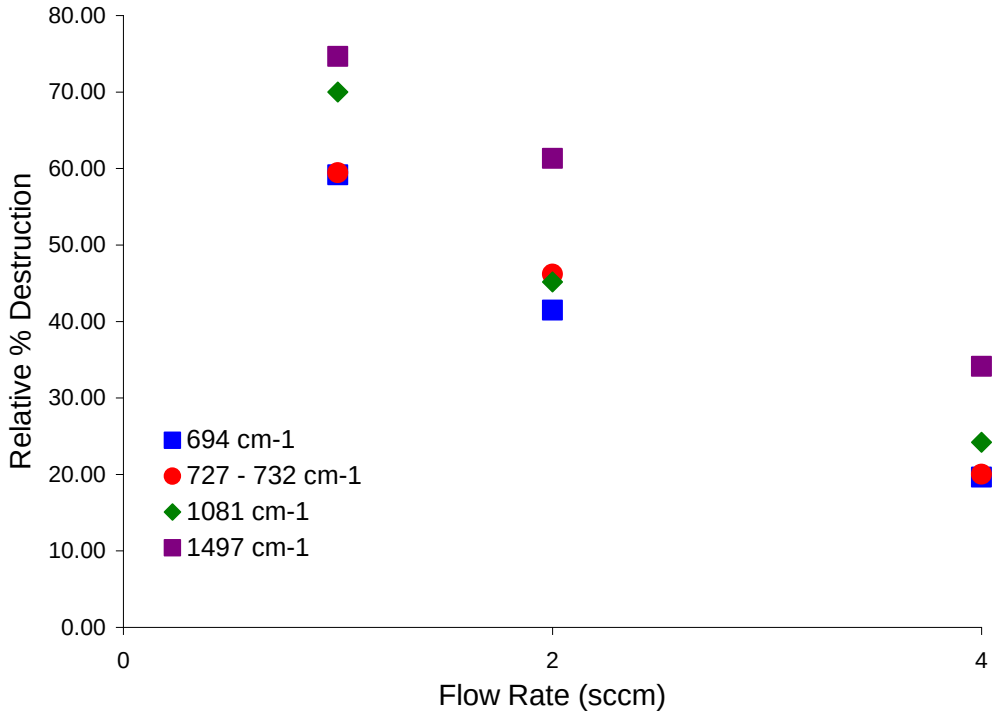

Figure 26. Relative percent destruction of toluene with respect to flow rate

The change in benzyl radical production with increasing flow rate is more easily seen when comparing spectra than the change in toluene destruction. As no benzyl radical is present in reference spectra, it is possible to simply compare the EB spectra and see the change in absorption magnitude. The benzyl radical peaks used for analysis are shown in Figure 27, and the decrease in magnitude with increasing flow rate can be observed.

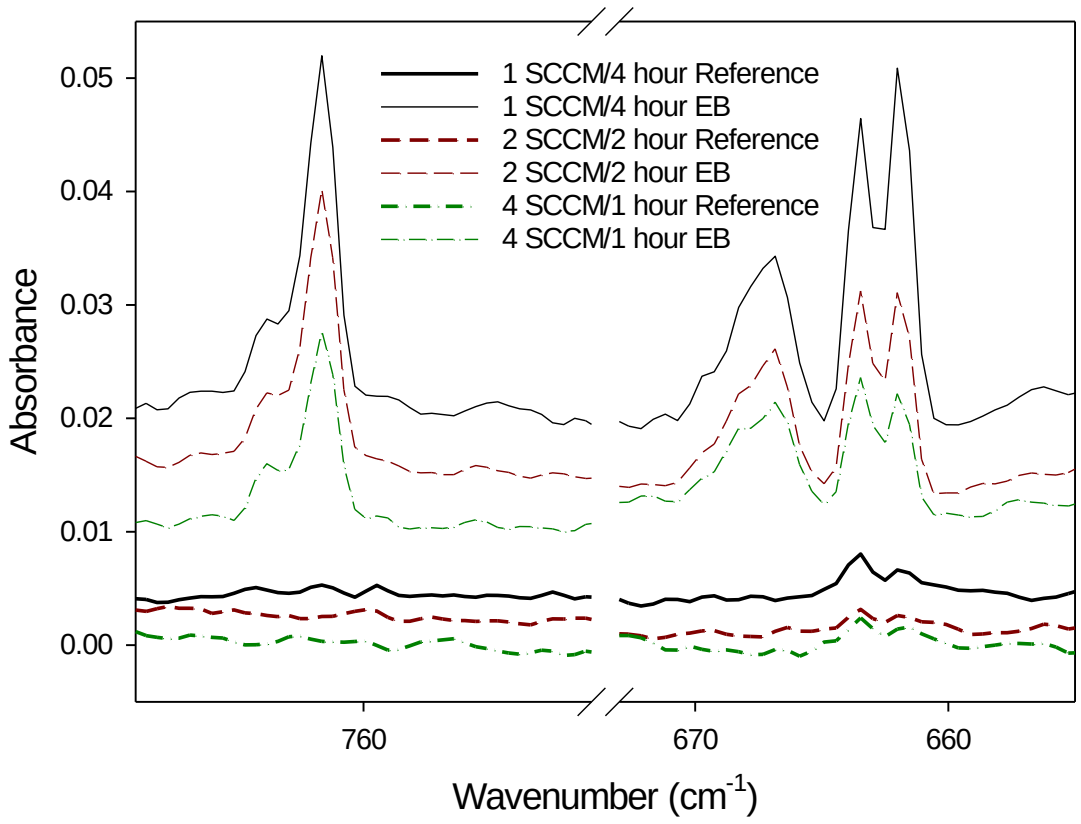

Figure 27. Benzyl radical peaks in electron bombardment and reference spectra from each flow rate/deposition time combination demonstrating that the low flow rate/long deposition combination (1 SCCM/4 hour) results in the greatest formation of benzyl radicals

The two benzyl radical peaks used for analysis were integrated in each EB spectrum, and the value for each peak was normalized against the values from the same peak from each different flow rate, dividing each peak integration by the largest value for that peak, as before. These values were plotted against flow rate, and a decrease in benzyl radical production with increasing flow rate is clearly seen (Figure 28).

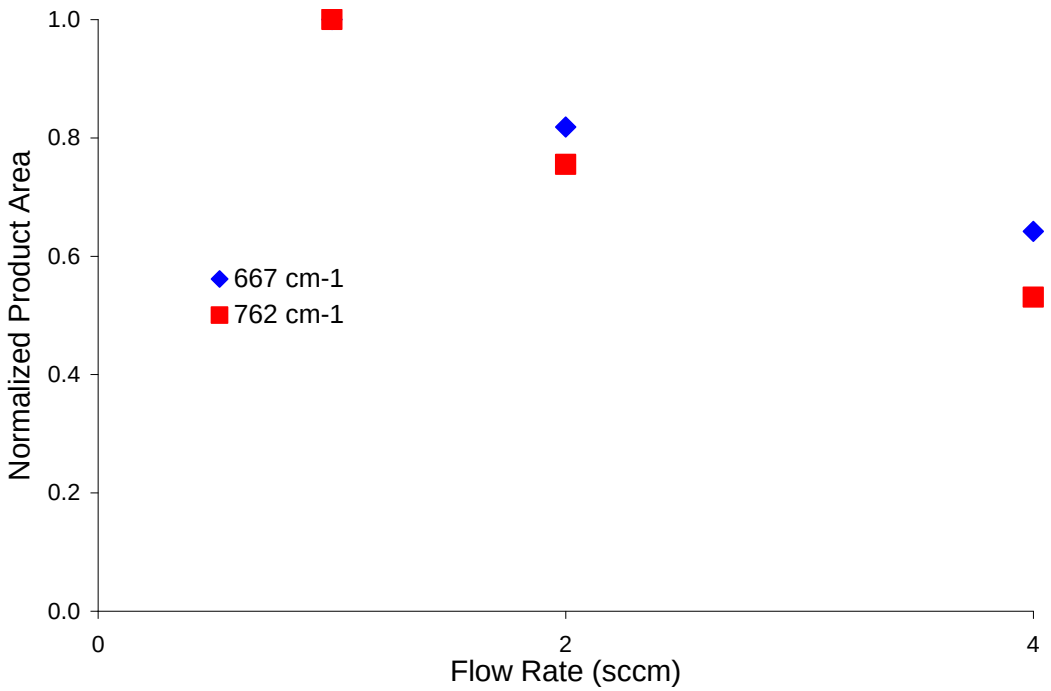

Figure 28. Normalized peak areas of benzyl radical absorbances with respect to flow rate

4.3.3.2 Varied flow rate – confirmation of trend

Due to the uncertainty present in the data obtained from the 4 SCCM/1 hour EB experiment in the previous set of experiments, a new set was performed. A new 1:1600 toluene:argon gas sample was prepared, and a reference experiment and an EB experiment were performed at 1 SCCM for 4 hours, and at 4 SCCM for 1 hour. The previous experiment set appeared to clearly show a decrease in both toluene destruction and benzyl radical production with increased flow rate. If the results from the 1 SCCM and 4 SCCM experiments in this set had appeared to contradict this trend, reference and EB experiments would have been performed at 2 SCCM for 2 hours to determine what new trend was occurring.

The toluene absorptions in each spectrum were integrated, and the relative percent destruction at each flow rate was again calculated. These values were plotted against the flow rate to clearly show the change in destruction with changing flow rate. This plot, and the reference and EB spectra are shown in Figure 29 and Figure 30, respectively.

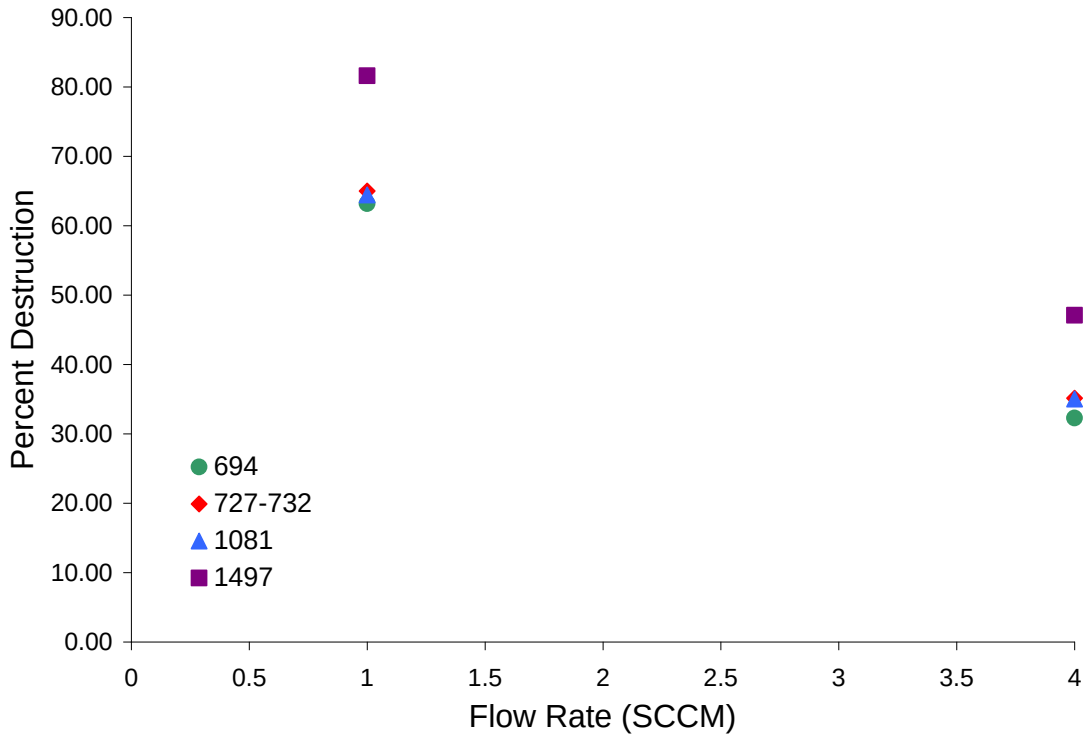

Figure 29. Relative percent destruction of toluene with respect to flow rate

These figures confirm the findings from the previous set of experiments – we again observe that increasing the flow rate while holding the total amount of gas deposited constant causes a decrease in toluene destruction, even though the total amount of toluene deposited increases with flow rate.

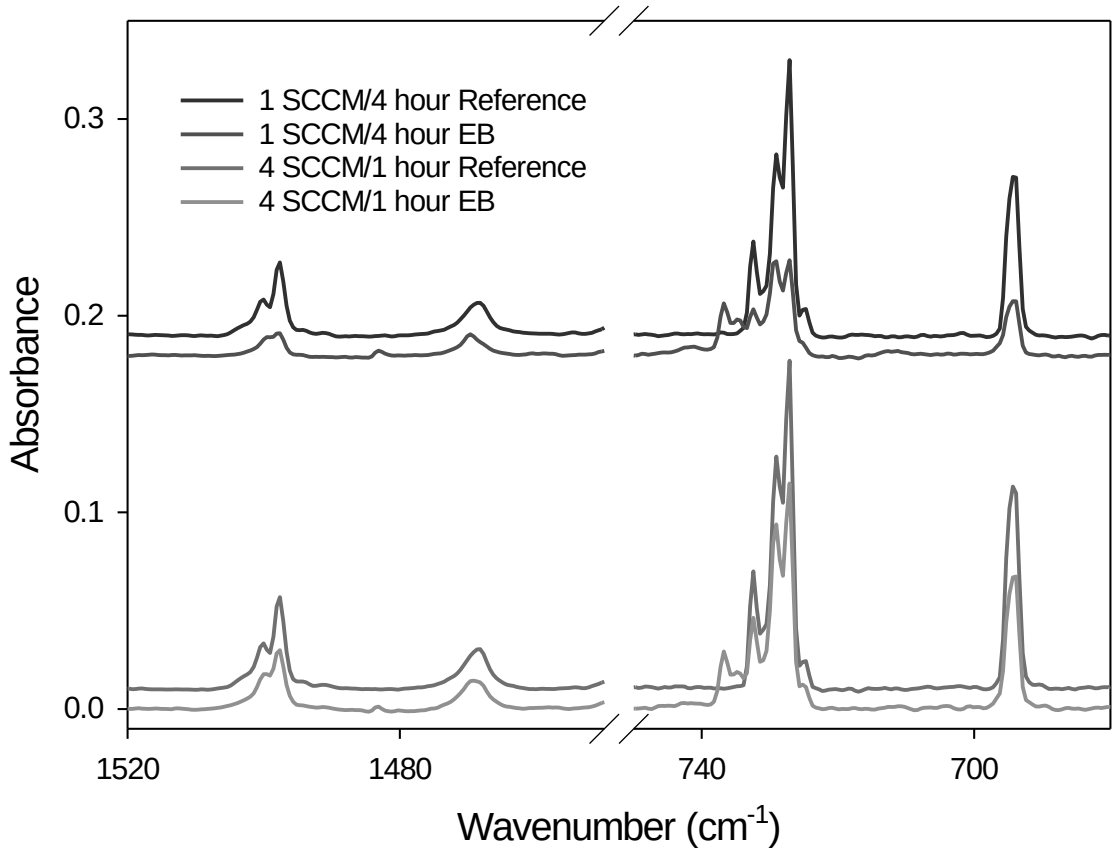

Figure 30. Toluene peaks in reference and electron bombardment spectra for both flow rate/deposition time combinations confirming that 1 SCCM/4 hours is the ideal flow rate/deposition time combination for toluene destruction

The data analysis performed on the benzyl radical absorptions in the previous set of experiments was also repeated for this set. The normalized peak areas of the two benzyl radical peaks were calculated and plotted against the flow rate, shown in Figure 31. The benzyl radical peaks are shown in Figure 32, and the change with changing flow rate is also visible here.

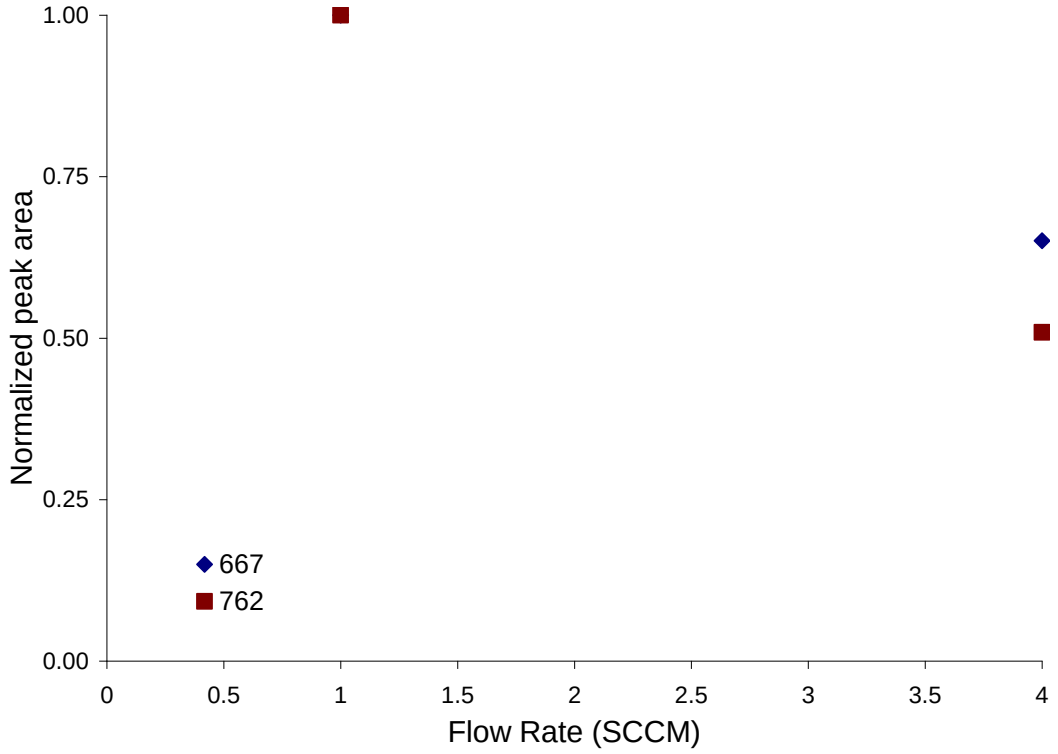

Figure 31. Normalized benzyl radical peak areas with respect to flow rate

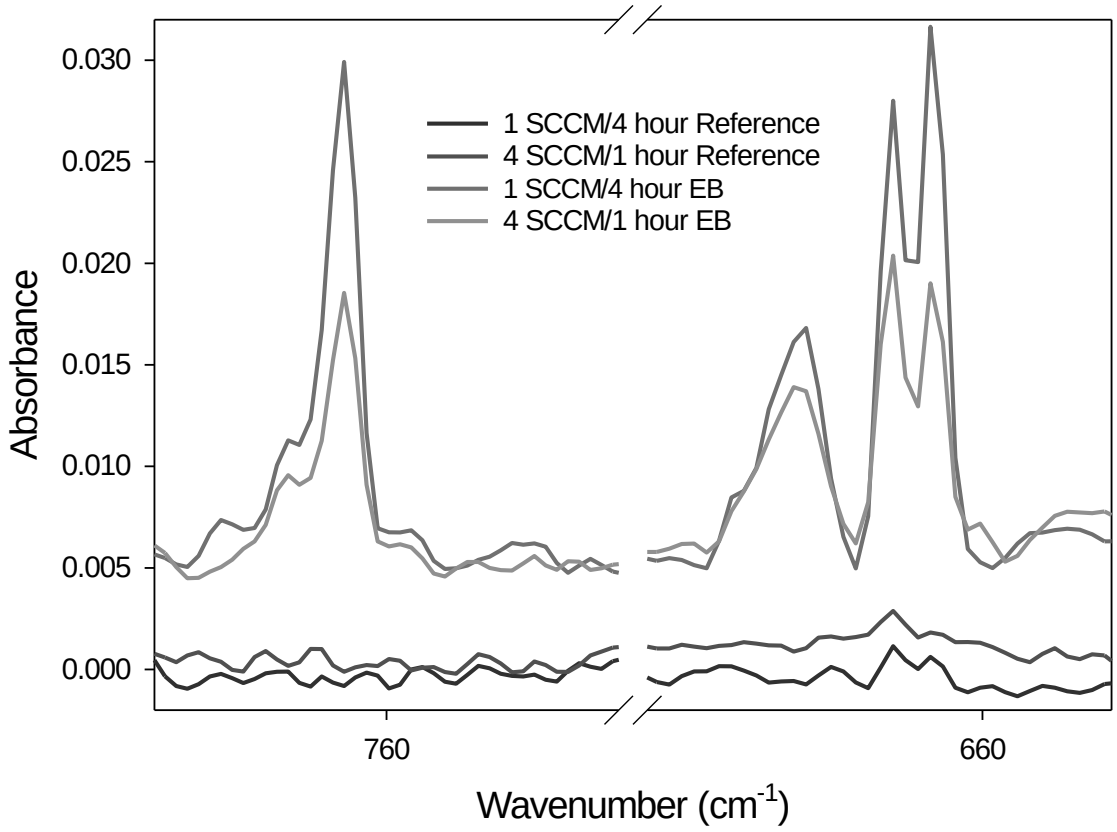

Figure 32. Benzyl radical absorptions in reference and electron bombardment spectra of both flow rate/deposition time combinations confirming that the 1 SCCM/4 hour flow rate/deposition time combination is ideal for production of benzyl radicals

As with the toluene analysis, these figures confirm the findings from the previous set of varied flow rate experiments. The production of benzyl radicals decreases with increasing flow rate. This observation was expected, based on the decreasing toluene destruction – if less toluene is destroyed, less benzyl radical is likely to be produced. Overall, these varied flow rate experiments demonstrated that increasing the sample flow rate negatively affects the experimental results, likely due to the fact that electrons are the limiting reagent. A decrease in both toluene destruction and benzyl radical

production was observed when the flow rate was increased. These results indicate that the optimal flow rate for benzyl radical production is 1 SCCM.

4.4 Toluene and oxygen mixtures

Once it was confirmed that benzyl radicals could be produced and observed in the EBMIS system, the next step was to try to effect their reaction with oxygen. To accomplish this goal, the next sets of experiments used gas samples containing mixtures of toluene and oxygen in argon. We found that the benzylperoxy radical could be made, and were able to partially characterize it.

4.4.1 1:2:1600 Toluene:O_2:Ar

A gas sample containing a 1:2:1600 mixture of toluene, oxygen, and argon was prepared. A reference experiment and a 20 μA electron bombardment experiment were performed, and spectra were acquired. After acquisition of the EB spectrum, the temperature control on the EBMIS system was used to heat the cold window to 25 K for 15 minutes, to anneal the matrix, and an additional spectrum was obtained. All experiments using this gas sample had deposition times of four hours.

The EB spectra of the toluene:O_2:Ar mixture revealed some new peaks, that were not previously observed in mixtures of toluene and argon without additional oxygen. The most promising of these peaks occurs at 954 cm^{-1}, within the range expected for the C–O stretch of an alkylperoxy radical[69,70,71,72,73] , the peak is not present in the reference spectrum, and does not appear in gas mixtures that do not contain both toluene and oxygen. Figure 33 shows the 954 cm^{-1} peak, and it is clearly visible that this is a new peak, occurring after electron bombardment of toluene/oxygen mixtures.

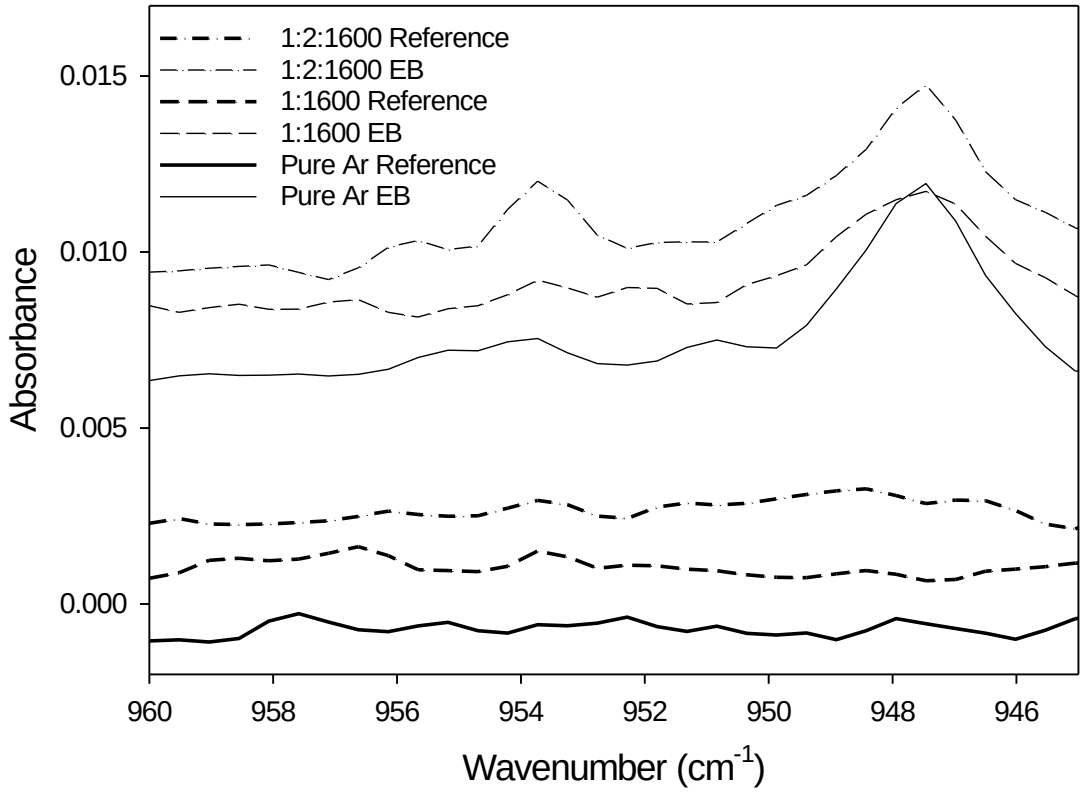

Figure 33. Electron bombardment spectrum of 1:2:1600 toluene:oxygen:argon, showing a peak at 954 cm^{-1} that is new when compared to EB and reference spectra of 1:1600 toluene:argon and pure argon gas samples, indicating a new compound created after electron bombardment of toluene-oxygen-argon mixtures

The effect of annealing the matrix on the observed spectra was also investigated. The relative percent destructions of a number of toluene peaks were calculated, in both the EB spectra and the annealed spectra. The destruction of toluene appeared to increase slightly with annealing, but the increase was not significant enough to determine whether it was a true increase in destruction, or if it was simply a change in peak profiles that appeared as a change in the magnitude of the peak integrations. Annealing also

appeared to cause a decrease in the magnitude of the new, unidentified peak at 954 cm^{-1} – this is shown in Figure 34.

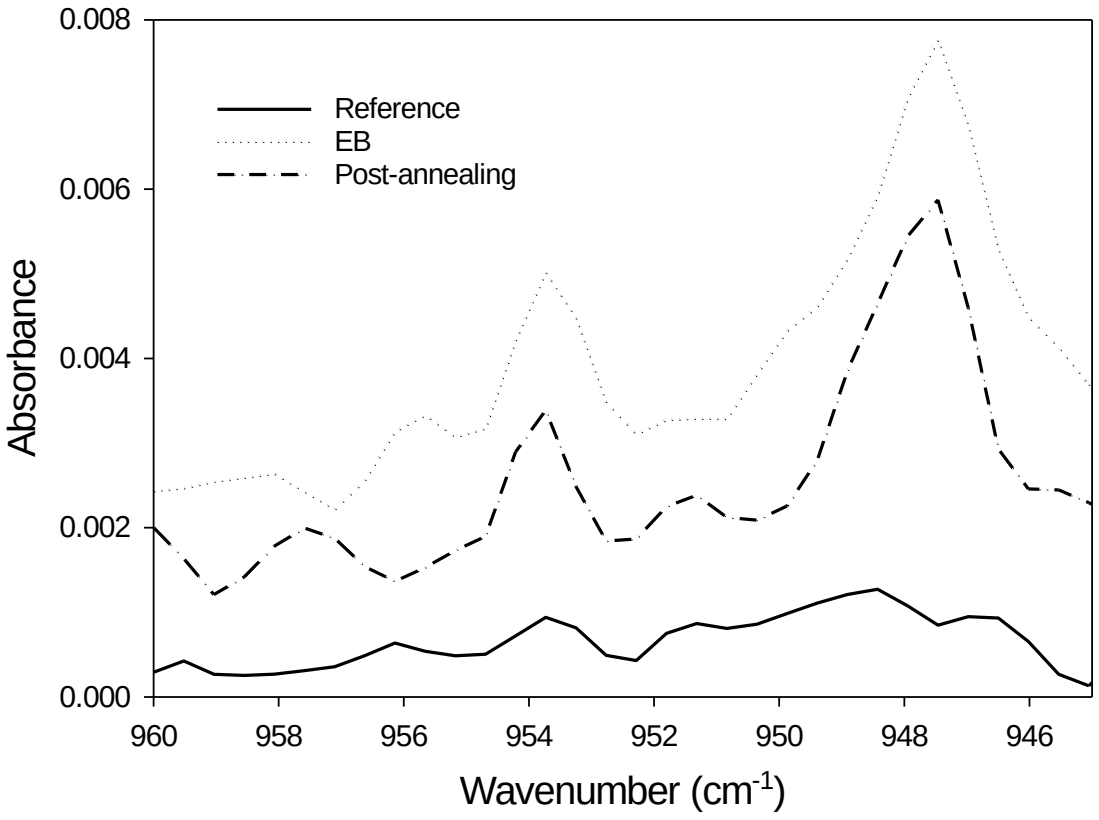

Figure 34. Reference, electron bombardment, and post-annealing spectra of 1:2:1600 toluene:oxygen:argon gas mixture, showing a slight decrease in magnitude of the unidentified 954 cm^{-1} peak with annealing

The new peaks that appeared upon electron bombardment of the toluene/oxygen mixture are promising. The next set of experiments was performed to try and increase the size of these peaks, and see if any more could be observed, by increasing the concentration of oxygen in the gas mixture.

4.4.2 1:8:1600 Toluene:O_2:Ar

This set of experiments used a gas mixture with a higher oxygen concentration than previous work – the gas sample was a 1:8:1600 toluene:O_2:Ar mixture. A reference experiment and an electron bombardment (20 μA electron current) experiment were performed, and a spectrum was obtained for each after a four hour gas deposition, and again after annealing the matrix at 25 K for 15 minutes.

The EB spectrum obtained from this gas mixture showed some additional new peaks, and some of the peaks that first appeared in the 1:2:1600 gas sample had increased in size. Figure 35 compares the size of the 954 cm^{-1} absorbance in the previous work to the peak observed with this gas mixture.

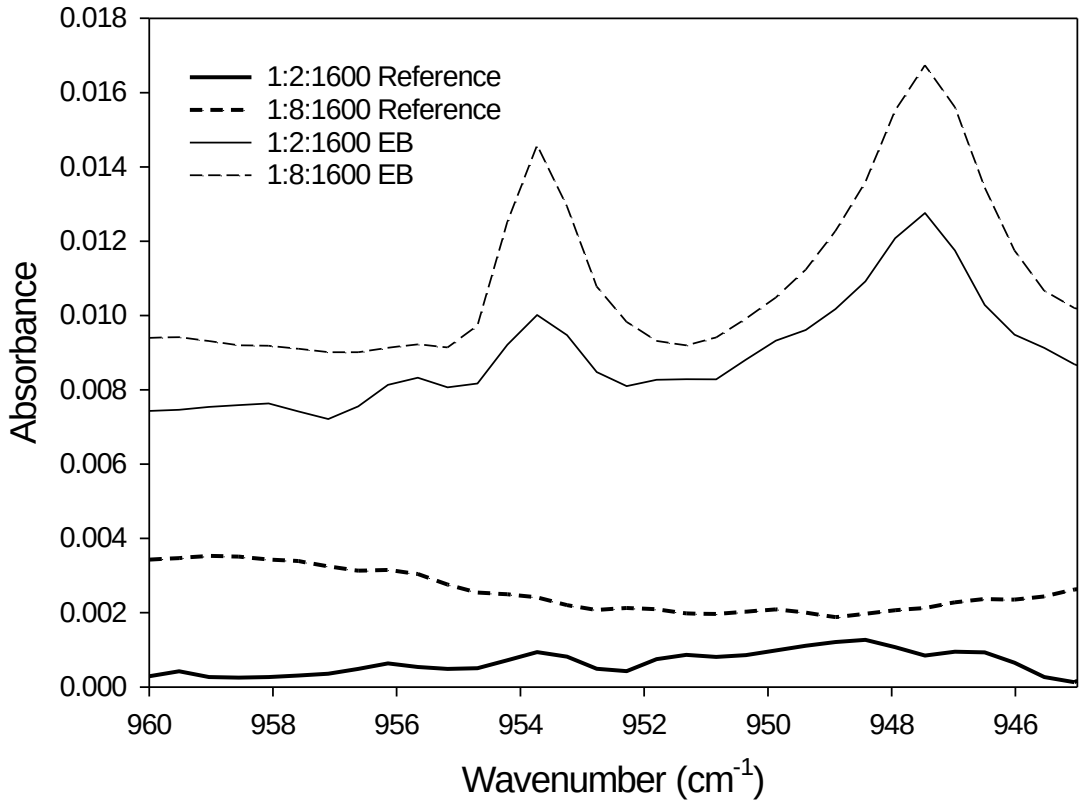

Figure 35. Reference and electron bombardment spectra of 1:2:1600 and 1:8:1600 toluene:O_2:Ar gas mixtures, showing increase in size of unidentified 954 cm^{-1} peak with increased oxygen concentration, indicating the presence of oxygen in the compound responsible for the absorption

Two additional absorptions were also identified as being potential benzylperoxy radical absorptions – a shoulder at 1104 cm^{-1} that was also present, though smaller in magnitude, in the 1:2:1600 gas sample, and a small peak at 1118 cm^{-1} that has not been observed previously. These two peaks are shown in Figure 36, and it is clear that they increase in size with the increase in oxygen concentration.

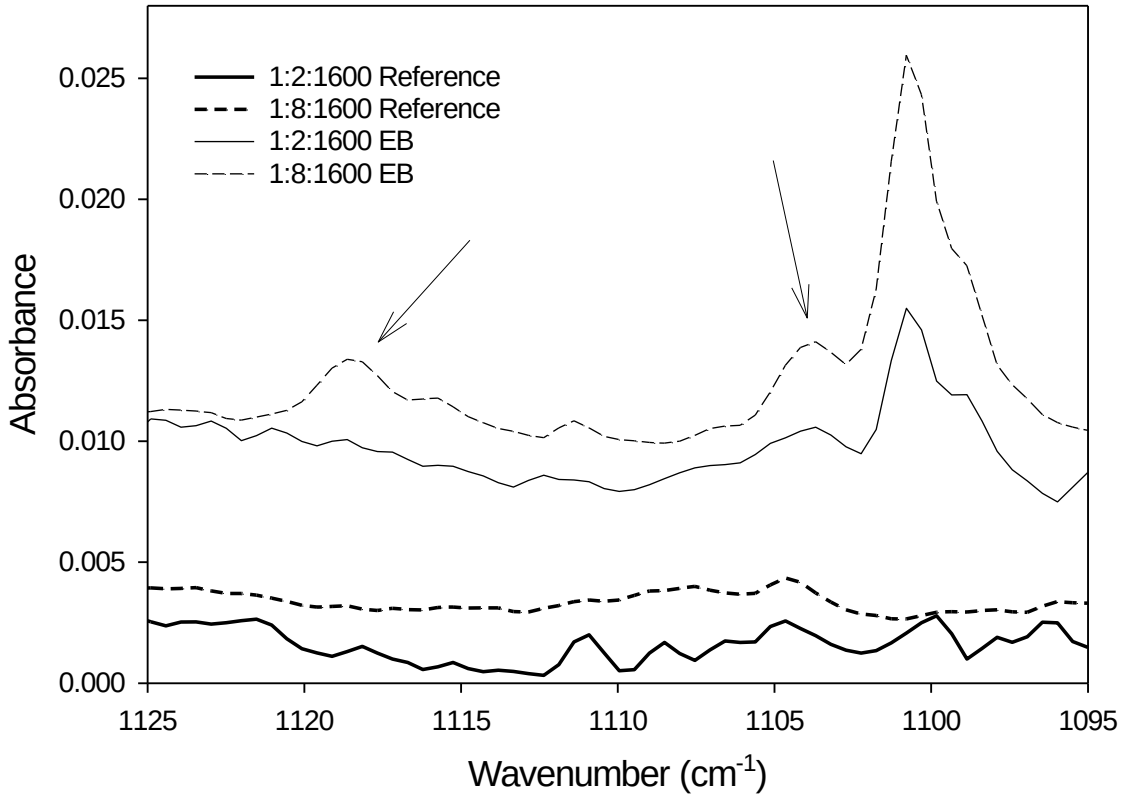

Figure 36. Reference and electron bombardment spectra from 1:2:1600 and 1:8:1600 toluene:O_2:Ar mixtures showing appearance of peaks at 1104 & 1118 cm^{-1} with increased oxygen concentration

The spectra obtained post-annealing were also analyzed, to determine what effect, if any, annealing had on the matrix. Similar to the previous toluene/oxygen work, a slight increase in toluene percent destruction was seen, along with a slight decrease in benzyl radical peak integration. Again, the changes were not large enough that they can definitely be said to be actual changes in toluene destruction or benzyl radical production rather than just a result of slightly shifting peak profiles.

The annealing had a definite effect on the new peaks that were observed, however. Figure 37 shows that the absorption at 1104 cm^{-1} increases with annealing, while the

absorptions at 954 and 1118 cm^{-1} both decrease, possibly indicating that they are associated with the same compound.

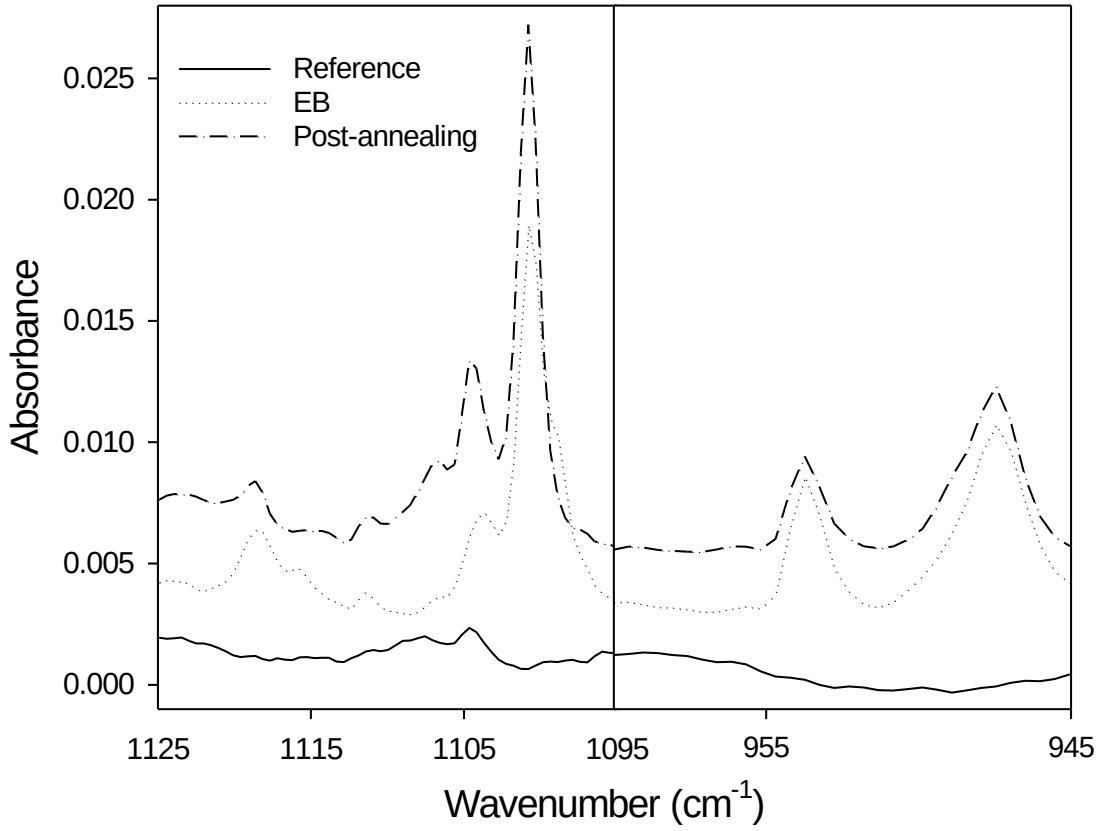

Figure 37. Reference, electron bombardment, and post-annealing spectra of 1:8:1600 toluene:O_2:Ar gas mixture, showing that annealing appears to decrease the magnitude of the 954 and 1118 cm^{-1} absorptions, while increasing the magnitude of the 1104 cm^{-1} absorption

After these sets of experiments were completed, a new spectrometer was obtained. Minor adjustments to the apparatus orientation were also made, to allow it to fit into the new spectrometer. Adjustments were also made to the anode and cathode potentials to avoid discharging at the anode.

4.5 New apparatus work

This set of experiments was performed using the same 1:8:1600 toluene:O_2:Ar sample as the previous work. The purpose was to determine whether the changes made to the apparatus setup had any effect on the resulting spectra.

Reference and 20 μA EB spectra were obtained. The absorbances observed in the EB spectrum were much larger than in previous spectra, so a second reference was obtained to determine if the cause of the increased absorptions was a change in flow rate, or an effect of changing the apparatus. As seen in Figure 38, although the first reference had more noise, the peak sizes in the two references were consistent.

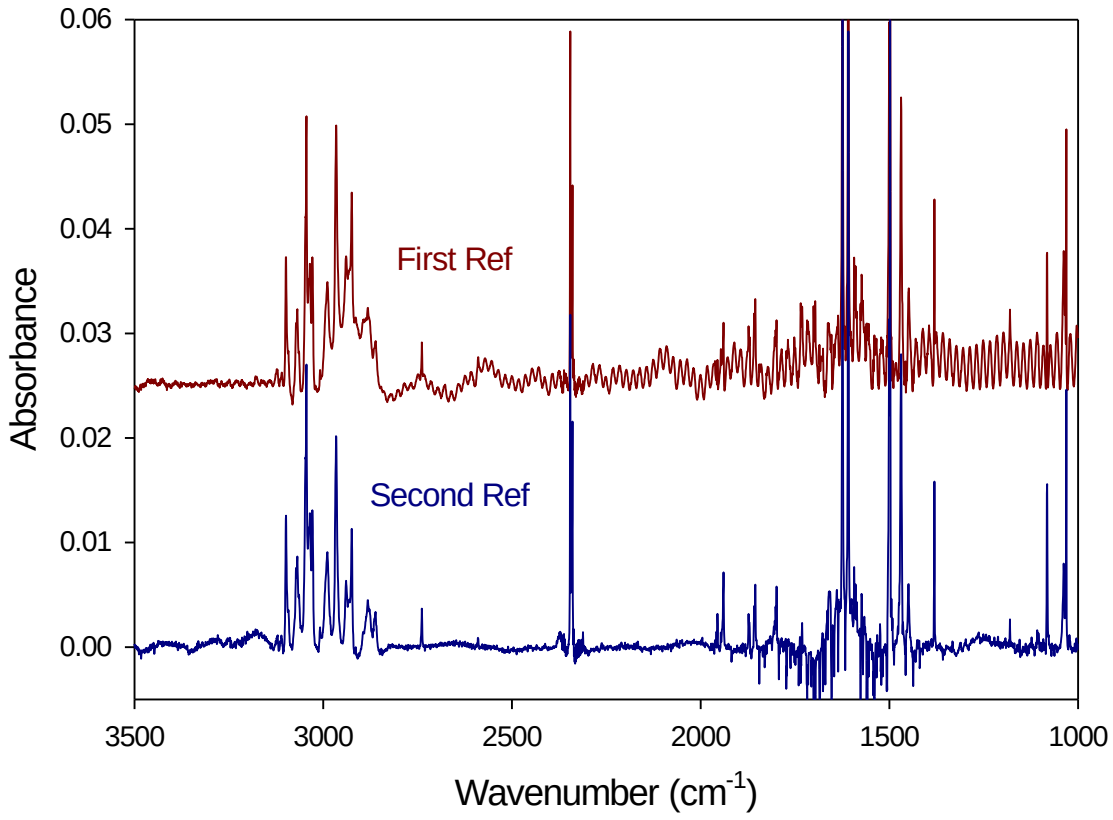

Figure 38. Reference spectra of a 1:8:1600 toluene:O2:Ar sample taken on the new apparatus

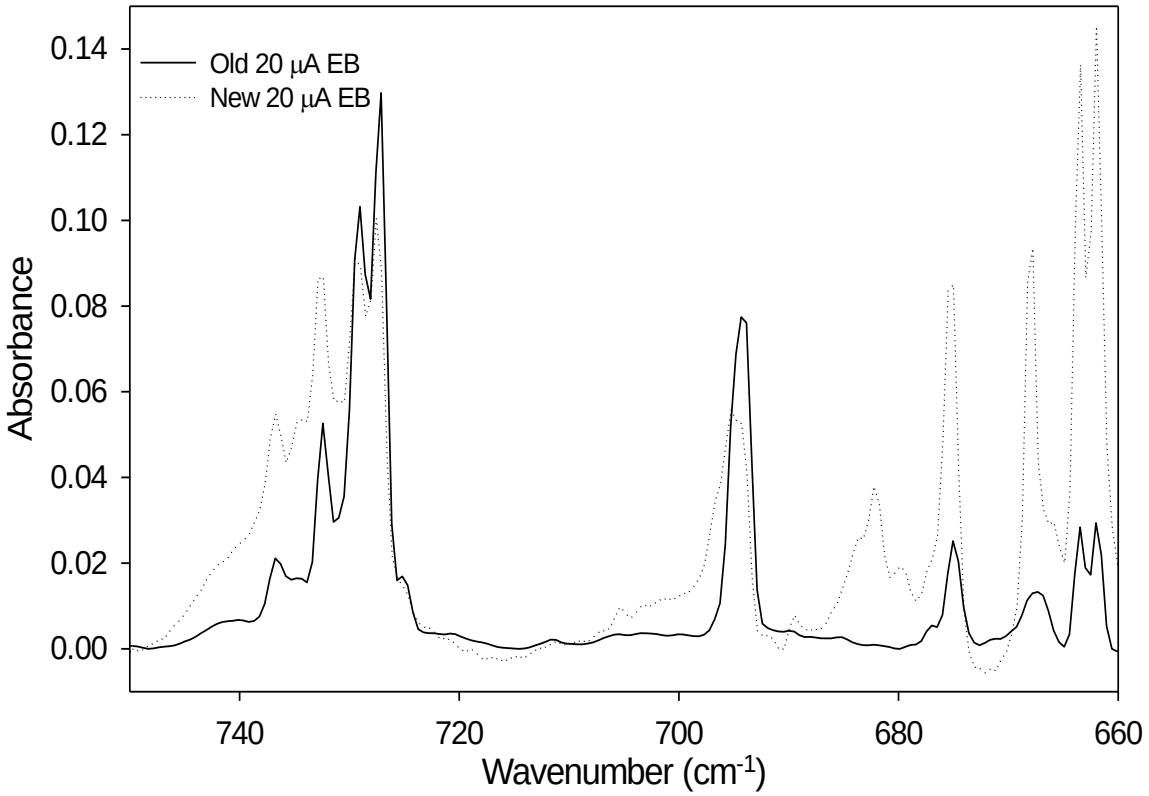

Figure 39. Comparison of 20 μA spectra taken on the old apparatus and the new apparatus, showing that toluene peaks remain consistent and observed increases in peak magnitude are occurring mainly in contaminant peaks

Figure 39 shows that the toluene peaks in the EB spectrum were consistent with those from before changes were made and the increased absorbances are mainly seen for contaminant peaks.

As mentioned previously, the cathode and anode potentials were changed, to avoid discharging at the anode. The previous work had been performed at cathode and anode potentials of -200 and +100, respectively. These potentials were changed to -240 and +60 for the work using the new apparatus.

4.5.1 Changing potentials

A new 1:8:1600 toluene:O_2:Ar sample was prepared, and a series of six experiments were performed – one reference and five electron bombardment. The electron bombardment experiments changed the anode potential while either changing the cathode potential as well, to maintain the same total potential, or leaving the cathode potential unchanged to vary the total potential difference. The EB spectra were all obtained at a current of 20 µA, and the potentials were as follows: anode/cathode (potential difference); +60/-240 eV (300 eV); +40/-240 eV (280 eV); +40/-260 eV (300 ev); +20/-240 eV (260 eV); and +20/-280 eV (300 eV).

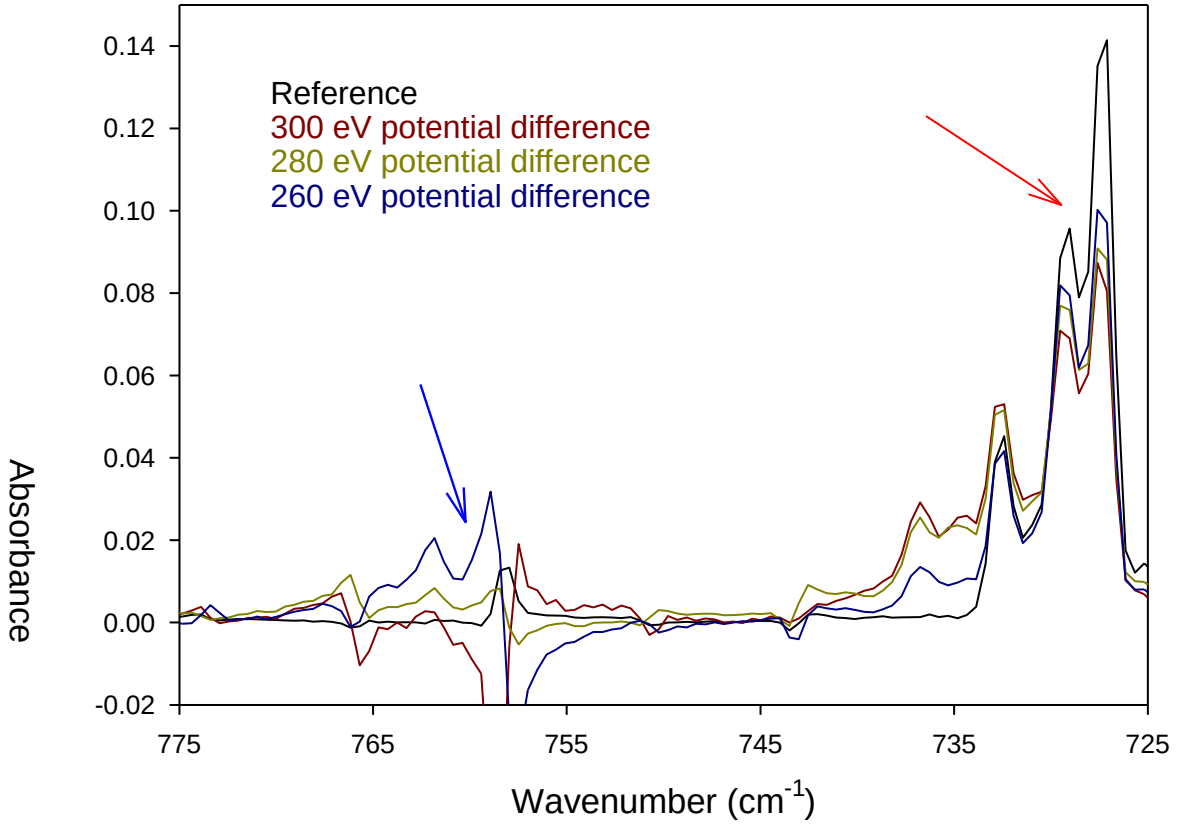

Figure 40. Reference and EB spectra of 1:8:1600 toluene:O_2:Ar sample, red arrow indicates toluene peak and blue arrow indicates product peak

Figure 40 shows that as the total potential difference decreases, product formation increases while toluene destruction decreases. The same trend is not seen in Figure 41 when the anode potential is decreased and the total potential difference is held steady. One potential reason for this is because there is uncertainty in the anode potential for this experiment – it may have climbed as high as +40, making the total potential difference 320 eV.

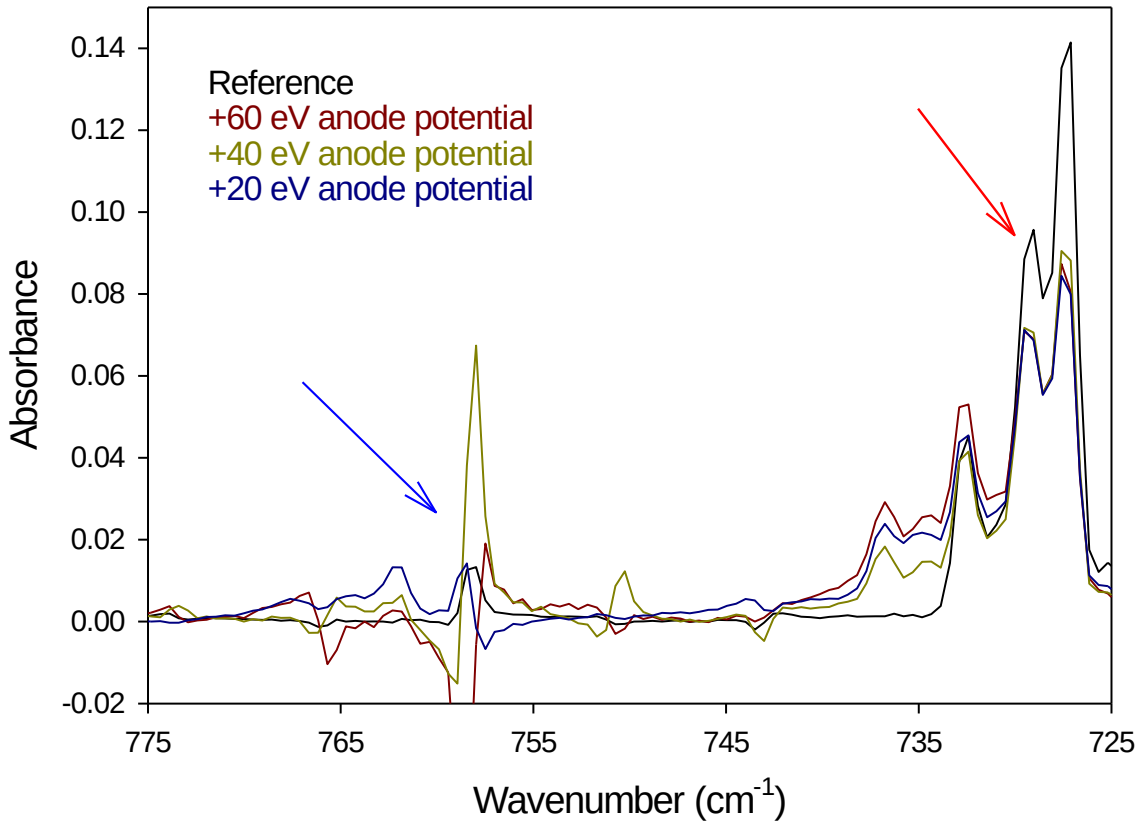

Figure 41. Reference and EB spectra (changing anode potential) of 1:8:1600 toluene:O_2:Ar sample, red arrow indicates toluene peak and blue arrow indicates product peak

4.6 Increased toluene concentrations

Since no definitive benzylperoxy radical peaks have yet been identified, experiments were performed with significantly increased concentrations of toluene, and no oxygen present. This was done to increase the amount of benzyl radical produced, as previous experiments had not produced much benzyl radical, and the production of benzylperoxy radicals is obviously more likely with more precursor present.

4.6.1 1:1000 Toluene:Ar

A sample was prepared containing a 1:1000 mixture of toluene and argon, almost double the concentration of toluene, compared to previous samples. A reference spectrum was obtained, along with three electron bombardment spectra. All EB spectra had a current of 20 μA, with varying cathode and anode potentials - +20/-280 eV, +40/-260 eV, and +60/-240 eV, the total potential difference for all experiments was 300 eV.

A fairly significant amount of ro-vibrational water was observed in both reference and electron bombardment spectra, so subtractions were performed to obtain cleaner spectra for analysis. Spectra were acquired of the cold window before deposition started, and were later subtracted from the post-deposition spectra. The factor by which the subtrahend file was multiplied was varied until an optimal factor was found that minimized ro-vibrational water interference in the spectra, while also avoiding altering the reactant and product absorbances. An example is shown in Figure 42, for the +20/-280 eV EB spectrum – the pre-deposition spectrum, post-deposition spectrum, and subtraction result spectrum are all shown.

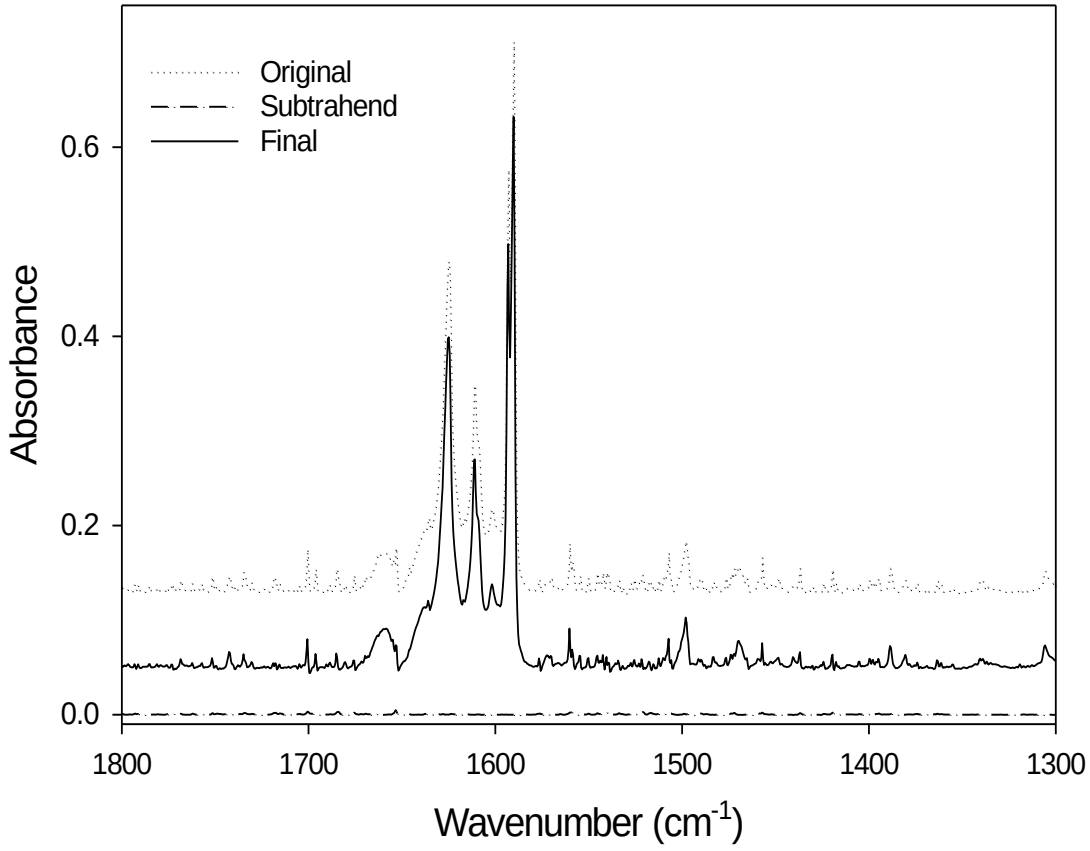

Figure 42. Original spectrum obtained post-deposition of 1:1000 toluene:Ar gas sample, along with subtrahend spectrum obtained pre-deposition, and resulting subtracted spectrum used for analysis, showing reduced noise in the final spectrum

Figure 43 shows the reference and EB spectra obtained, demonstrating the change caused by altering the anode and cathode potentials. Figure 44 compares the reference and +20/-280 eV EB spectrum to a reference and EB spectrum from 1:1600 toluene:Ar experiments. An increase in benzyl radical production was observed, so the toluene concentration was further increased for the next sets of experiments to try and obtain an even greater increase.

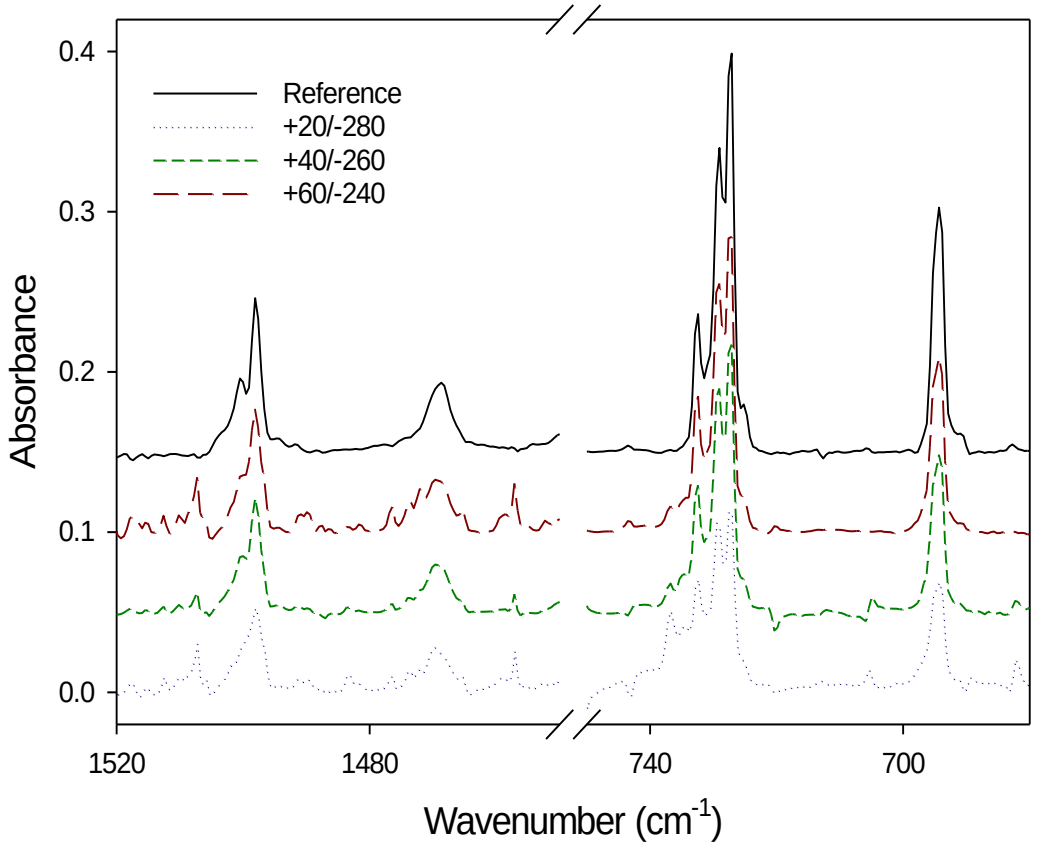

Figure 43. Reference and EB spectra from a 1:1000 toluene:Ar sample, illustrating the effect of changing anode and cathode potentials on the product spectra

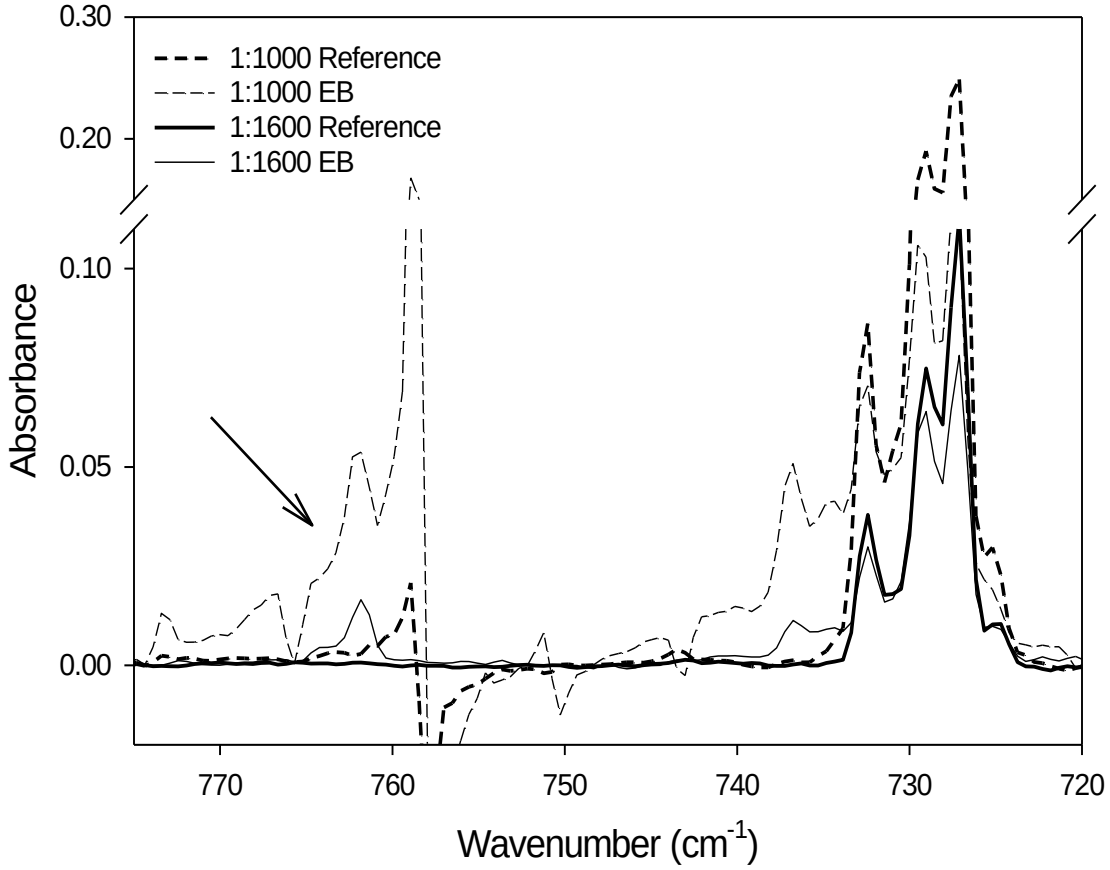

Figure 44. Reference and EB spectra from 1:1000 and 1:1600 toluene:Ar gas samples, arrow marks benzyl radical peak, which is seen to increase with increasing toluene concentration

4.6.2 1:200 Toluene:Ar

A 1:200 toluene:argon gas sample was prepared. The concentration of toluene in this sample is eight times that in the initial 1:1600 toluene:Ar samples, and five times that in the 1:1000 toluene:Ar samples used in the previous set of experiments. The vastly increased toluene concentration means that the resulting spectra will be less clean than previous spectra, but also that increased production of benzyl radicals is more likely.

A reference spectrum was obtained, along with two electron bombardment spectra. The anode and cathode for all EB experiments were set at +20 and -280 eV respectively, for a total potential difference of 300 eV. The first EB experiment was a four hour deposition with an electron current of 20 μA, and the second was a two hour deposition with an electron current of 30 μA.

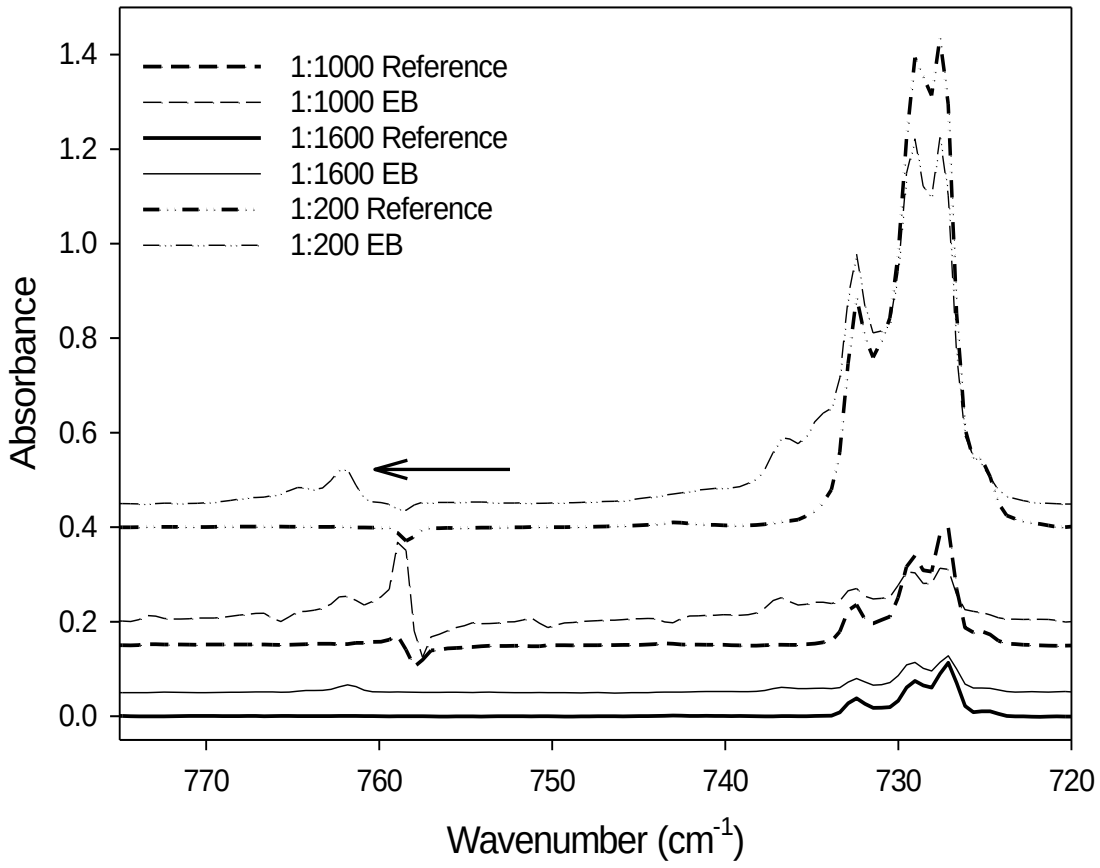

Figure 45. Reference and EB spectra from 1:200, 1:1000, and 1:1600 toluene:Ar gas samples, the arrow marks the 762 cm^{-1} benzyl radical peak, seen to increase significantly with increased toluene concentration

The benzyl radical absorption at 762 cm^{-1} was seen to increase with the increase in toluene concentration, as shown in Figure 45. When the peak is compared to those seen at toluene:Ar concentrations of 1:1000 and 1:1600, it is obviously larger, although when the peaks are integrated and their areas compared, the increase in size does not scale directly with concentration, as shown in Figure 46 – the red line shows the projected integration values if they did scale with concentration. Since this observation indicates that the benzyl radical plateaus at high toluene concentrations, and a 1:200 mixture is at the extremely high end of concentrations used in this lab, the concentration was not increased further. The next experiments re-introduced oxygen to the gas samples, in a final attempt to observe benzylperoxy radicals in the EBMIS system.

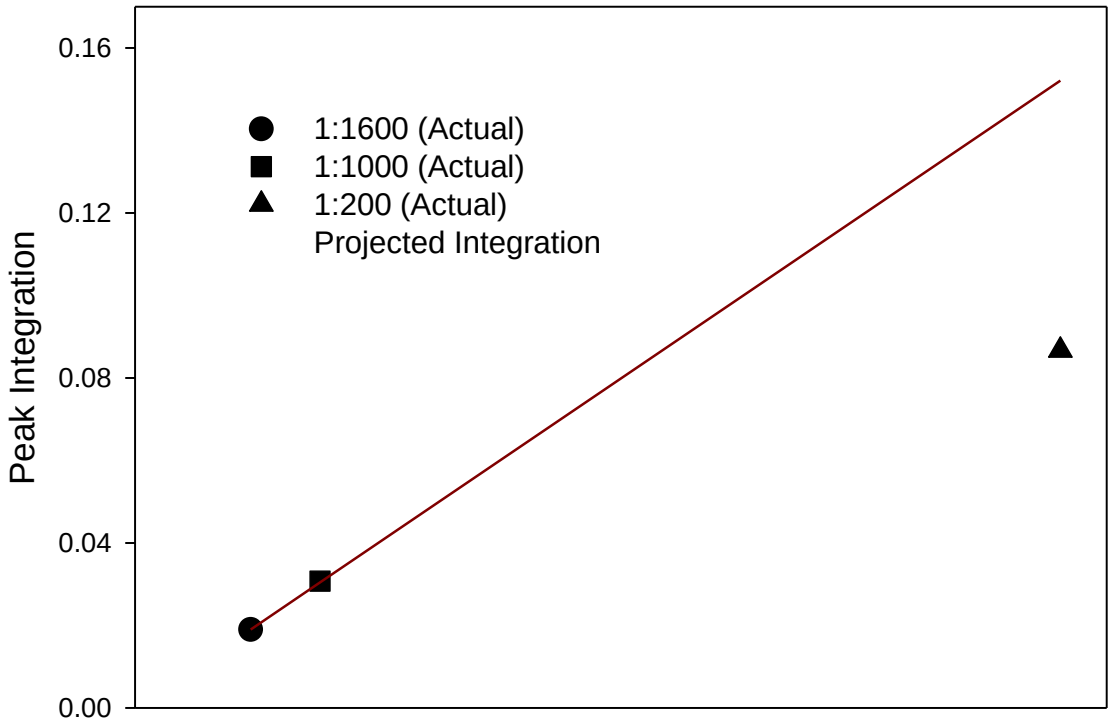

Figure 46. Integrations of 762 cm^{-1} benzyl radical peak from spectra obtained from 1:1600, 1:1000, and 1:200 gas samples, red line shows projected integration

4.6.3 1:1:200 Toluene:O_2:Ar

For this final set of experiments, a gas sample was produced containing very high concentrations of both toluene and oxygen – 1:1:200 toluene:O_2:Ar. A four hour reference deposition was run, without electron bombardment, and a spectrum acquired. Two electron bombardment experiments were performed, with anode and cathode potentials of +20 and -280 eV, respectively, and an electron current of 15 μA. The first was a four hour deposition, and the second had a deposition time of two hours. The spectrum acquired from the four hour deposition is used in analysis of these experiments.

Figure 47, below, shows the regions of the spectra around 954 and 1100-1120 cm^{-1}. respectively. These are the regions previously identified as containing absorptions potentially caused by benzylperoxy radicals. The 1:1:200 toluene:O_2:Ar reference and EB spectra are compared to determine whether any changes occur in the spectrum after electron bombardment.

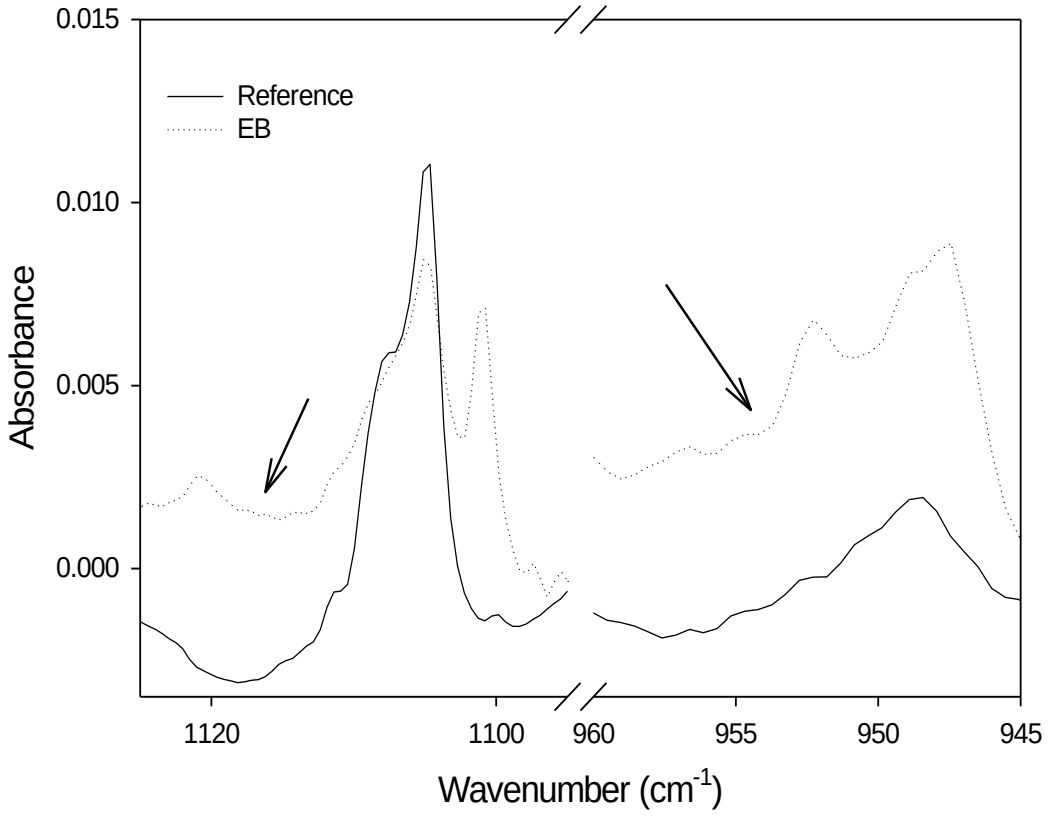

Figure 47. Reference and EB spectra from a 1:1:200 toluene:O_2:Ar gas sample in the region where absorptions tentatively assigned to the benzylperoxy radical have been observed, arrows mark areas of interest

Figure 48 compares the reference and EB spectra from the 1:1:200 toluene:O_2:Ar sample to those from the 1:8:1600 toluene:O_2:Ar sample. From these figures, it appears that the peaks that were observed in the previous spectra of toluene/oxygen mixtures

are present in these spectra, but have shifted slightly. The two new absorbances that appear in the 1:1:200 EB spectrum, at 1121 and 952 cm^{-1}, seem to correspond to the previously identified absorbances at 1118 and 954 cm^{-1}.

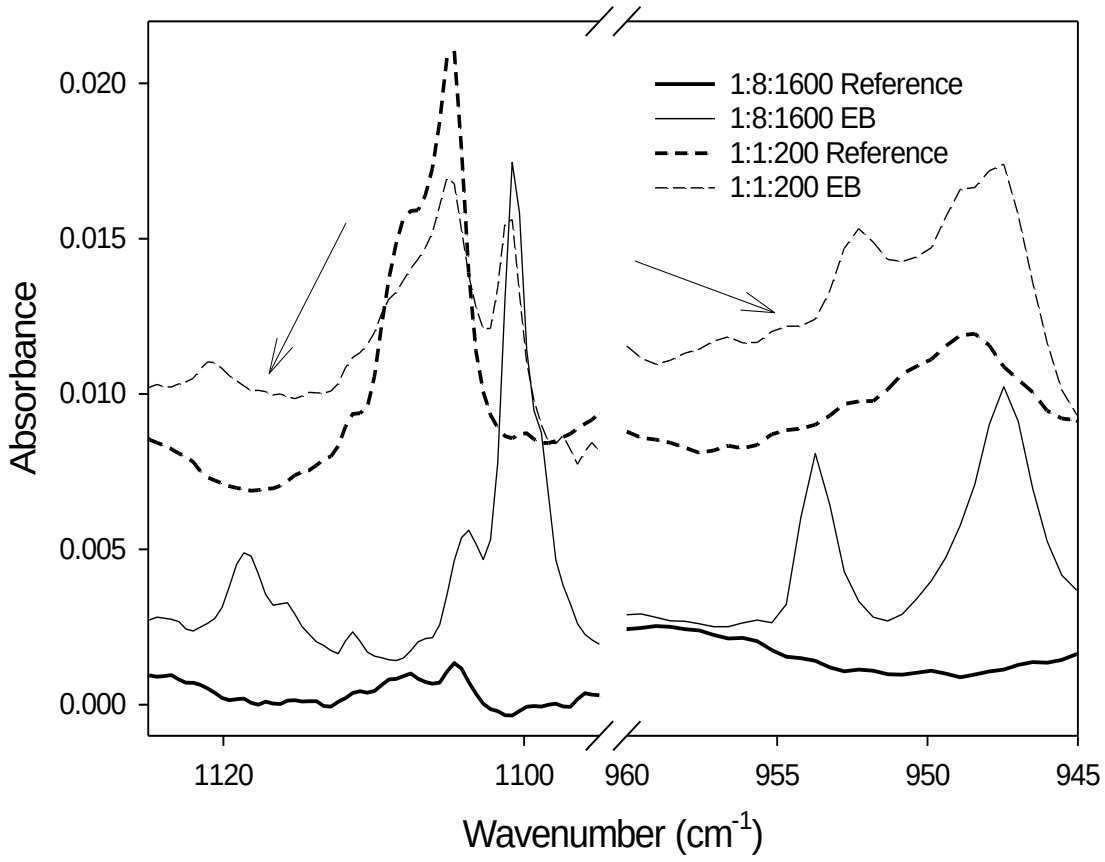

Figure 48. Reference and EB spectra from 1:1:200 and 1:8:1600 toluene:O_2:Ar gas samples, showing that absorptions previously observed at 954 and 1118 cm^{-1} appear to have shifted to 952 and 1121 cm^{-1} with the increase in concentration to 1:1:200

4.7 Ab initio calculations

Radical reactions with molecular oxygen are known to be highly exothermic, so the oxygen-benzyl radical reaction was assumed to be favorable in the EBMIS system. To confirm this assumption, a series of calculations were performed using Gaussian software (Gaussian 98, Rev. A.11.3, and Gaussview Rev 2.1).

The geometry, vibrational spectrum, total energy, and zero-point energy were calculated for several molecules: argon, the argon cation, oxygen, the oxygen cation, hydrogen, toluene, the toluene cation, the benzyl radical, the benzyl cation, the benzylperoxy radical, and the benzylperoxy cation. Initial calculations used the AM1 method[82], and the results were used as the starting point for more involved B3LYP calculations[83]. The B3LYP calculations started with the 3-21 basis set, and then moved up through the 6-31 set and then the 6-311 set to the 6-311Gdp basis set, using the result of each calculation as the starting point for the next calculation. One exception to this is the benzylperoxy cation, which was calculated starting from the 6-311Gdp results for the benzylperoxy radical in order to obtain a result where the molecule was intact. Gaussian software also calculates harmonic vibrational frequencies from the second derivative of the force constant matrix.

Table 2. Total energies (Hartrees) obtained from B3LYP 6-311Gdp calculations

Species	Spin State	Total Energy (Hartrees)
Argon (Ar)	singlet	-527.5532
Argon cation (Ar+)	doublet	-526.9711
Oxygen (O2)	triplet	-150.3648
Oxygen cation (O2+)	singlet	-149.9034
Hydrogen (H)		-0.5022
Toluene (Tol)	singlet	-271.6361
Toluene cation (Tol+)	doublet	-271.3199
Benzyl cation (Bz+)	singlet	-270.7237
Benzyl radical (Bz*)	doublet	-270.9902
Benzylperoxy cation (Bz-OO+)	singlet	-421.0380
Benzylperoxy radical (Bz-OO*)	doublet	-421.3797

Upon completing these calculations, the total energies obtained were tabulated (see Table 2 above), and used to calculate important reaction energies. These calculations and the results are shown in Table 3, below.

Table 3. Calculated reaction energies for important reactions

Reactions & Total Energies (Hartrees)					Reaction Energy		
					(Hartrees)	(kJ/mol)	(eV/particle)
Ar -527.5532	→	Ar+ -526.9711	+	e-	0.5821	1528.2734	15.8940
O2 -150.3648	→	O2+ -149.9034	+	e-	0.4614	1211.4444	12.5990
Tol -271.6361	→	Tol+ -271.3199	+	e-	0.3162	830.1563	8.6336
Tol -271.6361	→	Bz* -270.9902	+	H -0.5022	0.1437	377.3819	3.9248
Bz* -270.9902	+	O2 -150.3648	→	Bz-OO* -421.3797	-0.0247	-64.8980	-0.6749
Bz+ -270.7237	+	O2 -150.3648	→	Bz-OO+ -421.0380	0.0505	132.6691	1.3798
Bz* -270.9902	+	O2+ -149.9034	→	Bz-OO+ -421.0380	-0.1445	-379.2945	-3.9447

From these results, it is clear that the benzyl radical + oxygen reaction and the benzyl radical + oxygen cation reaction are both exothermic. This is expected, as they are both reactions involving reactants with unpaired electrons, and these calculations confirm that they should be favorable in the EBMIS system. Their reaction energies indicate that the reactions are highly exothermic, and that collisions between the benzyl radical and either oxygen or the oxygen cation should favour the production of the benzylperoxy radical, as long as the molecules' geometries are properly aligned, and the activation energy is not prohibitive.

Chapter 5

Discussion

5.0 Hydroxyl radicals from water

As discussed in the previous chapter, the main result of the argon-water set of experiments was the production of hydroxyl radicals from the electron bombardment of argon-water mixtures. This was confirmed by the observation of an absorbance at 3548 cm^{-1}, a characteristic absorbance of hydroxyl radicals[47]. The normal mechanism by which this occurs involves argon directly ionized by the electrons present in the system. This charged argon then ionizes the water in the gas mixture, creating H_2O^+. The excess energy present in this charged molecule is partially released during the dissociation of one of the hydrogen atoms, resulting in formation of either a hydrogen atom and hydroxyl cation, or a hydrogen cation and a hydroxyl radical. The ionization energy (E_I) of argon is 15.76 eV[84], while the ionization energy of water has been calculated most recently by Snow and Thomas[85] to be 12.6 eV. The ionized argon will collide with a water molecule, and will be neutralized via charge transfer, receiving an electron from water and leaving it with an amount of excess energy (E_e) equal to the difference between the two ionization energies[86].

When H_2O^+ is compared to neutral water molecules, the infrared absorbance wavenumbers of the cation are seen to be lower. The bond dissociation energy of the water cation was calculated to be 5.390 eV, slightly higher than that of the neutral molecule (4.988 eV), this indicates that the change in wavenumber is likely caused by structural change, rather than a bond weakening effect. These calculations were

performed using literature values for the ionization energies of the hydroxyl radical[87] and neutral water[88], and the dissociation energy of neutral water[89]. Using the ionization potentials of water and argon, the internal energy that remains in the water molecule after ionization is calculated - if this internal energy is greater than the bond dissociation energy of neutral water, then dissociation will occur. Based on the assumption that the bond dissociation energies of the cation will be lower than those of the neutral, H_2O^+ will also dissociate following ionization. In addition, ions generally neutralize in the electron bombardment apparatus, by capturing a free electron – this would release energy equal to the entire ionization potential of the water cation. The calculations below show how the remaining internal energy left after ionization is determined, and whether it is greater than the energy required for the dissociation of water.

$E_i(Ar)=15.76$ eV

$E_i(H_2O)=12.6$ eV

$E_e= E_i(Ar)-E_i(H_2O)$

$E_e=15.76$ eV – 12.6 eV

$E_e=3.16$ eV

$H_2O \rightarrow \bullet OH + H\bullet$

E_a = 440 kJ/mol[90]

E_a = 4.56 eV

One possible mechanism for the dissociation of the water cation is due to excess internal energy resulting from ionization, followed by the capture of a secondary electron. This will result in neutral fragments after dissociation, as shown below:

$H_2O^{+*} \rightarrow OH^{\bullet} + H^+$

$H^+ + e^- \rightarrow H$

A second mechanism reverses the order of these steps – the water cation captures a secondary electron after ionization, which neutralizes the ion and results in the release of the entire electron affinity of the cation. The resulting excess energy is significantly higher than the dissociation energy of the water cation, and dissociation will occur:

$$H_2O^{+}* + e^{-} \rightarrow H_2O^{**}$$

$$H_2O^{**} \rightarrow OH^{\bullet} + H^{\bullet}$$

The fact that there are significant quantities of electrons present in the apparatus makes either of these mechanisms possible. Mechanism 2 results in release of energy equal to the entire ionization potential of the molecule, providing enough energy for the dissociation of water to occur. Despite finding that it was possible to produce hydroxyl radicals via electron bombardment of water in the EBMI system, the yields that were observed were too low to be useful for the types of studies we wanted to pursue. No alternative source of hydroxyl radicals was viable in the electron bombardment system, and because of this we decided to move on to producing benzyl radicals directly in the EB apparatus. In the troposphere, one common reaction of a hydroxyl radical is the abstraction of a hydrogen atom, if it is possible to produce a more stable radical than $OH^{\bullet}$. As this is the main interest of this work and occurs after the first abstraction step, it was decided to skip the initial steps of the reaction, as they are quite straightforward, and move on to the direct production of the hydrogen abstraction product.

5.1 Oxygen ionization chemistry

The objective of this work was to generate benzyl radicals, and react them with oxygen inside the apparatus. This meant that it was necessary to understand the

independent chemistry of oxygen under similar conditions. The main results of this series of experiments were the observation of characteristic IR absorptions attributed to ozone and hydroperoxy radicals

The formation of ozone occurs via the combination of an oxygen molecule and an oxygen atom.

$O_2 + O\bullet \rightarrow O_3$

The single oxygen atoms are formed by dissociation of O_2, either due to excess energy remaining after ionization via charge-transfer from argon, direct ionization by electrons present in the apparatus, or capture of secondary electrons after ionization. The ionization energy of argon is 15.76 eV, as previously mentioned, and the ionization energy of oxygen is 12.07 eV[91]. The bond dissociation energy of the oxygen cation is 5.12 eV[92] - this value is larger than the excess energy that would remain after charge-transfer ionization, meaning that this cannot be the method by which dissociation of oxygen occurs. The electrons produced in the EBMI system have an energy of 300 eV, which is more than enough to ionize the oxygen molecules present, and leave them with sufficient excess energy to cause dissociation. Capture of a secondary electron after ionization by charge-transfer from argon would also cause dissociation of oxygen molecules. This would release the entire ionization energy of the oxygen cation, more than enough energy to overcome the oxygen-oxygen bond strength. Formation of ozone from the combination of an oxygen molecule and an oxygen radical has a reported rate constant[93] at 298K of 6.01×10^{-34} $cm^6 \cdot molecule^{-2} \cdot s^{-1}$, so when compared to an ionic termolecular reaction that will occur on every collision, which has a rate constant[94] of $10^{-29} - 10^{-30} cm^6 \cdot molecule^{-2} \cdot s^{-1}$, we can see that about 1 in every thousand or so collisions

will result in a reaction. This is reactive enough to produce noticeable quantities of product.

The hydroperoxy radicals formed in these experiments are likely being produced via the reaction of oxygen molecules with hydrogen atoms. The hydrogen atoms are likely a byproduct of the formation of hydroxyl radicals from background water present in the apparatus. The yield of hydroxyl radicals from water was fairly low, meaning that the yield of hydrogen atoms was also low, however hydrogen atoms have good mobility through the matrix, increasing their chances of encountering an oxygen molecule with which to react. The third-order rate constant of the $H + O_2$ reaction has been reported in a review by DeMore et al[93] to be 5.71×10^{-32} $cm^6 \cdot molecule^{-2} \cdot s^{-1}$. This shows that the reaction will occur in approximately 1 in every 5 collisions, so it is quite favourable – for comparison, the termolecular rate, mentioned previously, is 3×10^{-29} $cm^6 \cdot molecule^{-2} \cdot s^{-1}$ The oxygen molecules act as a scavenger for the hydrogen atoms, allowing us to see that they do result from dissociation of water – as hydrogen atoms will not be observed in an IR spectrum, they were not previously visible.

5.2 Production of benzyl radicals from toluene

Toluene is known to be a precursor of benzyl radicals in the atmosphere[49,50] , and ionization of toluene is known to lead to the benzyl cation[95]. This is the cationic analogue of the benzyl radical, and is a resonant stabilized product of the ionization of toluene, the other product being the tropyllium ion (a seven-membered aromatic ring cation, $C_7H_7^+$). The benzyl cation is produced with a yield of 35% when the ionizing electrons have an internal energy of 30 eV, according to work by McLafferty and Bockhoff[96]. The ease with which benzyl cations are produced from ionization of toluene

made this mechanism an appealing source of the benzyl radical, which would form upon neutralization of the benzyl cation in the EB apparatus.

A series of experiments, described in the previous chapter, were performed, and the main result was that it was in fact possible to produce benzyl radicals via the ionization of toluene in the EB apparatus. Further experiments were performed to optimize the conditions for benzyl radical production, the results indicated that benzyl radical production increased with increased electron current through the reaction cell, and that it decreased with increased sample flow rate.

One major reason that toluene makes a good source of benzyl radicals is the relative bond energies of the molecule. The C-H bonds in the methyl group have a bond energy of about 3.36 eV[97] while the C-C bond between the benzene ring and the methyl group has a bond energy calculated at 4.41 kcal/mol[98]. This means that the easiest, and therefore first, bond to be broken due to the excess internal energy present in the ionized toluene will be a methyl C-H bond, leaving the benzyl cation. The abundance of electrons present in the EBMI system means that the benzyl cation will be quickly neutralized, to form the benzyl radical. Ionization of toluene is the simplest, most direct method of benzyl radical formation in the EBMI apparatus.

Previous work from the Parnis lab supports the results obtained from the increased electron current experiments[86]. As the current increases, so does the density of the Ar^+ cations, decreasing the average time it takes the argon cations to encounter a toluene molecule. Benzyl radical production was seen to increase with electron current until it plateaus slightly above 30 mA. The reason for this plateau cannot be definitively explained, but it would appear that ionization of argon has saturated. While unconfirmed, one potential reason could be that although the total number of electrons in

the apparatus is increasing, not all of them are passing through the sample and ionizing the argon.

The results of the variable flow rate experiments were generally unsurprising. As the flow rate increases while the electron current remains the same, the number of argon atoms present in the reaction cell increases but the number of them that are ionized does not. This means that the time it takes an argon cation to encounter a toluene molecule will increase, as the cations are vastly outnumbered by neutral argon. Overall, the ideal conditions were found to be a low flow rate, 1 standard cubic centimeter per minute, and a moderate electron current, 20 – 30 mA.

5.3 Introduction of O_2 and toluene

The final step in this work was the electron bombardment of toluene-oxygen mixtures, in an attempt to produce the benzylperoxy radical via the reaction between benzyl radicals and oxygen. Radical-radical reactions are known to be generally favourable, having little or no energetic barrier[99], for example the reaction between hydroxyl radicals and hydrogen radicals requires no activation energy at all, and will proceed at gas-kinetic rates. For this reason, it was surprising that no new products were observed following these experiments, other than those products already identified after ionization of toluene and oxygen separately.

In a final attempt to produce the benzylperoxy radical, the concentrations of toluene and oxygen were increased. As the concentrations of the precursor species increased, new absorptions were observed at 1118 and 954 cm^{-1}, possible indications that a peroxy species was being produced. One piece of evidence for this identification is the fact that the wavenumbers of the absorptions characteristic of a number of other

peroxy species are known, and these values define a range into which the 1118 and 954 cm^{-1} absorptions could fit.

Alkylperoxy radical	*O-O Stretch(cm^{-1})*	*C-O Stretch (cm^{-1})*
CH_3O_2[69]	1112	902
$C_2H_5O_2$[70]	1112	838
i-$C_3H_7O_2$[71]	1101	789
t-$C_4H_9O_2$[72]	1124	730

In addition, Gaussian was used to produce a calculated vibrational spectrum of the benzylperoxy radical, and the resulting dataset includes normal mode wavenumbers consistent with the two observed peaks, at approximately 958 and 1125 cm^{-1}. Although there are no calculated values at exactly 1118 and 954 cm^{-1}, the calculated and experimental values would be expected to differ somewhat due to effects from the matrix and potential interaction with contaminants, etc., as well as inherent errors due to the computation itself.

The two new peaks observed at 1118 and 954 cm^{-1} increased in magnitude with increasing toluene and oxygen concentrations, which is another indication that the compound causing the absorptions is likely a product of the toluene and oxygen reaction. This observation, along with the fact that both calculated benzylperoxy vibrational spectra and experimental vibrational spectra of other peroxy species support the assignment of these peaks to a peroxy species lead us to the conclusion that it is quite likely that these peaks are produced by the benzylperoxy radical. Although the

available evidence is not entirely definitive, it is sufficient to support the tentative assignment of these peaks to the C-O (954 cm^{-1}) and O-O (1118 cm^{-1}) stretching modes of the benzylperoxy radical. Further experimental work would be required in order to confirm this peak assignment.

Chapter 6

Summary

Electron bombardment of toluene has been shown to produce benzyl radicals, which have been observed using FT-IR spectroscopy. When mixtures of toluene and oxygen were subject to electron bombardment in the EBMIS system, new product peaks were observed, two of which were identified as possible benzylperoxy radical absorptions. Based on computational work that was performed, formation of the benzylperoxy radical from the reaction between benzyl radicals and oxygen molecules is energetically favoured, and may occur if the barrier is not prohibitive.

This work has demonstrated that production of the benzylperoxy radical is possible in an EBMIS system, with an adequate supply of the benzyl radical precursor. This conclusion is supported by the observation of two new peaks, 1118 and 954 cm^{-1}, that can be assigned with some confidence to the benzylperoxy radical. This is a significant finding, as it means that investigations into the atmospheric reactions and fates of volatile organic compounds could be possible using the electron bombardment matrix isolation system.

It is likely that a major reason for the limited amounts of benzylperoxy radical formed was the fact that even with significantly increased toluene concentrations, only small quantities of benzyl radical could be produced. Early work had shown that hydroxyl radicals could be produced through electron bombardment of water, but only in small quantities. The initial plan had been to produce benzyl radicals through the reaction between hydroxyl radicals and toluene, but this was abandoned due to the insufficient production of hydroxyl radicals. If a method were developed to improve

hydroxyl radical production, this could be a better method than electron bombardment of toluene for benzyl radical production.

Lack of sufficient mixing/reaction time appears to be another major factor in the lack of significant product formation. To improve the issue of reaction time, the apparatus could be converted to a type of flow system, where the reactants would have significantly increased time to react with one another before being frozen in the argon matrix, as used by Y.P. Lee and his research group[100].

Overall, the work presented here was successful in determining that it is possible to investigate atmospheric reactions using an electron-bombardment matrix isolation system. Toluene was converted into benzyl radicals, which were in turn reacted with oxygen, producing two new infrared absorptions that have been tentatively identified as being caused by the benzylperoxy radical. Future work on this or similar projects should look into the use of a flow reactor setup, in order to maximize reaction time and improve product yield. If available, this could also involve the use of a microwave discharge as an efficient source of hydroxyl radicals.

[1] Gross, J.; *Mass Spectrometry: A Textbook*, Springer: New York. **2004**.

[2] Fridgen, T.D.; Parnis, J.M.; *J. Phys. Chem. A.* **1997**, 101, 5117.

[3] Parnis, J.M.; King, K.A.; Thompson, M.G.K.; *J. Mass. Spectrom.* **2009**, 44, 652.

[4] Thompson, M.G.K.; Parnis, J.M.; *J. Phys. Chem. A.* **2008**, 112, 12109.

[5] Szczepanski, J.; Roser, D.; Personetter, W.; Eyring, M.; Pellow, R.; Vala, M.; *J. Phys. Chem.* **1992**, 96, 7876.

[6] Tonokura, K.; Koshi, M.; *J. Phys. Chem. A* **2003**, 107, 4457.

[7] Whittle, E.; Dows, D.A.; Pimentel, G.C.; *J. Chem. Phys.* **1954**, 22, 1943.

[8] Kaye, G.W.C.; Laby, T.H.; *Tables of Physical & Chemical Constants,* 13th Ed., Longman Group Limited: London. **1966**.

[9] Cradock, S.; Hinchcliff, A.J.; *Matrix Isolation: A Technique for the Study of Reactive Inorganic Species*, 1st Ed., Cambridge University Press: Cambridge. **1975**.

[10] Parnis, J.M.; Thompson, M.G.K.; *J. Chem. Ed.*, **2004**, 81, 1196.

[11] Dunkin, E.R.; *Matrix Isolation Techniques: A Practical Approach*, Oxford University Press: New York. **1998**.

[12] Gaussian 03, Revision D.01, Frisch, M.J.; Trucks, G.W.; Schlegel, H.B.; Scuseria, G.E.; Robb, M.A.; Cheeseman, J.R.; Montgomery, J.A.; Vreven, T.; Kudin, K.N.; Burant, J.C.; Millam, J.M.; Iyengar, S.S.; Tomasi, J.; Barone, V.; Mennucci, B.; Cossi, M.; Scalmani, G.; Rega, N.; Petersson, G.A.; Nakatsuji, H.; Hada, M.; Ehara, M.; Toyota, K.; Fukuda, R.; Hasegawa, J.; Ishida, M.; Nakajima, T.;

Honda, Y.; Kitao, O.; Nakai, H.; Klene, M.; Li, X.; Knox, J.E.; Hratchian, H.P.; Cross, J.B.; Bakken, V.; Adamo, C.; Jaramilo, J.; Gomperts, R.; Stratmann, R.E.; Yazyev, O.; Austin, A.J.; Cammi, R.; Pomelli, C.; Ochterski, J.W.; Ayala, P.Y.; Morokuma, K.; Voth, G.A.; Salvador, P.; Dannenberg, J.J.; Zakrzewski, V.G.; Dapprich, S.; Daniels, A.D.; Strain, M.C.; Farkas, O.; Malick, D.K.; Rabuck, A.D.; Raghavachari, K.; Foresman, J.B.; Ortiz, J.V.; Cui, Q.; Baboul, A.G.; Clifford, S.; Cioslowski, J.; Stefanov, B.B.; Liu, G.; Liashenko, A.; Piskorz, P.; Komaromi, I.; Martin, R.L.; Fox, D.J.; Keith, T.; Al-Laham, M.A.; Peng, C.Y.; Nanayakkara, A.; Challacombe, M.; Gill, P.M.W.; Johnson, B.; Chen, W.; Wong, M.W.; Gonzalez, C.; Pople, J.A.; Gaussian, Inc. Wallingford, CT, 2004.

[13] Manahan, S.E.; *Environmental Chemistry*, 6th Ed., CRC Press: Boca Raton. **1994**.

[14] Health Canada, "Toluene – PSL1".

[15] Environment Canada, National Inventory Report 1990 – 2010: Greenhouse Gas Sources and Sinks in Canada, Government of Canada. **2012**.

[16] Suzer, S.; Andrews, L.; *J. Chem. Phys.* **1988**, 88, 916.

[17] Andrews, L.; *Ann. Rev. Phys. Chem.* **1979**, 30, 79.

[18] Milligan, D.E.; Jacox, M.E.; *J. Chem. Phys.* **1970**, 52, 3864.

[19] Breeze, P.A.; Burdett, J.K.; Turner, J.J.; *Inorg. Chem.* **1981**, 20, 3369.

[20] Suzer, S.; Andrews, L.; *J. Chem. Phys.* **1988**, 89, 5347.

[21] Knight, L.B.; Bostick, J.M.; Woodward, R.W.; Steadman, J.; *J. Chem. Phys.* **1983**, 78, 6415.

[22] Knight, L.B.; *Acc. Chem. Res.* **1986**, 19, 313.

[23] Fridgen, T.D.; Zhang, X.K.; Parnis, J.M.; March, R.E.; *J. Phys. Chem. A* **2000**, 104, 3487.

[24] Ehhalt, D.H.; *Phys. Chem. Chem. Phys*. **1999**, 1, 5401.

[25] Crutzen, P.J.; Zimmerman, P.H.; *Tellus 43AB*, **1991**, 4.

[26] Tang, X.; Madronich, S.; Wallington, T.; Calamari, D.; *J. Photochem. Photobiol., B*. **1998**, 46, 83.

[27] Wayne, R.P.; *Chemistry of Atmospheres*, 3rd Ed., Oxford University Press: New York. **2000**.

[28] Crutzen, P.J.; *Faraday Discuss.* **1995**, 100, 1.

[29] Montzka, S.A.; Krol, M.; Dlugokencky, E.; Hall, B.; Joeckel, P.; Lelieveld, J.; *Science*. **2011**, 331, 67.

[30] Tang, X.; Wilson, S.R.; Solomon, K.R.; Shao, M.; Madronich, S.; *Photochem. Photobiol. Sci*. **2011**, 10, 280.

[31] Berndt, T.; Böge, O.; *J. Phys. Chem. A*, **2007**, 111, 12099.

[32] Lee, W.; Baasandorj, M.; Stevens, P.S.; Hites, R.A.; *Environ. Sci. Technol*. **2005**, 39, 1030.

[33] Karl, M.; Dorn, H.-P.; Holland, F.; Koppmann, R.; Poppe, D.; Rupp, L.; Schaub, A.; Wahner, A.; *J. Atmos. Chem*. **2006**, 55, 167.

[34] Ruppert, L.; Becker, K.H.; *Atmos. Environ*. **2000**, 34, 1529.

[35] Librando, V.; Tringali, G.; *J. Environ. Manage*. **2005**, 75, 275.

[36] Anderson, P.N.; Hites, R.A.; *Environ. Sci. Technol*. **1996**, 30, 1756.

[37] Arey, J.; Obermeyer, G.; Aschmann, S.M.; Chattopadhyay, S.; Cusick, R.D.; Atkinson, R.; *Environ. Sci. Technol*. **2009**, 43, 683.

[38] Obermeyer, G.; Aschmann, S.M.; Atkinson, R.; Arey, J.; *Atmos. Environ*. **2009**, 43, 3736.

[39] Bunce, N.J.; Liu, L.; Zhu, J.; Lane, D.A.; *Environ. Sci. Technol*. **1997**, 31, 2252.

[40] Atkinson, R.; Arey, J.; *Environ. Health Perspect*. **1994**, 102, 117.

[41] Dillon, T.J.; Hoelscher, D.; Sivakumaran, V.; Horowitz, A.; Crowley, J.N.; *Phys. Chem. Chem. Phys*. **2005**, 7, 349.

[42] Markgraf, S.J.; Wells, J.R.; *Int. J. Chem. Kinet*. **1997**, 29, 445.

[43] Barnes, I.; Hjorth, J.; Mihalopoulos, N.; *Chem. Rev*. **2006**, 106, 940.

[44] Oksdath-Mansilla, G.; Penenory, A.B.; Albu, M.; Barnes, I.; Wiesen, P.; Teruel, M.A.; *J. Phys. Org. Chem*. **2010**, 23, 925.

[45] Atkinson, R.; *Pure & Appl. Chem*. **1998**, 70, 1335.

[46] Acquista, N.; Schoen, L.J.; Lide, D.R.; *J. Chem. Phys*. **1968**, 48, 1534.

[47] Cheng, B.-M.; Lee, Y.P.; Ogilvie, J.F.; *Chem. Phys. Lett*. **1988**, 151, 109.

[48] Cabral, B.J.C.; *Int. J. Quantum Chem.* **2005**, 103, 610.

[49] Molina, M.J.; Zhang, R.; Broekhuizen, K.; Lei, W.; Navarro, R.; Molina, L.T.; *J. Am. Chem. Soc*. **1999**, 121, 10225.

[50] da Silva, G.; Hamdan, M.R.; Bozzelli, J.W.; *J. Chem. Theory Comput.* **2009**, 5, 3185.

[51] Wilmshurst, J.K.; Bernstein, H.J.; *Can. J. Chem*. **1957**, 35, 911.

[52] Draeger, J.A.; *Spectrochim. Acta*, **1985**, 41A, 607.

[53] Keefe, C.D.; Pearson, J.K.; MacDonald, A.; *J. Mol. Struct*. **2003**, 655, 69.

[54] Bertie, J.E.; Apelblat, Y.; Keefe, C.D.; *J. Mol. Struct*. **2005**, 750, 78.

[55] La Lau, C.; Snyder, R.G.; *Spectrochim. Acta* **1971**, 27A, 2073.

[56] Hoops, M.D.; Ault, B.S.; *J. Phys. Chem. A*, **2006**, 110, 892.

[57] Brown, K.G.; Person, W.B.; *Spectrochim Acta*, **1978**, 34A, 117.

[58] Parker, J.K.; Davis, S.R.; *J. Am. Chem. Soc*. **1999**, 121, 4271.

[59] Kuş, N.; Sharma, A.; Reva, I.; Lapinski, L.; Fausto, R.; *J. Chem. Phys*. **2012**, 136, 144509.

[60] Baskir, E.G.; Maltsev, A.K.; Korolev, V.A.; Khabashesku, V.N.; Nefedov, O.M.; *Russ. Chem. Bull.* **1993**, 42, 1438.

[61] Fröechtenicht, R.; *J. Chem. Phys.* **1995**, 102, 4850.

[62] Koyanagi, M.; Uejoh, K.; *J. Lumin.* **1997**, 72-74, 511.

[63] Miller, J.H.; Andrews, L.; *J. Mol. Spectrosc.* **1981**, 90, 20.

[64] Andrews, L.; Miller, J.H.; Keelan, B.W.; *Chem. Phys. Lett.* **1980,** 71, 207.

[65] Fröechtenicht, R.; Hippler, H.; Troe, J.; Toennies, J.P.; *J. Photochem. Photobiol. A : Chem.* **1994**, 80, 33.

[66] Damm, M.; Deckert, F.; Hippler, H.; Rink, G.; *Phys. Chem. Chem. Phys.* **1999**, 1, 81.

[67] Parker, J.K; Davis, S.R.; *J. Phys. Chem. A,* **2000**, 104, 4108.

[68] Murakami, Y.; Oguchi, T.; Hashimoto, K.; Nosaka, Y.; *J. Phys. Chem. A.* **2007**, 111, 13200.

[69] Ase, P.; Bock, W.; Snelson, A.; *J. Phys. Chem.* **1986**, 90, 2099.

[70] Chettur, G.; Snelson, A.; *J. Phys. Chem.* **1987**, 91, 3483.

[71] Chettur, G.; Snelson, A.; *J. Phys. Chem.* **1987**, 91, 913.

[72] Chettur, G.; Snelson, A.; *J. Phys. Chem.* **1987**, 91, 5873.

[73] Mardyukov, A.; Sander, W.; *Chem. Eur. J.* **2009**, 15, 1462.

[74] Ayers, G.P.; Pullin, A.D.E.; *Spectrochim. Acta* **1976**, 32A, 1629.

[75] Ogawara, Y.; Bruneau, A.; Kimura, T.; *Anal. Chem.* **1994**, 66, 4354.

[76] Leroi, G.E.; Ewing, G.E.; Pimentel, G.C.; *J. Chem. Phys.* **1964**, 40, 2298.

[77] Schriver, A.; Schriver-Mazzuoli, L.; Vigasin, A.A.; *Vib. Spectrosc.* **2000**, 23, 83.

[78] Fridgen, T.D.; Parnis, J.M.; *J. Chem. Phys.* **1998**, 109, 2162.

[79] Andrews, L. and Spiker, R.C. *J. Chem. Phys.* **1972**, 76, 3208.

[80] Milligan, D.E. and Jacox, M.E. *J. Chem. Phys.* **1963**, 38, 2627.

[81] Jacox, M.E. and Milligan, D.E. *J. Mol. Spectrosc.* **1972**, 42, 495.

[82] Dewar, M.J.S.; Zoebisch, E.G.; Healy, E.F.; Stewart, J.J.P.; *J. Am. Chem. Soc*., **1985**, 107, 3902.

[83] Sousa, S.F.; Fernandes, P.A.; Ramos, M.J.; *J. Phys. Chem. A*, **2007**, 111, 10439.

[84] Velchev, I.; Hogervorst, W.; Ubachs, W.; *J. Phys. B*, **1999**, 32, L511.

[85] Snow, K.B.; Thomas, T.F.; *Mass Spectrom. Ion Processes*, **1990**, 96, 49.

[86] Parnis, J.M.; King, K.A.; Campbell, S.E.; Thompson, M.G.K.; *J. Mass. Spectrom.*, **2012**, 47, 89.

[87] Wiedmann, R.T.; Tonkyn, R.G.; White, M.G.; Wang, K.; McKoy, V.; *J. Chem. Phys.,* **1992**, 97, 768.

[88] Karlsson, L.; Mattson, L.; Jadrny, R.; Albridge, R.G.; Pinchas, S.; Bergmark, T.; Siegbahn, K.; *J. Chem. Phys*., **1975**, 62, 4745.

[89] Foner, S.N.; Hudson, R.L.; *J. Chem. Phys*., **1956**, 25, 602.

[90] Baulch, D.L.; Cobos, C.J.; Cox, R.A.; Esser, C.; Frank, P.; Just, T.; Kerr, J.A.; Pilling, M.J.; Troe, J.; Walker, R.W.; Warnatz, J.; *J. Phys. Chem. Ref. Data*, **1992**, 21, 411.

[91] Tonkyn, R.G.; Winniczek, J.W.; White, M.G.; *Chem. Phys. Lett*., **1989**, 164, 137.

[92] Vedeneev, V.I.; Gurvich, L.V.; Kondrat'ev, V.N.; Bond Energies, Ionization Potentials, and Electron Affinities, St. Martin's Press: New York, **1962**.

[93] DeMore, W.B.; Sander, S.P.; Golden, D.M.; Hanpson, R.F.; Kurylo, M.J.; Howard, C.J.; Ravishankara, A.R.; Kolb, C.E.; Molina, M.J.; JPL Publication 97-4, **1997**, 1.

[94] Spears, K. G. and Fehsenfeld, F.C.; *J. Chem. Phys*, **1972**, 56, 5698.

[95] Shen, J.; Dunbar, R.C.; Olah, G.A.; *J. Am. Chem. Soc.*, **1974**, 96, 6227.

[96] McLafferty, F.W.; Bockhoff, F.M.; *J. Am. Chem. Soc.*, **1979**, 101, 1783.

[97] Szwarc, M.; *J. Chem. Phys.*, **1948**, 16, 128.

[98] Yao, X.-Q.; Hou, X.-J.; Wu, G.-S.; Xu, Y.-Y.; Xiang, H.-W.; Jiao, H.; Li, Y.-W.; *J. Phys. Chem. A*, **2002**, 106, 7184.

[99] Pilling, M.J.; *Annu. Rev. Phys. Chem.*, **1996**, 47, 81.

[100] Su, Y.-T.; Huang, Y.-H.; Witek, H.A.; Lee, Y.-P.; *Science*, **2013**, 340, 174.